Solid-binding Proteins for Modification of Inorganic Substrates

Brandon Laurence Coyle

A dissertation submitted in partial fulfillment of the

requirements for the degree of

Doctor of Philosophy

University of Washington

2014

Reading Committee:

François Baneyx, Chairman

Dan T. Schwartz

Lilo Pozzo

Program Authorized to Offer Degree:

Department of Chemical Engineering

University of Washington

Abstract

Solid-binding Proteins for Modification of Inorganic Substrates

Brandon Laurence Coyle

Chair of the Supervisory Committee
Dr. François Baneyx
Chemical Engineering

Robust and simple strategies to directly functionalize graphene- and diamond-based nanostructures with proteins are of considerable interest for biologically driven manufacturing, biosensing and bioimaging. In this work, we identify a new set of carbon binding peptides that vary in overall hydrophobicity and charge, and engineer two of these sequences (Car9 and Car15) within the framework of various proteins to exploit their binding ability. In addition, we conducted a detailed analysis of the mechanisms that underpin the interaction of the fusion proteins with carbon and silicon surfaces. Through these insights, we were able to develop proteins suitable for dispersing graphene flakes and carbon nanotubes in aqueous solutions, while retaining protein activity. Additionally, our investigation into the mechanisms of adhesion for our carbon binding peptides inspired a cheap, disposable protein purification system that is more than 10x cheaper than commonly used His-tag protein purification. Our results emphasize the importance of understanding both bulk and molecular recognition events when exploiting the adhesive properties of solid-binding peptides and proteins in technological applications.

Table of Contents

List of Tables

List of Figures

Acknowledgements

I owe and enormous amount of thanks to all the people that have supported me through my journey in graduate school. First and foremost, to my family, who have always encouraged me in everything I have pursued and been unquestionably supportive. Along with my grandma Grace who has always inspired me to always take a positive outlook in any situation.

I am also deeply indebted to my advisor and mentor, François Baneyx, who has helped shape my science reasoning and continues to inspire me to strive for something more in both science and life. Also, to my committee members who have helped guide my project: Dan Schwartz, Lilo Pozzo, Marco Rolandi, and Beth Traxler. Additionally, I owe a special thank you to all the great people I have met along the way of which there are too many to name, but especially to my lab group members: Miki, Brent, James, Brian, Weibin, Rosie, Jessica, and Mike; without you guys I couldn't have made it through. Through all the pranks, jokes, and conversations that covered everything from A-Z while pipetting away in the lab.

Most importantly, I'd like to thank the 2 most important girls in my life, my loving daughter Ayana who has always encouraged me to be a better person and brings a smile to my face every day. She inspires me through her courage, strength, and energy. And last but not least, her "puppy sister," Addy, who has been a major influence through her constant licks and happiness. She reminds me that the little things can be the best things.

Introduction

Nanotechnology, exploits the unique physico-chemical properties of materials in the 1-100 nm size range to create new structures, systems and devices. While nanotechnology is relatively new to humanity, nature has long used nanoscale molecules such as proteins, lipids, carbohydrates, DNA and RNA. Biomimetics bridges these two worlds by taking inspiration from nature to create new materials or technologies. This thesis focuses on combining biology and materials science for the creation of hybrid functional materials that bring together the unique functionalities of the natural and synthetic materials into a single, more technologically relevant system.[2, 3]

1.1 Biological modification of nanomaterials

Synthetic nanomaterials are important because matter exhibits unique functional properties at the nanoscale. While the field has immense potential, it is difficult to control and manipulate nanomaterials with the degree of precision required for the production of functional devices and architectures in two- and three-dimensions.

Biology uses organic macromolecules to exert remarkable control over the formation and assembly of nano- and microscopic inorganic structures under ambient conditions of temperature, pressure, and pH.[4-6] For example, mollusk shells derive their mechanical strength from the brick and mortar layering of $CaCO_3$ aragonite platelets (**Figure 1.1**) which provides a fracture toughness 3-4 times higher than that of disordered aragonite layers.[7] This ability to change structural characteristics through nanoscale manipulation and bottom up manufacturing

occurs frequently in nature. In contrast, many of our most advanced manufacturing techniques are top down techniques that require many coat and expose steps.

1.2 Selection methods for inorganic binding peptides

Because organisms only produce only a limited amount of inorganic materials, alternative approaches have been developed to build 'designer' proteins suitable for mineralizing, binding and organizing materials of engineering interest. Combinatorial display technologies have been a major tool in enabling this molecular biomimetic approach to materials synthesis.[6, 8] In 1985, George Smith modified the genome of the M13 filamentous bacteriophage by fusing an antibody epitope to one of the viruses' minor coat proteins and showed that the modified bacteriophage was capable of binding to the antibody.[9] This seminal work laid the foundation for the development of the Ph.D. M13 bacteriophage display system[10] which has become the most widely used technology for the identification of solid binding peptides (SBPs). In M13 display, random sequences of amino acids are expressed as fusions to the N-terminus of the p3 minor coat protein to yield a library of virions that can be screened for candidates capable of binding to a particular antibody, protein or even solid material (**Figure 1.2A**). Three libraries are commercially available from New England Biolabs (Beverly, MA, USA): linear heptapeptide (Ph.D.-7) and dodecapeptide (Ph.D.-12) libraries, and the Ph.D.-C7C library in which random heptapeptides are constrained by a disulphide bond between flanking cysteine residues to restrict the conformational space sampled by the inserts (**Figure 1.2B**). Each random sequence is displayed at 3–7 copies (usually five) at the end of the bacteriophage that normally binds to the conjugative F pilus of *E. coli* (**Figure 1.2A**). Typical Ph.D. libraries contain about 10^9 primary clones but phages are usually amplified so that up to 55 copies of the same sequence might be

present in the working library. Non-commercial systems in which random peptides are fused to the p7 or p9 minor coat proteins (**Figure 1.2A**) have also been built.[11] However, they have not been used as extensively as the Ph.D. system. It should also be noted that while it is possible to fuse peptides to the p8 major coat protein to display them at nearly 2700 copies on the virion surface, this approach is not well suited for combinatorial screens because certain basic sequences inhibit phage biogenesis.[12]

Cell surface display is an alternative to phage display in which random peptides are exposed on the cell surface by virtue of being fused to (or within) a membrane-anchored protein. While a number of such technologies have been developed over the years,[13-15] the prevailing cell surface display tools in the materials science community are the FliTrx system (which used to be – but is no longer – commercialized by Invitrogen, Carlsbad, CA) and yeast surface display. In FliTrx display (**Figure 1.2C**), disulfide-bonded dodecapeptides are displayed at multiple copies within defective *E. coli* flagella. This is done by replacing the protruding CGPC active site of the cysteine oxidoreductase thioredoxin 1 (TrxA) by random peptides and inserting the resulting fusions within a permissive site of the major flagellar protein FliC (**Figure 1.2B**).[16] Yeast surface display operates under similar principles, but relies on C-terminal fusions to the *Saccharomyces cerevisiae* Aga2p protein which projects from the cell wall (**Figure 1.2D**).[13, 17] As a result, random sequences can efficiently interact with their targets. The size of both libraries is limited by the efficiency of transformation. The FliTrx system has a diversity of about 10^8, which is only a small fraction of the 4.1×10^{15} possible sequence space. Yeast surface display libraries can be built to a diversity of 10^9 primary clones, but the process is labor-intensive and it is more common to use libraries of $\approx 10^7$ members that can be produced in a single day.[13]

Ribosomal and mRNA display technologies do not rely on a host organism to connect genotype and phenotype. As a result, transformation is not needed and libraries can contain as many as 10^{13} to 10^{14} unique members.[18] Such a degree of diversity is sometimes required to identify strong consensus motifs, e.g. when searching for high-affinity protein ligands. However, inorganic surfaces are inhomogeneous in terms of roughness, oxidation state, and crystallography. As a result, SBPs obtained after 3–5 rounds of biopanning typically do not converge towards a consensus sequence of amino acids. This is not to say that they do not share materials-specific physicochemical characteristics, as exemplified graphically (**Figure 1.3**) for five different inorganic compounds.[19-22]

To summarize, library diversity is generally not an issue when looking for solid-binding peptides (SBPs), peptides that bind to the same material share physicochemical characteristics, and most of the sequences reported in the literature have been isolated using the few *in vivo* display systems that were both robust and commercially available.

1.3 Carbon nanomaterials

Carbon nanostructures represent a major emerging class of synthetic nanomaterials. In nature, carbon typically occurs in two crystal structures, diamond and graphite. Diamond is comprised solely of sp^3 hybridized carbon atoms and forms a rigid, hard structure as the result of the interpenetrating FCC lattices that compose its unit cell crystal structure (**Figure 1.4B**). The other crystal form, graphite, is composed of sp^2-hybridized carbon atoms that lay in a flat hexagonal lattice (**Figure 1.4A**). Due to the double-bonded carbon atoms in this sp^2 orientation, a weak π bond extends perpendicular to the carbon lattice. Many alternative structures exist at the nanoscale

1.3.1 Fullerenes

Prior to the discovery of fullerenes in 1985, carbon was thought to exist in 2 allotropes, graphite and diamond. However, during the examination of carbon fragments, it was found that a species of material consisting of 60 carbon atoms was the predominate material.[23] These fragments were later called fullerenes, which are singe nanometer diameter carbon cages made of carbon hexagons and pentagons that look similar to a soccer ball. These nanoscale carbon variants possess properties unlike either diamond or carbon. For instance, they have been reported to exhibit anti-viral activity through complex formation with HIV protease,[24] and although they exhibit strong anti-oxidant capacity *in vivo*,[25] they can create oxygen radicals at high quantum efficiency.[26] This confinement of carbon at the nanoscale reveals unique properties that are unknown in the bulk carbon counterparts.

1.3.2 Carbon nanotubes

Carbon nanotubes[27] (CNTs) were discovered in 1991 when needle-like structures were found at the negative electrode of the arc discharge devices used to mass produce fullerenes. They are best described as a single layer of graphite rolled into a tube that can exist in a single (SWNT) or multi-walled state (MWNTs). CNTs exhibit different chiralities including zigzag, armchair, and chiral (**Figure 1.5A-C**), depending upon how their sp2-hybridized hexagonal rings aligns with the tube axis.[28] Additionally, the conductance can change depending on these structures. CNTs can be either metallic or semi-conducting in terms of electron propogation based on their chiral vector.[29] These structural differences make it difficult to obtain a uniform/single type of CNT nanotubes, which are required for use in electronic devices. For

example, a typical purification may require creation through CVD on metal catalyst, separation of CNTs from impurities through chemical treatments, length sorting and diameter sorting, and finally sorting for metallic or semi-conducting based on reactivity with different additives.[30-32] The end material is worth the extensive work due to the exciting thermal, electrical and mechanical properties cannot be matched by bulk materials.[33, 34] For example, a CNT can transfer heat at a rate that it 10-fold that of copper, a material used in many applications requiring rapid heat transfer,[35] while the electrical conductivity of a single CNT is up to 1000 times greater than copper,[36] and greater than 10 times the tensile strength of stainless steel.[37]

1.3.3 Graphene

Graphene, a free-standing, single layer of graphite which was discovered in 2004[38] has generated considerable excitement in the scientific community (the number of research publications referring graphene have increased exponentially and at a faster rate than those on CNTs following their initial discovery).[39] Graphene is the thinnest and strongest material known to humans,[40] with electronic and thermal properties that are even better than CNTs.[41-53] A major benefit is that it has no chirality. However, unlike CNTs, graphene has no bandgap, which makes it metallic in character.[42]

1.3.4 Graphene nanoribbons

Graphene nanoribbons (GNRs) are the by-product of constricting one plane of a sheet of graphene. GNRs are important because they can be either metallic or semiconducting depending on their edge structure (zigzag or armchair, respectively). Additionally, semiconducting GNRs have a bandgap that depends on ribbon width (1-10 nm) and edge doping.[54-56] The opening of a

bandgap allows nanoribbons to be used as for building transistors. Interestingly, it is possible to go one step further and create an all-graphene field effect transistors where wide graphene nanoribbons act as the metallic source and drain electrodes are connected by a thinner semiconducting graphene nanoribbon.[57]

1.4 Biomolecular Interactions

The graphite nanostructures introduced above are difficult to manipulate due to their propensity to form insoluble aggregates in aqueous solutions. This limitation has been handled in a number of ways with varying degrees of success. Dispersion in aqueous solvents can be achieved by direct chemical modification through treatment with HNO_3/H_2SO_4 or H_2O_2, but these treatments also alter the unique properties of carbon nanotubes by creating carbocylic acid groups at the surface, which break the integrity of the carbon lattice and reduce the electronic and thermal properties.[58, 59] Graphitic nanomaterials may also be dispersed with surfactants,[60] peptides,[61-63] proteins,[64] sugars,[65, 66] or DNA[67] that create potential sites for further modification without destructing the carbon lattice of the material.

1.4.1 DNA-assisted dispersion

$\pi-\pi$ stacking is responsible for the aggregation of graphitic structures. It also complicates the construction of functional devices that incorporate these materials using aqueous solutions. Sonication is suitable for dispersing aggregates in aqueous solvents but carbonaceous materials quickly re-aggregate in the absence of stabilizing agents. Since DNA acquires its structure and stability through π- π stacking of adjacent nucleotides, it was theorized that the open π bonds in single stranded DNA (ssDNA) molecules might be suitable to passivate the surface of graphitic

nanostructures. Indeed, sonication of graphitic nanomaterials in the presence of ssDNA yields stable dispersions. Later, it was even discovered that different DNA sequences had affinity to differing chiralities, and this was exploited to purify specific chirality semi-conducting SWNTs.[32, 67, 68] Using this technique, purities of 70-90% of specific chirality CNTs was achieved.[32] Since synthetic CNTs can have different sizes and chiralities, the availability of monodisperse solutions of a single CNT type and length is critical for future nanoelectronics applications. Current state of the art technologies require several processing steps to obtain pure CNTs of a single type, so unique applications such as DNA-assisted resuspension and purification through ion-exchange are intriguing.

1.4.2 Peptide-assisted dispersion

Small peptides offer more flexibility than ssDNA for the solubilization of sp^2-hybridized materials because amino acid side chains can be chemically derivatized. Both rational design and phage-display have been used to identify peptides that bind to graphitic nanostructures. In 2003, Wang and colleagues reported on the identification of highly specific CNT binding peptides by phage display,[62] and two of these sequences, the strong binder B1 [HWKHPWGAWDTL] and the weak binder B3 (HWSAWWIRSNQS) were further investigated by Tomásio and colleagues.[69] Using molecular dynamics simulation, the team found that the tryptophan (W) ring formed adhesive groups that remained in direct π-stacked contact with the surface of CNTs while histidine (H) residues interacted with bulk water and created stable conformations of the peptide. Replacing tryptophan residues with tyrosine and phenylalanine (two other aromatic residues) lowered peptide affinity for carbon nanotubes.[69, 70]

Dieckmann and colleagues expanded upon this work by using rational design to develop a peptide that would disperse CNTs. The amphiphilic helical peptide nano-1 (Ac-E(VEAFEKK)(VAAFESK)(VQAFEKK)(VEAFEHG)-$CONH_2$) [where Ac indicates N-terminal acetylation, $CONH_2$ indicates C-terminal amidation] was designed to not only bind and disperse carbon nanotubes in aqueous solutions, but also control the assembly of the peptide coated CNTs.[61] This effect aggregation of the peptide-coated CNTs could then be modulated by the ionic strength of the solution.[61]

Naik *et al* used M13 phage display to identify peptides binding to graphene nanoplatelets.[71] Surprisingly, the dominant peptide, GBP1 (EPLQLKM), does not share any homology with the peptides selected by Wang against CNTs in spite of the fact that the only difference between the two substrates is curvature. In a later study, the Naik group colleagues used molecular dynamics to study the structure of graphene binding peptides on graphene using a dodecamer of sequence GAMHLPWHMGTL which is more similar to those reported by Wang.[62, 71] The peptide formed an α-helix in solution, was helical but was distorted on the graphene surface with the tryptophan in intimate contact through π-stacking.[72]

1.4.3 Protein-assisted dispersion

Graphitic nanostructures can also be solubilized and modified with proteins although there is a risk for denaturation since carbon-based materials are hydrophobic. The first approach to conjugate proteins to sp^2-hybridized nanomaterials is through covalent reaction with carboxylic acids groups created on the surface of the CNTs, as discussed in chapter 1.4. These methods have been reviewed in detail by Nyogi *et al*,[73] and the major limitation with is the

disruption of the CNTs lattice which degrades the thermal and electronic conductance that they are prized for.

Proteins can also adsorb non-specifically to graphitic nanostructures [64, 74, 75] or following treatment with polymers, detergents, or esters;[76-78] which allow proteins to adhere as a secondary layer coating graphitic nanostructures. Unfortunately, biological activity is not consistently retained. For example, α-chymotrypsin lost 99% of its soluble activity when used to coat CNTs that had been sonically separated in dimethylformamide, while soybean peroxidase retained 3-28% enzyme activity depending on enzyme loading.[79] Fourier-transform infrared spectroscopy revealed that α-chymotrypsin was unfolded while SBP retained most of its secondary structure.[79]

1.5 Applications

1.5.1 Complex and multifunctional nanostructures

In addition to providing an environmentally friendly route to nanofabrication through biomineralization, one of the main advantages of designer proteins is that they can be modified by genetic engineering to build complex architectures that are suitable for harnessing unique nanoscale properties or imparting useful functionalities to hybrid nanostructures. In an early demonstration of protein-driven multi-material assembly, Brown constructed 6GB-bio, an artificial protein consisting of six tandem repeats of a gold binding peptide (QATSIGVEKLAGMAESKPTKT) fused to the biotin acceptor peptide GGLNDIFEAQKIEWHEDS.[80, 81] Following *in vitro* biotinylation of the C-terminal tail with the enzyme biotin holoenzyme synthetase (BHS), 6GB-bio was immobilized onto streptavidin-coated polystyrene spheres. These conjugates were next assembled onto larger gold particles by relying on interactions between the fusion protein's gold binding domains and the Au surface

(**Figure 1.6A**).[80] More recently, an FtsZ variant containing an N-terminal biotin acceptor peptide was used to couple avidin-coated magnetic beads through GTP-induced polymerization of the biotinylated protein (**Figure 1.6B**). The protein filaments were 2–4 nm thick and 200–800 nm in length and often aligned into larger sheets.[82]

Metal-enhanced fluorescence (MEF) is a near-field phenomenon in which the photo-luminescence of a fluorophore (e.g. a quantum dot) is increased through interactions with the local electric field of metal nanoparticles exposed to incident illumination.[83] Although it is a very attractive means of increasing brightness, MEF requires precise control of the distance separating quantum dot and metallic particles as loss of enhancement occurs when the separation is too large while fluorescence is quenched if the metal is too close.[84] Taking advantage that proteins are in the correct size range to harness field enhancement effects, Leong *et al.*[85] made use of a biotinylated gold binding peptide called *l*-AuBP2 (WALRRSIRRQSY), gold nanoparticles and a fabricated gold nanoarray to tune the distance separating biotinylated quantum dots and gold nanostructures. In the optimal architecture (consisting of the fabricated gold array, and successive layers of biotinylated *l*-AuBP2, streptavidin, biotinylated quantum dots, streptavidin, biotinylated *l*-AuBP2, and gold nanoparticles; **Figure 1.6C**) a separation of 17.5 nm between Au nanostructures and quantum dots creates a plasmonic 'hot spot' around the nanocrystal that leads to a 15-fold increase in emission brightness.[85]

In addition to the biotin-streptavidin system, other protein–protein interactions can be exploited to build complex architectures. **Figure 1.6D** provides a good illustration of the process. Starting with a TrxA derivative incorporating the CT43 ZnS-mineralizing peptide, we fused tandem repeats of the B from *Staphylococcus aureus* protein A to the N-terminus of the protein to endow it with the ability to bind to the F_c fragment of several classes of IgG. The resulting

chimera not only remained suitable for the production of luminescent ZnS nanocrystals but its BB domain could bind antibodies with a K_d of 60 nM.[22] Furthermore, addition of a small amount of transition metal ions during the biomineralization process changed the maximum emission wavelength from 430 nm (undoped) to 480 nm (Cu^{2+}) or 590 nm (Mn^{2+}), and the amount of antibodies bound by the quantum dot protein shell could be controlled by modifying the molar ratio of BB-TrxA::CT43 to IgG.[21]

In this thesis, we explored the development of a peptide sequences that can bind specifically to sp^2 substrates. Graphene and CNTs are composed of sp^2 carbon and we examined the difference in peptides that bind to sp^2 carbon materials versus sp^3 carbon such as diamond. We found two peptides, Car9 and Car15 discussed in chapter 2, that share a similar affinity to sp^2 carbon substrates but one is a promiscuous binder that could bind to sp^2, sp^3, and silica substrates. Through further examination of the promiscuous peptide sequence, we found that it bound to silica through more than simple ionic interactions. This was interesting because we were able to exploit this interaction to develop a quick purification system on cheap silica substrates. We found costs that were 10x lower than traditional His-tag purification. These tagged proteins could able bind and release from silica sol-gels or even be added to precursor solutions to for silica sol-gels that have an embedded target protein. Finally, we exploited a combination of both the silica and sp^2 carbon binding tags on a single protein to develop protein coated CNTs that bind to silica or oxidized silicon substrates. Eventually, we hope to exploit this to create CNT-based devices on silicon substrates.

1.6 Figures

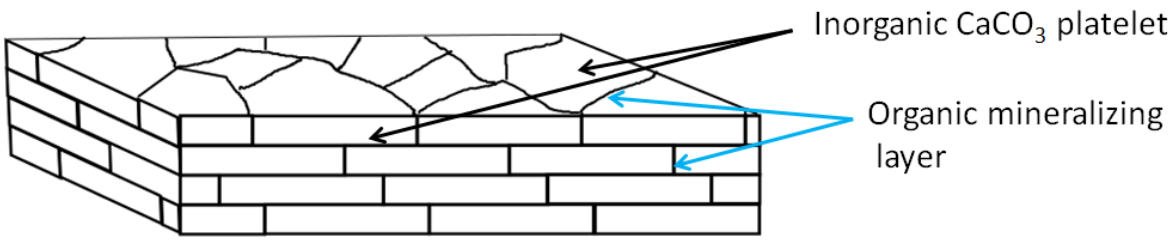

Figure 0.1 Schematic representation of nacre. Stacked aragonite platelets interfaced by an organic mineralizing layer within a mollusk shell.

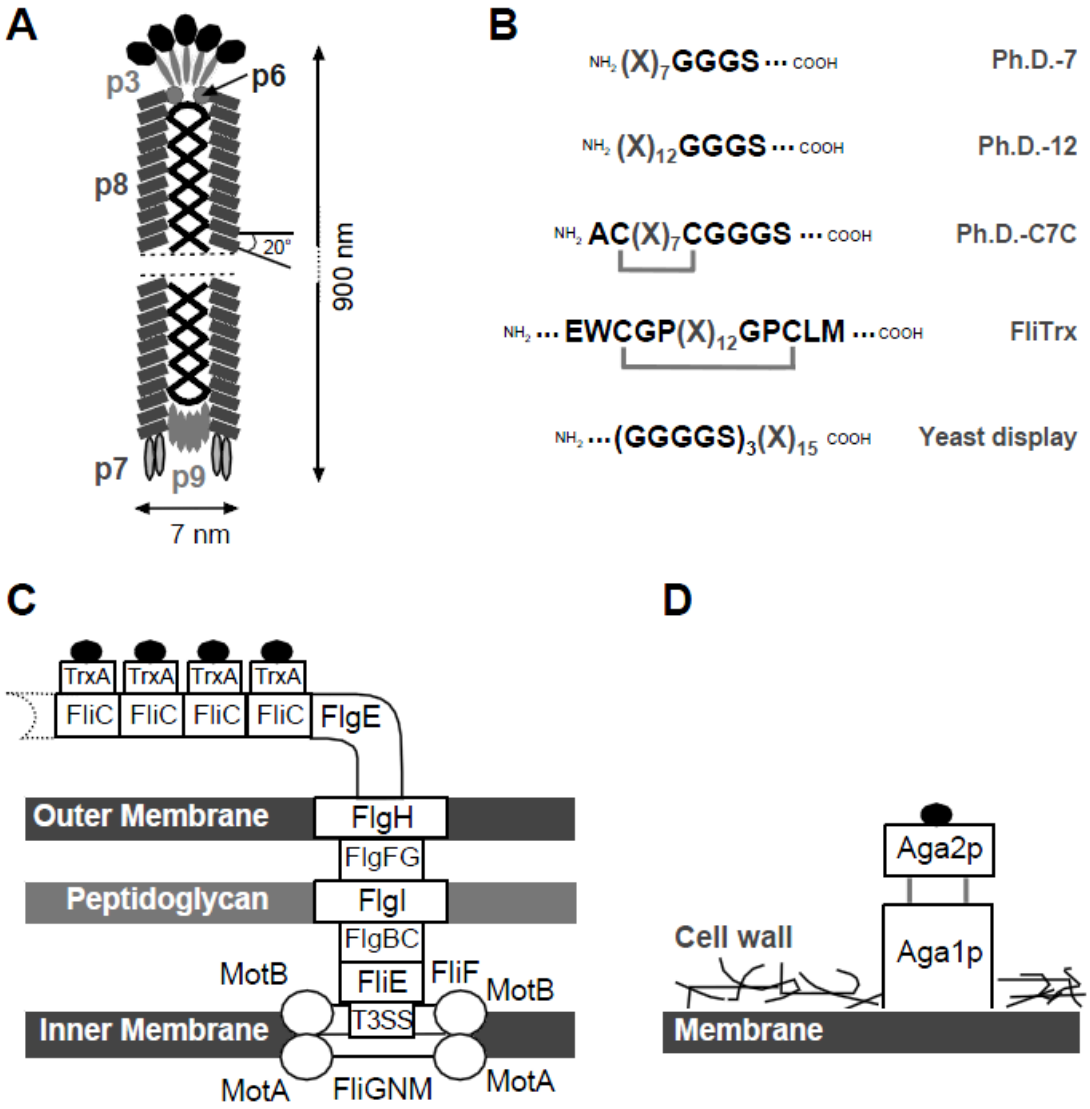

Figure 0.2 (A) Schematic representation of an M13 bacteriophage identifying capsid proteins and geometric parameters. (B) Structure of random peptides displayed as N-terminal fusions to the p3 protein in the Ph.D.7, Ph.D.–12 and Ph.D.-C7C systems, as internal fusions in the FliTrx system, and as C-terminal fusions in the yeast display system. Random amino acids are denoted × and grey lines correspond to disulphide bonds. (C) Schematic structure of the *E. coli* cell envelope and defective flagella architecture used in in FliTrx display. Black ovals corresponds to random peptides inserted within TrxA which is itself fused within FliC. (D) Schematic representation of the *S. cerevisiae* cell envelope in the yeast display system. Aga2p which bears the random peptide (black oval) as a C-terminal fusion is connected to Aga1p through two disulphide bridges (grey lines).

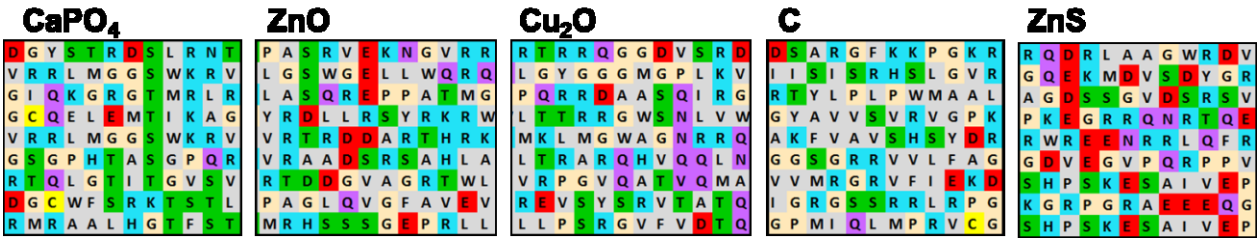

Figure 0.3 SBPs do not converge towards a consensus sequence but share materials-specific characteristics. Patterns are graphical representation of the physicochemical properties of nine solid binding dodecapeptides selected on zinc sulphide (ZnS), zinc oxide (ZnO), cuprous oxide (Cu_2O), calcium phosphate ($CaPO_4$) and carbon (C) substrates via FliTrx display system. Shades of grey correspond to different side-chains chemistries (cysteine, yellow; acidic, red; amide, blue; neutral, tan; hydrophobic, gray; hydroxyl, purple)

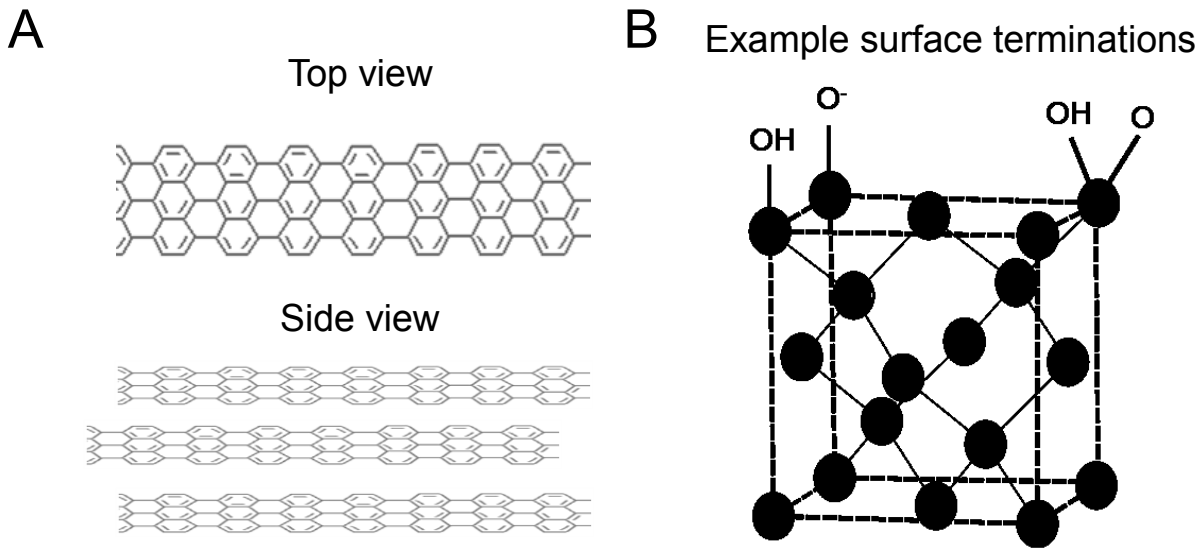

Figure 0.4 Naturally occurring carbon crystal lattices (A) graphite: stacked sheets of hexagonal carbon rings with resonating double bonds. Single unit cell is known as graphene (B) diamond: interpenetrating face centered cubic lattices of tetrahedrally bonded carbon atoms – indicated are potential sites for surface terminations such as -OH, -OOH, $-O^-$ functional groups.

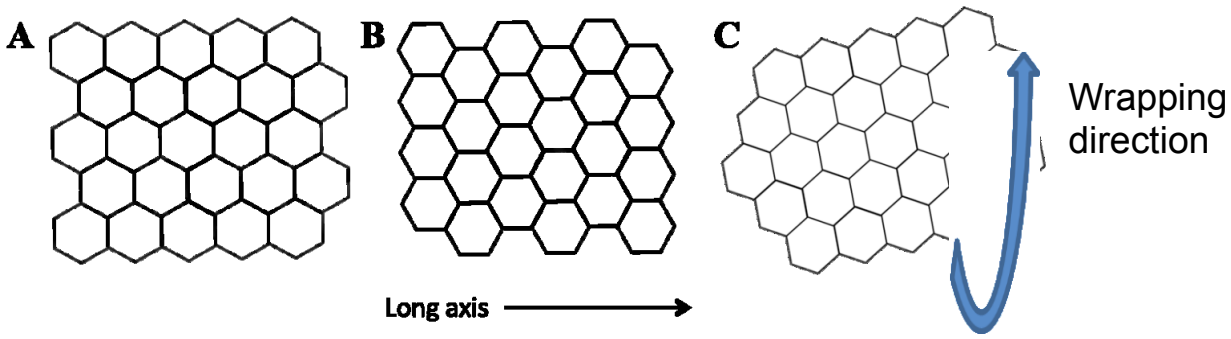

Figure 0.5 Top-down schematic representation of carbon nanotube chirality due to the different configurations of a wrapped graphene sheet (A) armchair, metallic (B) zigzag, semi-metallic or semi-conducting depending on diameter (C) chiral, semi-conducting or semi-metallic

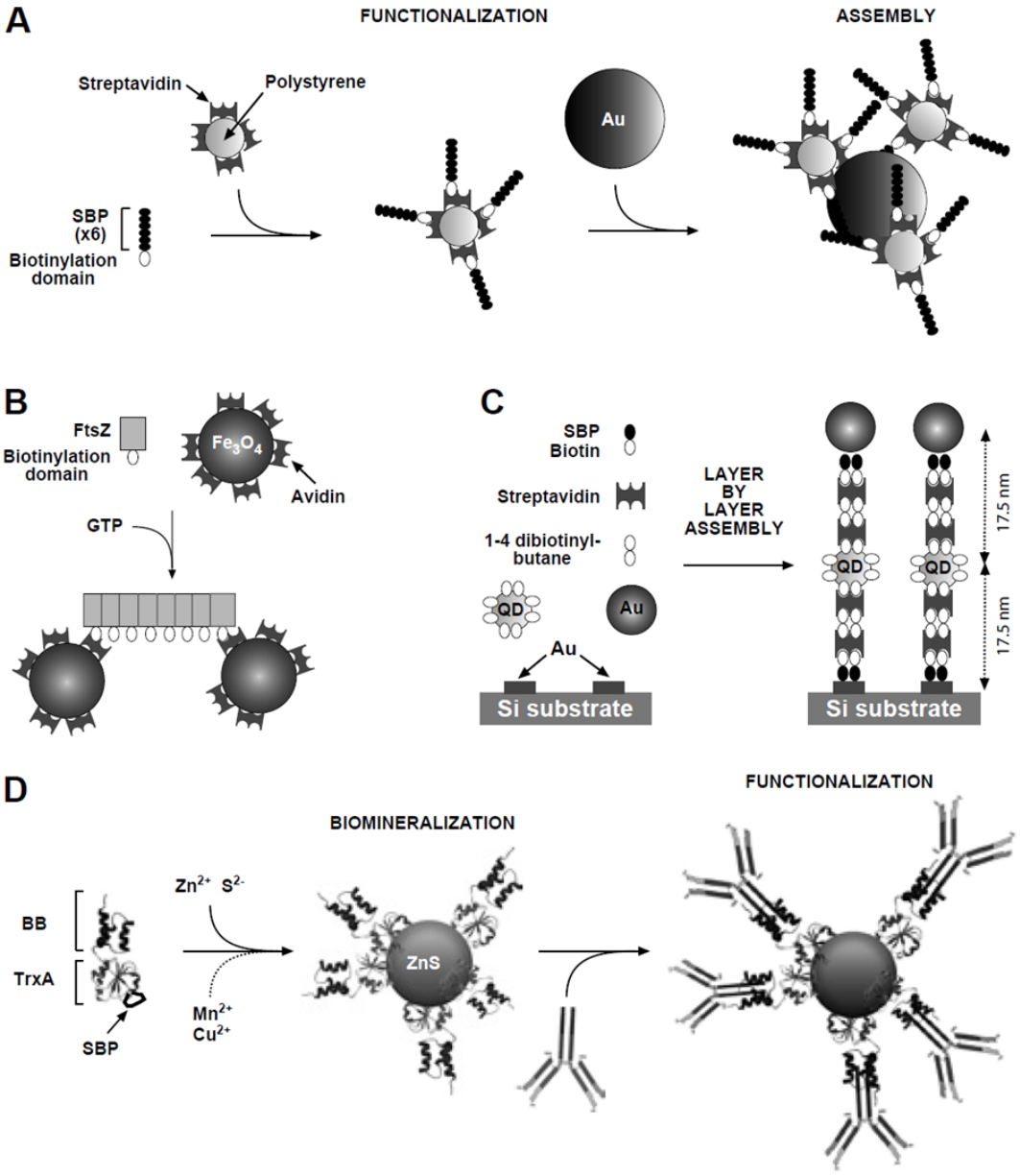

Figure 0.6 Using designer proteins to build complex architectures. (A) A fusion between six repeats of a gold binding peptide and a biotinylation domain is used to assemble streptavidin-coated polystyrene spheres onto larger gold particles. (B) A fusion between a biotinylation domain and the cell division protein FtsZ is used to couple avidin-coated magnetic particles via GTP-induced polymerization. (C) A biotinylated gold binding peptide, biotin-coated quantum dots (QDs), 1,4-dibiotinyl-butane and streptavidin are used to precisely separate patterned gold structures and gold nanaparticles so that a plasmonic hot spot is generated around the QD. (D) A fusion between an antibody-binding domain (BB) and a ZnS-binding TrxA derivative is used to mineralize and cap ZnS nanocrystals that can be derivatized with antibodies.

Preferential Adhesion of Carbon Binding Designer Proteins to sp^2 vs sp^3 hybridized carbon substrates

1.7 Introduction

Solid-binding peptides (SBPs), designer proteins that incorporate them, and organisms that display them have emerged as powerful tools to synthesize and assemble functional materials through environmentally benign processes.[86-90] It is now straightforward to rapidly isolate SBPs against virtually any material of interest by combinatorial technologies, exploit their adhesive properties for surface attachment, interface modification and part-to-part assembly, or harness their chemical reactivity or synthetic properties to promote or modulate the nucleation and growth of inorganic phases.[86, 87, 89, 91-93] While SBPs have great potential for enabling the fabrication of functional hybrid materials with programmed composition, crystallography and topology, the mechanisms through which they interact with solids are far from clear. A better understanding of these phenomena is key to the development of robust, biologically driven and controlled manufacturing processes.

Because of their superior mechanical, thermal, electrical and electronic properties, carbon-based nanomaterials have attracted considerable interest for applications ranging from composite materials to energy storage and next generation nanoelectronics.[41, 44, 46, 94] Carbon nanostructures, particularly sp^2-bonded ones such as nanotubes and graphene, also hold promise in biosensing, drug delivery and bio-imaging applications.[95-97] To interface with the biological world, naturally hydrophobic carbon nanomaterials must first be dispersed into aqueous solutions. This is typically done by chemical modification, which impacts functional properties, or the use of

detergents or solubilizing agents that often denature proteins.[98-100] Peptides that have been designed[101, 102] or selected[103-107] for carbon binding provide an attractive alternative to chemical approaches to disperse, functionalize and manipulate carbon nanostructures. However, only proteins provide a versatile solubilizing framework whose structure and function can be engineered at will.[86] Here, we report on the isolation of a new set of carbon binding peptides and perform a detailed investigation of how Thioredoxin A (TrxA) derivatives incorporating two of these peptides within their framework interact with carbonaceous substrates. The implications of our results for the mechanisms of carbon molecular structure recognition are discussed.

1.8 Materials and Methods

1.8.1 Carbon Binding Peptides and Proteins

The FliTrx cell surface display system (Invitrogen) was used to identify disulfide-constrained, carbon binding dodecapeptides (Car) using a previously described protocol[108] and 12 mm siliconized glass discs (Hampton Research) coated with a carbon film (≈ 25 nm) by thermal evaporation in an Edwards Auto306 instrument.

1.8.2 Cell Binding

GI826 (F^- *lacI*^{q} *amp*C::P_{trp}cI Δ*fliC* Δ*motB eda*::Tn*10*) cells expressing FliTrx::Car fusions on their flagella were grown overnight at 25°C in 5 mL of IMC medium (0.2% amicase, 0.5% glucose, 1 mM $MgCl_2$, 100 μg/ml ampicillin) supplemented with 10 μg/mL carbenicillin. At A_{600} ≈ 1.5, aliquots corresponding to 10^9 cells (2 mL) were transferred to 125 mL shake flask containing 25 mL of IMC supplemented with carbenicillin and 100 μg/mL tryptophan to induce recombinant protein synthesis. After 6 h of growth, the A_{600} of samples was normalized to 1 (10^9

cells/mL) with IMC media and 5 mL of cells were contacted with carbon-coated glass discs in a 60 x 15mm polystyrene petri dish with shaking at ≈ 50 rpm. After 15 min, cells were removed by pipetting, and the discs were washed three times with 5mL of IMC media for 5 min. The discs were next transferred to the stage of an optical microscope and imaged with a 50x objective. The number of adhesive cells was determined by counting 5 randomly selected fields for two independent experiments. .

1.8.3 DNA Manipulations and Protein Purification

Plasmids encoding *E. coli* Thioredoxin 1 (TrxA) variants incorporating carbon binding (Car) peptides within their active were constructed as described.[109] BL21(DE3) cells harboring the resulting pTrx-CarX plasmids (where X denotes a particular carbon binding sequence) were grown overnight at 37°C in 25 mL Luria Broth (LB) supplemented with 34 μg/mL chloramphenicol. Seed cultures were used to induce 500 mL of supplemented LB medium and growth was allowed to proceed at 37°C to $A_{600} \approx 0.5$. Flasks were transferred to a 25°C water bath for 10 min and protein synthesis was induced with 1mM isopropyl β-*D* thiogalactopyranoside (IPTG). After 6 hours, cells were harvested by centrifugation at 7,000*g* for 5 min. TrxA::Car9 was purified as previously described.[109] TrxA::Car15 was first recovered by subjecting the cells to osmotic shock[110] in the absence of $MgCl_2$ which is detrimental to TrxA release.[111] The protein was purified to near homogeneity by ion exchange chromatography on a Whatman DE52 column. Typical protein concentration was 50 μM (0.67 mg/mL).

1.8.4 Protein Interaction with Carbon Surfaces

All carbon surfaces were characterized by Raman spectroscopy (**Figure 6.1**). Glassy carbon (200-400 μm) spherical powder and explosion diamond powder (210-250 μm) were purchased from SPI Supplies. Multi-walled carbon nanotubes (MWNT; 6-9 nm × 5 μm) synthesized by catalytic chemical vapor deposition were purchased from Sigma-Aldrich. For carbon allotrope discrimination experiments, glassy carbon and diamond powders were transferred to a 20 mL glass vial, washed with acetone, methanol and ddH_2O, and subjected to three additional wash cycles in 50 mM sodium phosphate buffer, pH 7.5. Liquid was removed by aspiration and powders were dispensed into microcentrifuge tubes so that each sample corresponded to equivalent surface area (≈ 2,500 mm^2). The latter was determined by measuring average particle diameter through microscopy analysis and calculating their surface area by assuming that they were nonporous, perfect spheres. Proteins (250μL from a 2.5μM solution) were added to the powders and the mixtures were incubated for 1h at room temperature. The supernatant was removed and the powders were washed twice with sodium phosphate buffer. The remaining liquid was removed by aspiration and powders were mixed with 675 μL of active reagent from Pierce bicinchoninic acid (BCA) protein assay (Thermo Scientific). Adsorbed proteins were quantified using a calibration curve constructed with bovine serum albumin, as described by the manufacturer. For MWNT resuspension experiments, ≈ 1 mg of material was added to a glass vial containing 3 mL of protein at 2.5 μM. The mixture was cooled by immersion in a mixture of EtOH and ice and subjected to 2 min of sonication with a micro-tipped sonicator at 12W, 100% duty cycle (Branson Sonifier 450).

1.8.5 Analytical Techniques

QCM measurements were performed on a KSV Z500 instrument using a custom-build Teflon liquid cell and 5 MHz Au quartz crystals (International Crystal Manufacturing) onto which carbon had been evaporated. Before each experiment, crystals were rinsed with ethanol and subjected to UV-ozone treatment for 20 min in a UVO-cleaner (Jelight Co). After addition of 1mL of sodium phosphate buffer, the 3rd, 5th and 7th harmonic frequency changes were monitored until equilibrium was reached (20-30 min) Aliquots of protein (≈ 2, 5, 10 and 20 μL, increasing as maximum surface coverage was approached) were injected and the system was allowed to return to equilibrium. The process was repeated until the protein concentration reached 840 nM. QCM frequency response data and linear least-squares regression was used to construct a Langmuir adsorption isotherm and deduce the values for maximum frequency change (Δf_{max} at full monolayer coverage) and equilibrium dissociation constant (K_d). By using the calculated values for Δf_{max} we were able to plot the surface coverage from the knowledge of Δf at each protein concentration.

Surface Plasmon Resonance measurements were conducted on homemade SPR glass chips coated with a ≈ 2 nm titanium adhesion layer, a ≈ 48 nm evaporated gold film, and a ≈ 4 nm evaporated carbon film. Chips were cleaned with ethanol and UV-ozone as above and mounted on a 4-channel flow cell SPR sensor from the Institute of Photonics and Electronics (Prague, Czech Republic) includes temperature control (25°C) and a peristaltic pump for controlled flow at 50 μL/min. The SPR design is based on an attenuated total reflection and measures wavelength modulation. We note that because carbon coating attenuates the plasmon, SPR data

cannot be used to determine absolute protein concentration at the surface but as a relative measurement of binding affinity.[112]

For atomic force microscopy (AFM), highly oriented pyrolytic graphite (HOPG) substrates (10 x 10 x 2 mm; SPI supplies) were cleaved with adhesive tape to reveal a pristine graphite surface and 150 μL of protein solution at the indicated concentration was deposited by pipetting. After 10 min, the chip was rinsed for 30 sec with ddH_2O using a squeeze flask and dried with filtered air. AFM images were collected in tapping mode on a Veeco Multimode V AFM with Veeco TESP Si (Sb) doped cantilevers.

1.9 Results

1.9.1 Identification of Carbon Binding Peptides

We used the FliTrx flagellar display system[113] to identify disulfide-constrained dodecapeptides capable of conferring to *E. coli* the ability to adhere to evaporated carbon, a disordered and sp^2-hybridized material.[114] As typically observed when biopanning on inorganic targets,[91-93] the putative carbon-binding (Car) peptides did not converge towards a consensus sequence when the inserts of over 30 clones were sequenced. Also as expected,[108] there were large differences in the avidity of cell surface displayed Car sequences for carbon. In fact, we observed an almost 20-fold difference in the number of *E. coli* binding to carbon chips when different Car peptides were displayed on the cell surface within the context of defective flagella (**Table 2.1; Figure 2.1**).

Two of the sequences found to promote high-avidity cell binding (Car9 and Car15) contained a tyrosine (Y) and Car15 also specified tryptophan (W). The presence of aromatic amino acids, in particular that of tryptophan, was not unexpected since these residues have previously been

implicated in mediating the binding of peptides to carbon nanotubes, carbon nanohorns and graphene surfaces via π-stacking.[103, 105, 106, 115-119] On the other hand, Car14 led to poor cell adhesion in spite of containing a tryptophan and the aromatic-free Car16 sequence was capable of mediating (weak) cell adhesion to carbon substrates.

1.9.2 Construction and Purification of Carbon-Binding Designer Proteins

To better understand how two sequences of distinct pI and hydrophobicity (**Table 2.1**) can both confer high-avidity binding to carbon surfaces, we constructed derivatives of *E. coli* Thioredoxin 1 (TrxA) containing a disulfide-constrained Car9 or Car15 sequence in place of the native Cys-Gly-Pro-Cys active site. The TrxA scaffold has the advantages of being fully compatible with the FliTrx system[113] and of projecting its active site loop outwards,[120] which allows for efficient contact between inserted solid binding peptides and their cognate materials.

Figure 2.2A shows that the TrxA::Car9 fusion protein was indeed almost completely soluble. It could be rapidly purified by incubating crude cell extracts at high temperature in order to precipitate thermolabile host proteins and recovering the target protein in a nearly pure form by anion exchange chromatography, as described.[109] By contrast, nearly 85% of the total TrxA::Car15 produced was found in the insoluble cell fraction (**Figure 2.2B**), even though cells were cultured at 25^{o}C to minimize protein misfolding.[121] Such aggregation-prone behavior is consistent with the much higher overall hydrophobicity of the Car15 sequence compared to Car9. Yet, the fact that 15% of the total protein produced is soluble indicates that Car15 can pack its hydrophobic core in a conformation that does not promote inclusion body formation.

In order to selectively purify these TrxA::Car15 conformers, we took advantage of the observation that authentic TrxA can be released from the *E. coli* cytoplasm by an osmotic shock

procedure that is normally used to purify periplasmic proteins.[110] The presence of the Car15 sequence had no noticeable on impact on the osmotic release of TrxA (which is believed to occur through mechano-sensitive channels in the *E. coli* inner membrane)[111] and we were able to recover soluble and pure TrxA::Car15 by subjecting the osmotic shock fluid to a single anion exchange chromatography step.

1.9.3 TrxA::Car9 and TrxA::Car15 Adsorb to Evaporated Carbon through Distinct Mechanisms

We next quantified the affinity of the purified designer proteins for carbon by quartz microbalance (QCM) measurements using QCM crystals that had been coated with an evaporated carbon film (an amorphous, but mostly sp^2-hybridized surface).[122] **Figure 2.3** shows that while the "empty" TrxA framework had little to no affinity for this substrate, the presence of Car9 or Car15 led to high affinity binding with calculated equilibrium dissociation constants (K_d) of 50 nM for TrxA::Car9, and 90 nM for TrxA::Car15. These values are comparable to one another and typical of the room temperature K_d measured with other inorganic-binding designer proteins on their cognate substrates.[123-127]

To gain further information on the nature of binding, we evaporated a thin carbon film onto a gold-coated glass chip and conducted surface plasmon resonance (SPR) measurements with this substrate using a multichannel flow cell. As expected from QCM results, authentic TrxA did not significantly interact with the carbon surface when flowed over the SPR chip at a concentration of 1 μM and a flow rate of 50 μL/min (**Figure 2.4A, gray**). Under the same conditions, TrxA::Car9 (green) rapidly adsorbed and did so with sigmoidal initial kinetics that became more obvious when the protein concentration was lowered to 100 nM (**Figure 2.4B**). Such behavior is

typically indicative of a cooperative adsorption mechanism.[128] By comparison, TrxA::Car15 bound to carbon with typical first order kinetics but did so with a lower k_{on} adhesion rate (**Figure 2.4C**). In addition, the two proteins exhibited very different desorption behaviors: while about a third of TrxA::Car9 could be removed from the surface upon washing with buffer (**Figure 2.4A-B, arrow**), TrxA::Car15 remaining quantitatively bound to the substrate (**Figure 2.4A and C**). Equilibrium dissociation constants extracted from these data (**Figure 6.2)** were 40 nM for TrxA::Car9 and 85 nM for TrxA::Car15, in very good agreement with QCM measurements. Taken together, the above data suggest that although the Car9 and Car15 carbon binding peptides confer TrxA similar affinity for amorphous carbon under equilibrium conditions, the underlying adsorption mechanisms are distinct.

1.9.4 Car15 is an Effective Graphene Binding Peptide

We turned to atomic force microscopy (AFM) to better understand how Car15 and Car9 mediate the attachment of TrxA to carbon. Because the surface roughness of evaporated carbon (> 5 nm) would have complicated the analysis, we imaged the adsorption of TrxA::Car9 and TrxA::Car15 at five different concentrations on highly ordered pyrolytic graphite (HOPG), a multilayered sp^2–hybridized material with surface chemistry and long-range order similar to that of graphene. At a concentration of 50 nM, TrxA::Car9 formed discrete aggregates on HOPG terraces and preferentially adhered to the high-energy step edges (**Figure 2.5C**). TrxA::Car15 was more evenly distributed with no distinct preference for edges or terraces (**Figure 2.5G; Figure 6.3C-D**). At 100 nM, TrxA::Car15 nearly achieved monolayer coverage (**Figure 2.5H**). Surface decoration remained incomplete with TrxA::Car9 under the same conditions and it seemed to proceed from the edges and onto the terraces as the protein concentration increased

(**Figure 2.5C-D; Figure 6.3A-B**). Complete surface coverage was reached at 500 nM TrxA::Car9 (**Figure 2.5E**) and 250 nM TrxA::Car15 (**Figure 2.5I**). Of note, control experiments conducted with wild type TrxA showed that the protein framework did not adhere to HOPG in the absence of inserted Car sequences at concentrations as high as 1 μM (**Figure 6.2**).

We reasoned that if TrxA::Car15 binds to sp^2-hybridized carbon more efficiently than TrxA::Car9, it should also prove superior at dispersing graphene nanostructures that tend to aggregate in polar solvents due to their high surface area and hydrophobicity. To test this hypothesis, approximately 1 mg of multi-walled carbon nanotubes (MWNTs) was sonicated in buffer alone or in the presence of ≈ 2.5 μM of TrxA, TrxA::Car9 or TrxA::Car15, and the solutions were allowed to stand at room temperature for 24h. Consistent with our expectations, TrxA::Car15 was the only protein capable of maintaining the nanotubes in suspension (**Figure 2.6**). We conclude that Car15 binds to graphitic surfaces with high-affinity and specificity and that it can be used at low concentration to solubilize MWNTs, and, presumably, other sp^2-bonded carbon nanostructures of engineering interest.

1.9.5 Carbon Allotrope Discrimination

Graphite and graphene are sp^2-bonded materials in which carbon atoms are arranged into planar hexagonal rings. In diamond, the other naturally abundant form of crystalline carbon, atoms are sp^3-hybridized and organized as two interpenetrating face-centered cubic (FCC) lattices. To determine if Car9 and Car15 would exhibit selectivity for these two carbon allotropes, we acquired glassy carbon (a nonporous, fullerene-related and sp^2-bonded material)[129] and explosion diamond powders in the same size range (200-400 μm). We calculated the average surface area per weight for both substrates using microscopy analysis and assuming a spherical

geometry for both particles (**Figure 2.7, inset**). Next, we incubated the cleaned powders at equivalent surface area (2,500 mm^2) with 2.5 μM of TrxA, TrxA::Car9 or TrxA::Car15 and used a standard BCA assay to determine how much protein remained particle-bound after two cycles of washing. Under these conditions, comparable amounts (≈ 1μg) of authentic TrxA adsorbed to both powders through non-specific interactions (**Figure 2.7**). While the presence of a Car9 insert nearly doubled the amount of protein bound to either powder, there was no statistical difference in the ability of TrxA::Car9 to recognize sp^2- over sp^3-hybridized carbon. By contrast, about 3μg of TrxA::Car15 adsorbed to glassy carbon compared to ≈ 1.5 μg on diamond, leading to a 2:1 discrimination factor between the two carbon allotropes.

1.10 Discussion

As previously observed by other investigators in the case of C_{60}-specific antibodies,[130] and designed[101, 102] and selected[103-107] graphene-binding peptides, we found that the aromatic residues tryptophan, tyrosine and phenylalanine were important to drive the high-affinity binding of displaying cells to amorphous carbon, presumably because these amino acids are capable of forming π-π interactions with sp^2-hybridized regions. Nevertheless, neither the presence of a strong physisorbing amino acid such as tryptophan,[116-118] nor that of a local region of high hydrophobicity guarantees efficient carbon binding (**see, e.g. Car14; Figure 2.1 and 2.8**). In fact, cells displaying peptides that completely lack aromatic content and are reasonably hydrophilic (**e.g., Car16; Figure 2.8**) are still capable of weakly adhering to carbon, perhaps because their sequences are enriched in basic residues (arginine and lysine) that interact with negatively charged hydroxyl, carbonyl, ether and ketone groups dangling from the edge of sp^2-hybridized domains at pH 7.5.[131]

Compared to solid-binding peptides, cells and viruses, solid-binding proteins offer the advantages of multiple SBP insertion with positional control of placement, addition of biological functionalities (e.g., ligand binding, enzymatic activity, etc) via genetic engineering, and solubility enhancement.[86] The latter is particularly true of TrxA, a small, fast-folding, and thermostable protein that has a long history of improving the solubility of aggregation-prone fusion partners.[132, 133] Here, we found that insertion of the Car15 sequence within the active site loop of TrxA greatly compromised its ability to fold (**Figure 2.5**). Clearly, if hydrophobic sequences such as Car15 are insoluble within the context of TrxA, it is hard to imagine how they could be fully soluble as synthetic peptides and at the concentrations (typically 100 μM to 3 mM) where studies with synthetic carbon-binding peptides are often performed. However, by taking advantage of the unusual ability of TrxA to partition with periplasmic contents upon osmotic shock,[111] we were able to selectively purify the soluble (and thus properly folded) subpopulation of TrxA::Car15 conformers. The availability of this protein and that of the easily purified TrxA::Car9 allowed us to conduct a detailed analysis of the interactions of two otherwise isogenic carbon-binding proteins with various carbon surfaces.

While the high affinity of Car15 for carbon is well explained by the "classic" theory – a region of high local hydrophobicity with a π-π–hybridizing tryptophan at its core[106, 117] – that of Car9 is more likely to originate from a combination of electrostatic interactions (between arginine and lysine residues and negatively charged dangling groups) and weaker[118] π-stacking between phenylalanine and sp^2-bonded carbon rings. Such differences in adsorption mechanisms are consistent with the first order and tight binding of TrxA::Car15 to amorphous carbon relative to the sigmoidal adsorption kinetics and weaker binding that we observed with TrxA::Car9 by SPR (**Figure 2.4B**). They also account for the higher propensity of TrxA::Car9 to decorate

HOPG step edges relative to TrxA::Car15 (**Figure 2.5 and Figure 6.3**). Indeed, electrostatic interactions have been proposed to play an important role in the preferential binding of an aromatic-free peptide to the edges of graphene.[134]

These distinct adsorption modalities have important practical implications for the dispersion, functionalization and manipulation of carbon (nano)structures as well as for the selective recognition of carbon allotropes (**Figure 2.6 and 2.7**). For instance, TrxA::Car15 binds with a high degree of specificity to sp^2-hybridized carbon and is thus highly suitable for solubilizing carbon nanotubes. By contrast, the reliance of TrxA::Car9 on electrostatics for carbon binding means that although it is suitable for functionalizing both glassy carbon and diamond, it cannot stably disperse nanotubes. It will be interesting to determine if the Car9 and Car15 carbon binding peptides will be useful to achieve direct asymmetric functionalization of the ends/edges and sides/planes of carbon nanotubes and graphene nanostructures with proteins.

1.11 Conclusions

In this study, we used cell surface display to isolate a new set of carbon binding peptides and conducted a detailed characterization of two of these sequences within the context of TrxA fusion proteins. We showed that equivalent carbon binding affinities can be achieved through very different adsorption kinetics and molecular recognition mechanisms, and demonstrated a direct correlation between adsorption modality, carbon nanostructure dispersion and carbon allotrope discrimination. As our understanding of carbon-peptide interactions grows and matures, it should be possible to build designer proteins that provide full control over carbon nanostructure functionalization, manipulation and assembly towards powerful bio-enabled electronics and sensors.

1.12 Tables

Table 0.1 Physico-chemical characteristics of selected carbon binding peptides

Name	Sequence[a]	M_r (Da)	pI	Hydropathy[b]
Car9	*CGP*DSARGFKKPGKR*GPC*	1346.6	11.1	-1.900
Car14	*CGP*AGGGVVLWQAQD*GPC*	1200.3	4.3	+0.267
Car15	*CGP*RTYLPLPWMAAL*GPC*	1431.8	8.8	+0.525
Car16	*CGP*EEVRRPLGQARV*GPC*	1409.6	9.6	-1.000

[a]. Amino acids are color-coded as follows: hydrophobic, gray; acidic, red; basic, cyan; hydroxyl side chain, green; aromatic (yellow). Invariant tripeptides flanking the dodecamers are italicized.

[b]. Average hydropathy score are based on the Kyte and Doolittle scale.[1] Positive scores denote hydrophobic sequences while negative scores denote hydrophilic sequences. The higher (respectively, lower) the score, the more hydrophobic (respectively, hydrophilic) the sequence is.

1.13 Figures

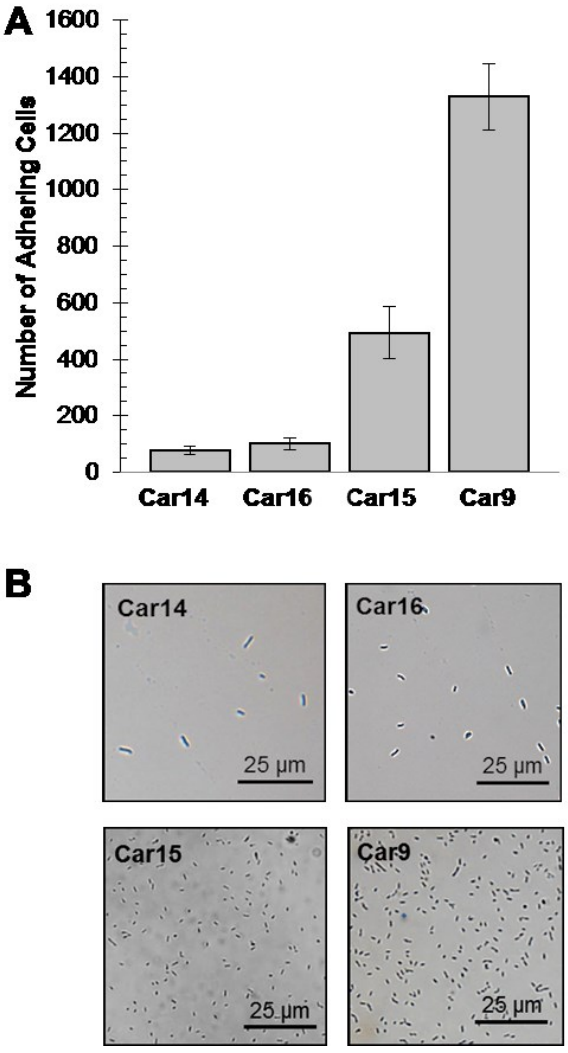

Figure 0.1 Adhesion of cells expressing different carbon-binding peptides on their flagella to carbon-coated surfaces. (A) *E. coli* GI826 cells harboring plasmids encoding the indicated FliC::Trx::Car fusions (where Car denotes a carbon binding peptide) were contacted with carbon-coated cover slips. After washing, slides were transferred to the stage of a microscope and the number of cells present in a field was counted at 500-fold magnification. Error bars were obtained for 5 different fields and two separate experiments. (B) Characteristic appearance of carbon-coated slides following incubation

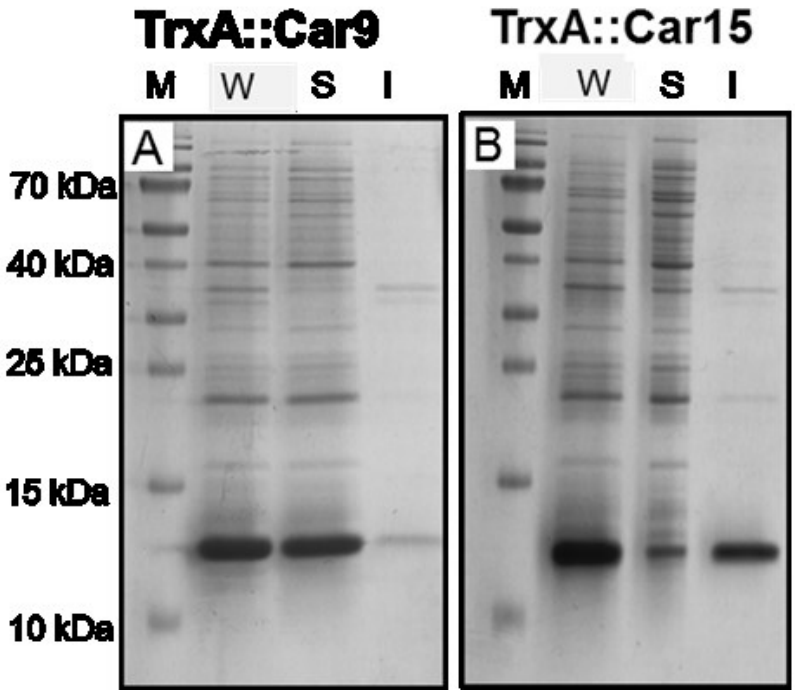

Figure 0.2 Solubility of carbon-binding TrxA derivatives. E. coli BL21(DE3) cells harboring plasmids encoding the TrxA::Car9 (A) or TrxA::Car15 (B) fusion proteins were grown, induced and harvested as described in 2.2.2. Whole cells (W) were separated into soluble (S) and insoluble (I) fractions and samples corresponding to identical amount of cells were resolved on reducing SDS minigels.

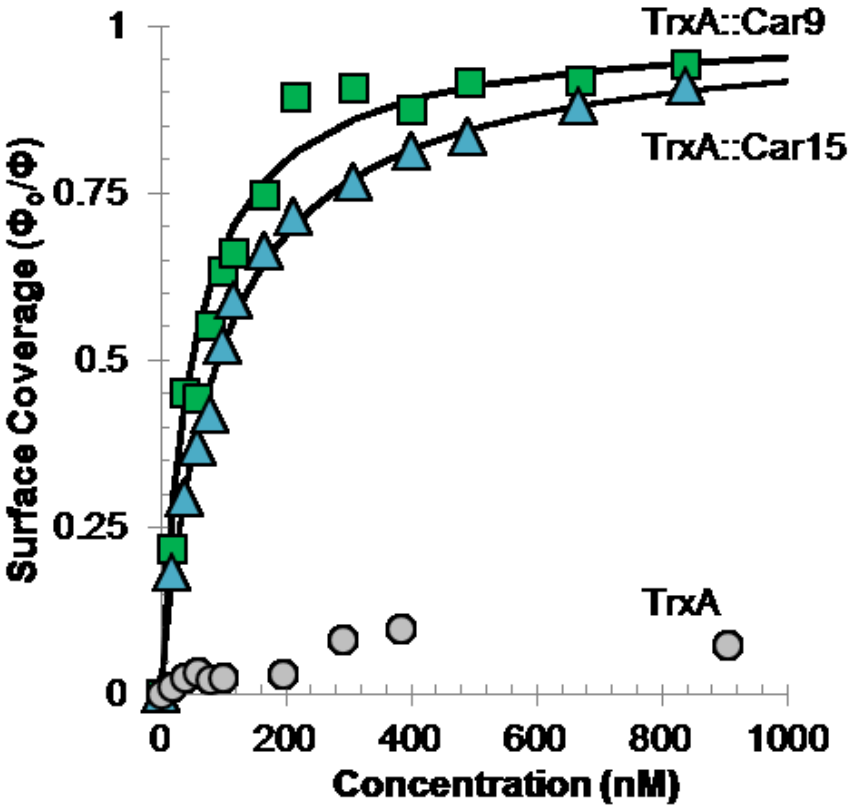

Figure 0.3 QCM analysis of the adsorption of carbon-binding TrxA derivatives to amorphous carbon. Authentic TrxA (circles), TrxA::Car9 (squares) or TrxA::Car15 variants (triangles) were incubated at the indicated concentrations on carbon-coated QCM crystals. Fractional surface coverages were determined as described in Methods. Solid lines correspond to Langmuir isotherms from which equilibrium dissociation constants were extracted.

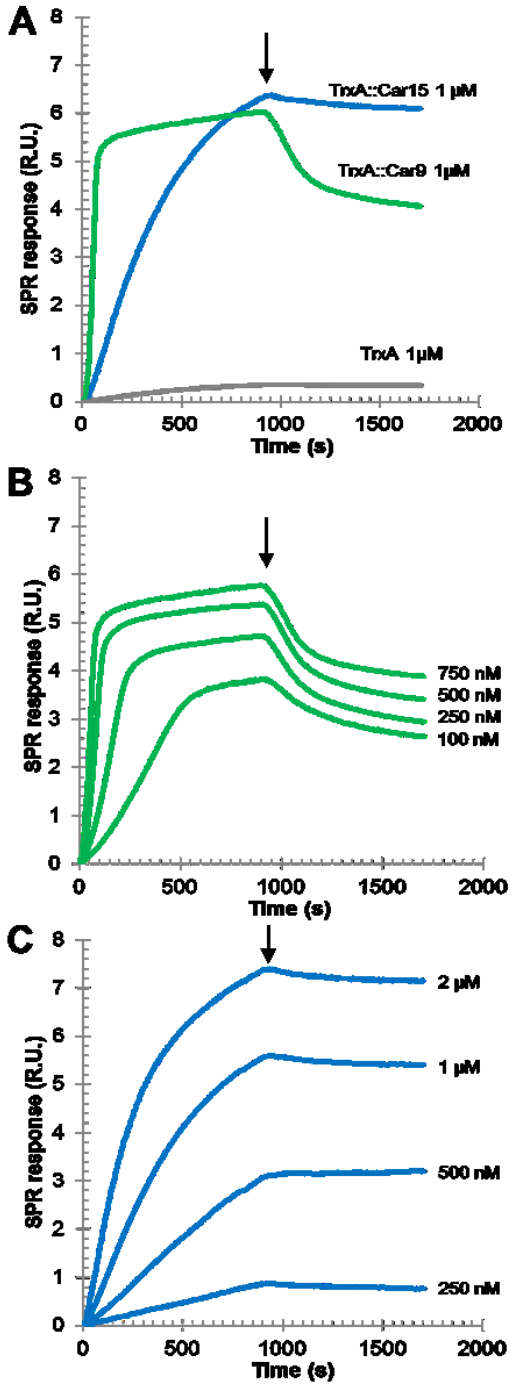

Figure 0.4 SPR analysis of the adsorption of carbon-binding TrxA derivatives to amorphous carbon. . (A) Authentic TrxA (grey), TrxA::Car9 (green) or TrxA::Car15 variants (blue) were flowed over a carbon-coated SPR chip at 1 µM concentration. Pure buffer was flowed after 15 min (arrows). Sensograms were obtained at the indicated concentrations of TrxA::Car9 (B) or TrxA::Car15 (C) for K_d calculation. See text and Chapter 6 for details.

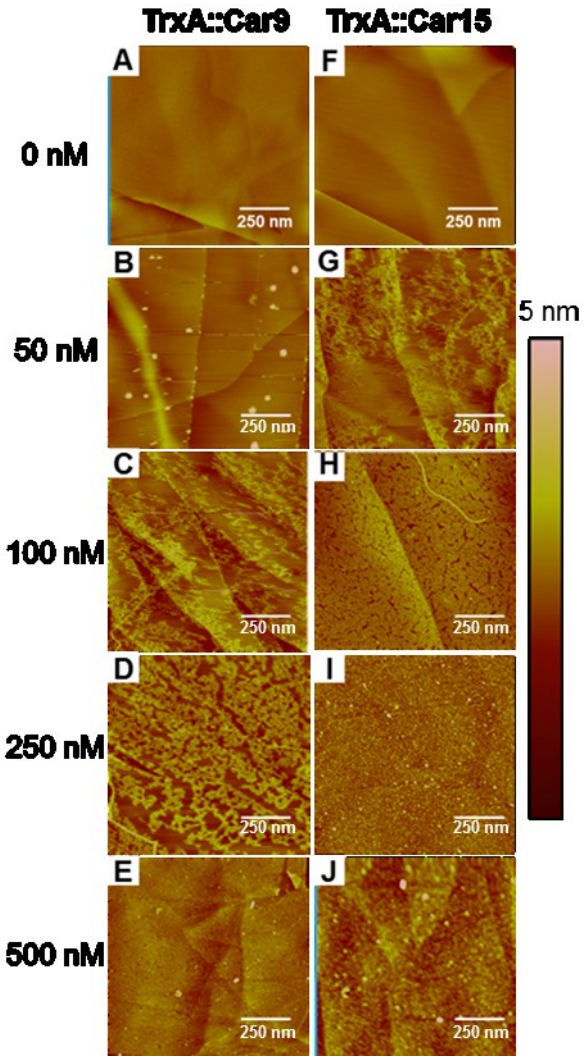

Figure 0.5 AFM analysis of the adsorption of carbon-binding TrxA derivatives to HOPG. TrxA::Car9 (A-E) or TrxA::Car15 (F-J) in 50 mM phosphate buffer and at the indicated concentrations were contacted for 10 min with freshly cleaved HOPG. Surfaces were imaged by AFM after washing and drying. The scale bar corresponds to 250 nm.

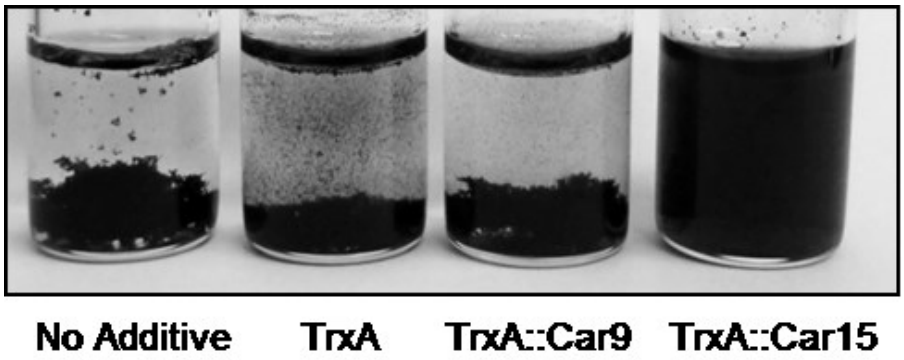

Figure 0.6 Dispersion of multi-walled carbon nanotubes by carbon-binding TrxA derivatives. MWNT (≈ 1mg) were sonicated in the absence of additive or in the presence of 2.5 μM of authentic TrxA, TrxA::Car9 or TrxA::Car15. Samples were photographed after 24h.

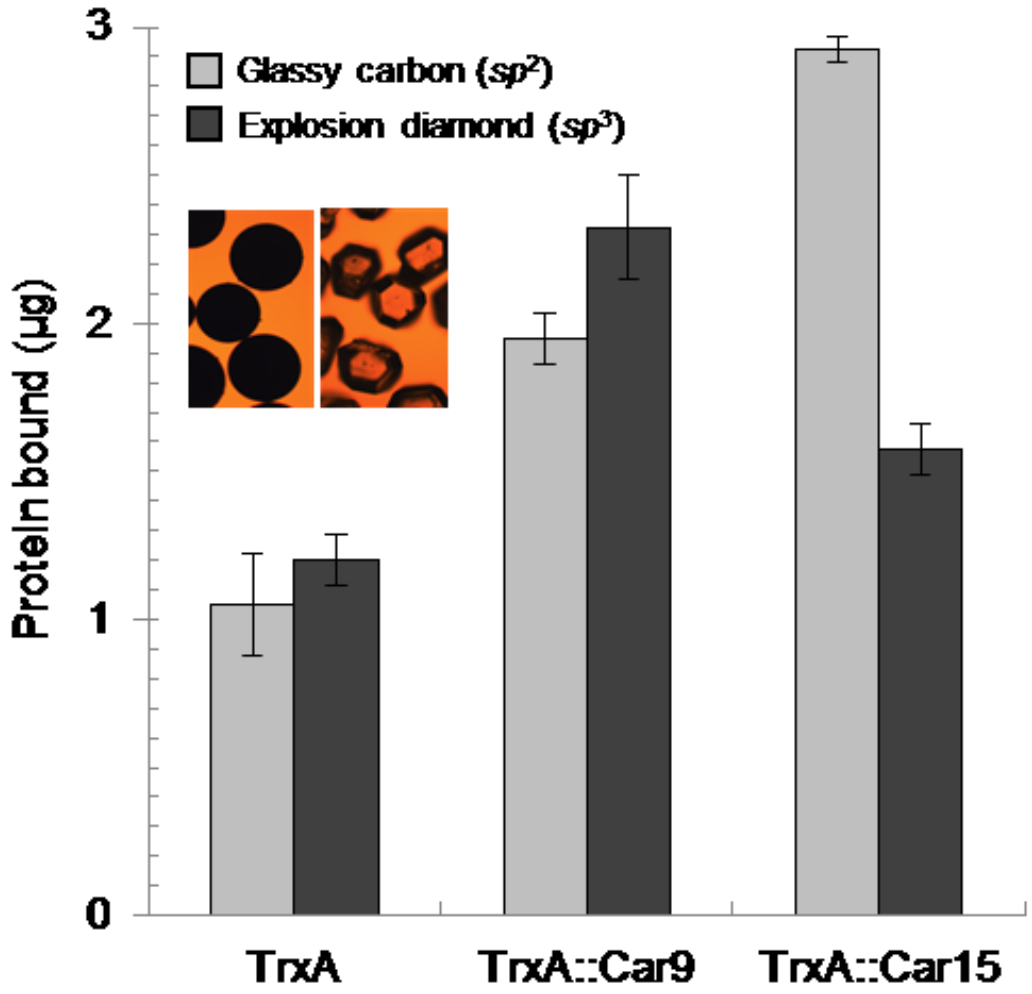

Figure 0.7 Adsorption of carbon-binding TrxA derivatives to sp2- and sp3-hybridized carbon powders. Authentic TrxA, TrxA::Car9 or TrxA::Car15 (2.5 µM) were incubated for 1h with glassy carbon or explosion diamond powders at equivalent surface areas. The amount of bound protein remaining after washing was determined by BCA assay. Insets show the appearance of the glassy carbon (left) and detonation diamond (right) powders.

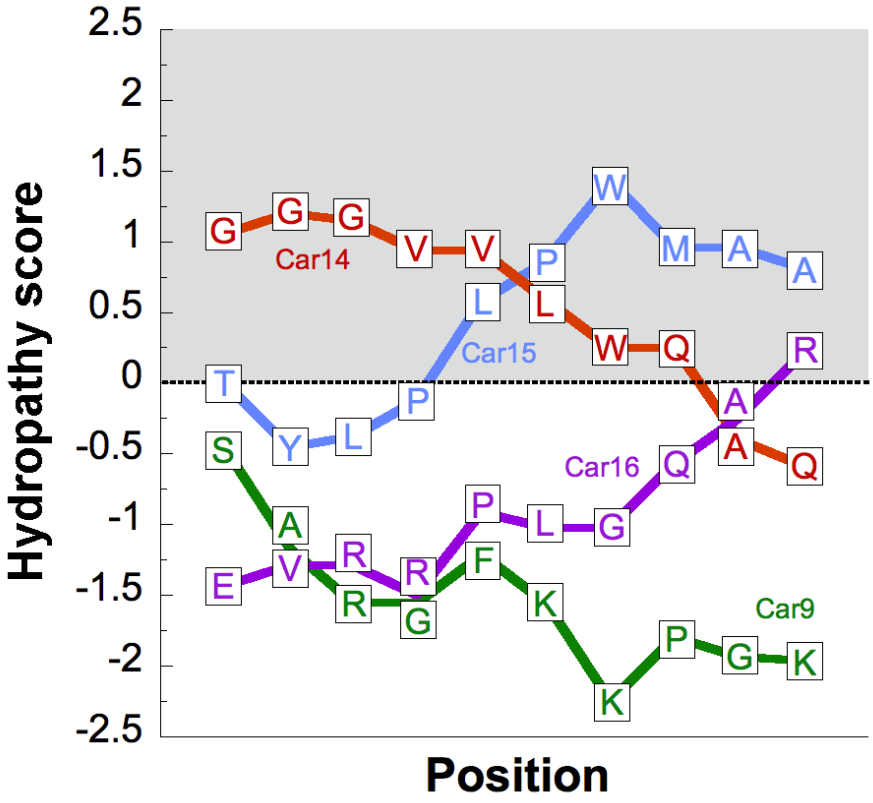

Figure 0.8 Positional dependency of the hydrophobicity in carbon-binding peptides. The local hydrophobicity of the indicated Car sequences flanked by invariant tripeptides (Table 1) was determined with the ExPASy ProtScale tool (http://web.expasy.org/protscale/) using the Kyte and Doolittle hydrophobicity scale[1] and a sliding window of 9 residues (thus, the first calculated hydropathy score is for the second residue of a Car dodecapeptide). Positive scores denote hydrophobic character.

A Cleavable Silica-Binding Affinity Tag for Rapid and Inexpensive Protein Purification

1.14 Introduction

Affinity tags have revolutionized protein purification by enabling one-step recovery of recombinant proteins from contaminating species. Tags are generally fused to the N- or C-terminus of expression targets and range in size from full-length proteins that bind with high affinity to immobilized substrates (e.g., maltose binding protein and glutathione S transferase) to short peptides recognized by immobilized antibodies or proteins (e.g., FLAG, c-myc and Streptag).[135, 136] By far, the most widely used affinity tag is the hexahistidine (His) extension which confers high affinity for transition metal ions (e.g. Ni^{2+} and Co^{2+}) immobilized on a solid support through a coordinating ligand (e.g., nitrilotriacetate; NTA).[137] While such resins are significantly cheaper than immobilized antibodies and proteins, they remain expensive. For example, the estimated cost of purifying a His-tagged protein on Ni-NTA has been estimated to be $2 per mg of purified protein.[138]

Because purification costs are primarily associated with the price of the stationary phase, and to a lesser extent with that of the eluent, the development of affinity purification schemes relying on abundant materials is desirable (**Table 7.1**). One such material is silica gel, a porous and vitreous form of SiO_2, which has been extensively used as a chemically-modifiable stationary phase for chromatography because it engenders low pressure drops and can be produced with controlled particle and pore sizes.[139] To date, however, few attempts have been made at using underivatized silica for protein purification.

Here, we show that Car9, a dodecapeptide that we previously identified for its ability to bind carbonaceous substrates,[140] exhibits micromolar affinity for silica gel. By exploiting the fact that this interaction can be disrupted by L-lysine, we develop and validate a new affinity purification scheme that supports rapid and inexpensive protein purification. We also describe a companion strategy for precise excision of Car9-based C-terminal tags.

1.15 Materials and Methods

1.15.1 DNA Manipulations and Protein Purification

Plasmid pBLN200, a pET-24a(+) (Novagen) derivative in which the T7 promoter has been replaced by a DNA segment encoding the *araC* gene and the arabinose-inducible P_{BAD} promoter was described elsewhere.[141] Plasmid pBLN200-Car9 (**Fig 7.1)** was constructed by inserting a *Hin*dIII-*XhoI* cassette encoding a GGGS linker and the Car9 dodecamer into the same sites of pBLN200. Genes encoding GFPmut2, MBP and His6-mCherry were PCR-amplified on *Nde*I-*Hin*dIII fragments and inserted into the same sites of pBLN200-Car9. Derivatives of pBLN200 encoding the wild type proteins were also built. All DNA constructions and initial expression experiments were in Top10 cells (Top10 (F^- *endA*1 *recA*1 *hsdR*17 (r^-_k,m^+_k) λ^- *supE*44 *thi*1 *gyrA*96 *relA*1 ϕ80Δ*lac*Δ*M15*Δ(*lacZYA-argF*)U169 *deo*R). Plasmids were also introduced in *E. coli* KS272 (F' Δ*lacX*74 *galE galK thi rps*L(*strA*) Δ*phoA*)[142] and in SF100 (KS272 Δ*ompT*. [143] Seed cultures (25 mL) were used to inoculate 500 mL of LB medium supplemented with 50 µg/ml kanamycin and cells were grown to $A_{600} \approx 0.5$ at 37°C. Cultures were transferred to a 25°C water bath for 10 min and protein synthesis was induced by addition of 2% L-Arabinose. Cell growth was conducted at 25°C to remain consistent with previous work. All Car9 derivatives were also grown at 37°C during expression with similar soluble protein expression

(data not shown). After 6h of cultivation at the same temperature, cells were harvested by centrifugation at 7,000*g* for 5 min, resuspended in 35 mL of 20 mM Tris-HCl pH 7.5 (Buffer A) supplemented with 2 mM EDTA, and disrupted by 6 rounds of sonication for 3 min at 30% duty cycle using a Branson sonifier. Lysates were clarified by centrifugation at 10,000*g* for 15 min. GFPmut2, MBP, and mCherry were purified to near homogeneity by ion exchange chromatography on a Whatman DE52 column. Typical concentration was 50 μM (0.67 mg/mL).

1.15.2 Characterization of Protein-Silica Interactions

The homemade Surface Plasmon Resonance (SPR) chips used in our experiments consisted of a glass substrate coated with a ≈ 2 nm titanium adhesion layer, a ≈ 48 nm evaporated gold film, and a ≈ 4 nm silicon film deposited by plasma enhanced chemical vapor deposition. Chips were cleaned by ethanol and UV-ozone treatment and mounted on a 4-channel flow cell SPR sensor from the Institute of Photonics and Electronics (Prague, Czech Republic). SPR experiments were conducted with purified TrxA, TrxA::Car9, GFPmut2 and GFPmut2-Car9 as previously described.[140]

Silica gel (60-220 μm particles with 6 nm pores) was purchased from Sigma-Aldrich. For fluorescence depletion assays, the gel was washed several times with Buffer A to remove fines and the indicated amount of settled powder was transferred to pre-weighed PCR tubes. Proteins (150 μL from 2.5 μM stock solutions) were added and the mixtures were incubated for 1h at room temperature. Supernatants were removed and the fluorescence was quantified on a Hitachi F-4500 fluorescent spectrophotometer with excitation at 488 nm and emission slit width set at 2.5 nm. Protein concentrations were quantified using a calibration curve constructed with dilutions of GFPmut2 and GFPmut2-Car9, as appropriate.

1.15.3 Tag Cleavage by OmpT

For the experiments of Fig. 5A, cultures Top10 cells harboring pBLN200-GFPmut2-Car9 were grown to $A_{600} \approx 0.5$ at 37°C in 25 mL of LB medium supplemented with 50 µg/ml kanamycin. Flasks were transferred to 25°C for 10 min and protein synthesis induced by addition of 2% L-Arabinose. After 6h, samples (3 mL) were harvested by centrifugation at 7,000*g* for 5 min, resuspended in 5 mL of Buffer A supplemented with 2 mM EDTA, and disrupted by 3 rounds of French pressing. Lysates were separated into soluble and insoluble fractions by centrifugation at 10,000*g* for 15 min. Clarified lysates were kept on ice for 30 min and subjected to methanol/chloroform extraction as described.[144] Proteins were resuspended in SDS loading buffer and samples corresponding to identical amounts of cells[145] were fractionated by gel electrophoresis. For the experiments of **Figure 3.5B**, KS272 or SF100 cells harboring pBLN200-GFPmut2-Car9 were grown and lysed as above. Unbroken cells were removed by centrifugation at 10,000 *g* for 15 min, and lysates were incubated at 0°C or 25°C for 1h. Clarification and protein precipitation was performed as above.

For the tag removal experiments of **Figure 3.6**, SF100 cells transformed or not with pML19 were grown at 37°C in 25 mL LB medium supplemented with 100 µg/mL carbenicillin. Cells were harvested after 5h of growth at 37°C and the absorbances at 600 nm (A_{600}) were normalized to OD = 3. Culture aliquots (2 mL) were washed 3 times with 50 mM sodium phosphate pH 7.5 with intervening 5000*g* centrifugation steps. After the final wash, cells were resuspended in 100 µL of 50 mM phosphate buffer pH 7.5 containing purified GFPmut2-Car9 at 10 µM final concentration. After 30 or 45 min incubation at room temperature, cells were sedimented at 5000*g*, and aliquots of the supernatants were fractionated by SDS-PAGE.

1.15.4 Purification of Tagged Proteins on Silica Gel Columns

Silica gel (3g) was washed thoroughly with Buffer A and the slurry was incubated with 5 mL of clarified cell lysate prepared as above. After overnight incubation at 8^{o}C with gentle agitation, the gel was transferred to a 1 cm inner diameter chromatography column (GE Healthcare) that was washed at 1 mL/min with buffer A until no protein was detected in the effluent (> 5 column volumes). Target proteins were eluted in ≈ 45 mL using the same flow rate of buffer A supplemented with 1 M L-lysine. Protein concentrations were determined using the BCA protein assay (Thermo Scientific) and bovine serum albumin as a standard.

1.15.5 Disposable Setup for Rapid Purification

Silica slurry (3 g; ≈ 5 mL) was loaded in the barrel of a 30 mL syringe that had been plugged with glass wool and connected to a second 30 mL syringe through a plastic 2-way valve. A perforated plastic disc was placed on top of the bed to keep the stationary phase settled. Clarified lysate (5 mL) prepared as above, were dispensed on top of the bed, the valve was opened and the fluid was aspired at a flow rate of ≈ 30 mL /min. The time between dispensing the lysate and aspiration is less than 5 seconds. When the top of the bed was reached, the valve was closed and 30 mL of Buffer A was added to the top barrel and drawn through the bed as above. The wash process was repeated 3 times for a total wash volume of 90 mL (no protein could be detected at larger wash volumes). GFPmut2-Car9 was eluted with Buffer A supplemented with 1 M L-lysine. The first 5 mL (corresponding to wash buffer) were discarded and 60 mL of elution buffer were passed through. The protein was concentrated on a 10-kDa cutoff Amicon ultra centrifugal filters (Millipore).

1.16 Results and Discussion

1.16.1 Car9 is as a Silica-Binding Peptide

Previously, we used the FliTrx cell surface display system[113] to identify disulfide-constrained dodecapeptides that discriminate between allotropes of carbon.[140] One of these binders, called Car9 (amino acid sequence DSARGFKKPGKR using the one letter code), was found to bind to graphitic materials through a combination of electrostatic interactions (between basic K and R residues and negatively-charged hydroxyl and carbonyl groups dangling from the materials' edges) and π- π interactions (between the F residue and the planar 6-carbon rings of graphene-based materials).[140] Because silica (SiO_2) surfaces are rich in hydroxyl-terminated silanol groups (**Figure 3.1A**), we hypothesized that Car9 may also function as a silica binder. As an initial test of this idea, we conducted surface plasmon resonance (SPR) experiments using TrxA::Car9, a derivative of *E. coli* thioredoxin 1 (TrxA) that specifies a disulfide-constrained Car9 sequence flanked by CGP and GCP tripeptides in place of the protein's native CGPC active site. The fusion protein along with wild type TrxA were expressed and purified as described [140] and chemical vapor deposition was used to coat surface SPR chips with a thin film of silicon that spontaneously develops an SiO_2 layer upon exposure to oxygen.[146] SPR experiments conducted at a protein concentration of 1 μM revealed that TrxA::Car9 adsorbed to these chips with rapid kinetics (**Figure 3.1B, squares**) and that more than half of this material was retained when the chip was washed with buffer to remove loosely bound material (arrow). By contrast, wild type TrxA did not appreciably bind to silica (**Figure 3.1B, circles**), unambiguously establishing that disulfide-constrained Car9 is a silica binding peptide in addition to being a carbon binder.

1.16.2 A linear version of Car9 endows GFP with silica-binding ability

Conversion of solid binding peptides from a disulfide-constrained to a linear conformation can affect their ability to bind to their cognate solids and modulate their ability to control the nucleation and growth of inorganic phases.[140, 147-151] To determine if presentation in a disulfide-bonded loop is required for Car9 to bind silica and to facilitate the construction of fusion proteins containing a C-terminal Car9 extension, we inserted a DNA cassette specifying a flexible GGGS linker and the Car9 dodecamer downstream of the arabinose-inducible P_{BAD} promoter of pBLN200[141] (**Figure 7.1**). Using this system, we appended Car9 to GFPmut2, an improved folding mutant of *A. victoria* GFP containing the S65A, V68L and S72A substitutions,[152] and purified wild type and tagged proteins by conventional ion exchange chromatography. As expected from its charged and hydrophilic nature and the fact that it is separated from its fusion partner by a flexible linker, Car9 had no deleterious effect GFPmut2 optical properties (**Figure 7.2**).

We next constructed Langmuir adsorption isotherms using silica-coated SPR chips and increasing concentrations of purified GFPmut2-Car9 or GFPmut2. Fig. 2 shows that while the parental protein had little affinity for silica (circles), GFPmut2-Car9 bound to the SiO_2 surface in a concentration dependent manner and with a calculated equilibrium dissociation constant (K_d) of 1 μM (squares). This value is identical to that reported for the interaction of His-tagged proteins and Ni-NTA-coated surfaces.[153]

To confirm the above results with a form of silica that is relevant to chromatography, a constant amount of GFPmut2-Car9 or GFPmut2 (10 μg) was incubated with increasing loads of silica gel for 1h at room temperature and the fluorescence remaining in the supernatant was quantified by spectroscopy. GFPmut2-Car9 progressively partitioned in the solid phase (**Figure**

3.3A) and nearly all of the fluorescent material was depleted from the supernatant in the presence of ≈ 35 mg of silica gel (**Figure 3.3C, squares**). By contrast, GFPmut2 adsorbed nonspecifically to the matrix and the majority of the untagged protein remained in the supernatant even when we added 5 times the amount of silica gel needed to quantitatively pull down GFPmut2-Car9 (**Figure 3.3B and 3.3C, circles**). In summary, linear Car9 is fully functional for binding to silica gel and it does so with an affinity and capacity suitable for the development of chromatography schemes.

1.16.3 L-Lysine is an Effective Eluent for Releasing Car9 Fusions from Silica Gel

Easy removal of proteins from the stationary phases to which they selectively adsorb is a prerequisite for the development of useful purification schemes. We therefore tested a number of conditions to elute GFPmut2-Car9 from silica gel. Although the tag contains 5 basic residues, neither high ionic strength buffers (5 M NaCl or 5 M $MgCl_2$), nor alkaline solutions (up to pH 10) proved effective at releasing the protein. Taken together with other studies,[154, 155] these results suggest that the binding of Car9 to silica not only involves electrostatic interactions between basic residues and silanol groups but also hydrophobic contacts between the central phenylalanine and siloxane groups (**Figure 3.1A**).

We reasoned that because Car9 specifies four lysines (a positively-charged residue whose side chain has a hydrophobic character), the free amino acid might prove useful as a competitive eluent. Indeed, incubation of silica-bound GFPmut2-Car9 with a solution of 1M L-lysine led to efficient release of functional (fluorescent) protein from the particles (**Figure 3.4A**).

To validate this strategy, clarified extracts from SF100 (Δ*ompT*; see below) cells expressing GFPmut2-Car9 were incubated with silica gel and loaded on a FPLC column that was washed at

1 mL/min with buffer to remove contaminants. Addition of 1M L-lysine to the buffer led to efficient elution of GFPmut2-Car9 with a purity of ≈ 80% (**Figure 3.4B**). To demonstrate broad applicability, we fused the Car9 tag to the C-termini of MBP and mCherry (a monomeric derivative of *Dicosoma* sp. DsRed)[156] and repeated the above experiment. These two targets could be recovered with ≈ 90% and 80% purity, respectively based on intensity analysis via ImageJ gel analysis (**Figure 3.4B**). This was completed with no attempt at optimizing loading or elution conditions.

From the above experiments, we estimate that the binding capacity of silica for Car9-tagged proteins is ≈ 4 mg per mL of settled slurry. This is comparable to the capacity of Ni-NTA for His-tagged proteins (5-10 mg per mL) and that of cross-linked amylose for MBP (7-10 mg per mL). Additionally, eluent costs compared to Ni-NTA remain relatively equal. However, at $0.10 per mg of purified protein, the cost of purifying Car9-tagged proteins on silica is more than 10 times cheaper than affinity schemes based on Ni-NTA or amylose resins.

1.16.4 The Car9 Tag is Cleaved by Outer Membrane Protease OmpT

During initial expression and purification experiments in Top10 cells, we noticed the appearance of two large fragments of GFPmut2-Car9 degradation when soluble cell extracts were held on ice (**Figure 3.5A**, lane S, black arrows). There was no GFPmut2 degradation under the same conditions (**Figure 7.3**) and GFPmut2-Car9 remained intact in undisrupted cells or when deposited into inclusion bodies (**Figure 3.5A**, lanes WC and I, respectively). These results suggested that a cell envelope-associated protease was recognizing the tag at two different positions. Because fusion of the linker-Car9 region to GFPmut2 introduces an Lys-Lys dipeptide at the fusion joint, and because the tag itself contains an internal Lys-Lys as well as a C-terminal

Lys-Arg sequence (**Figure 3.5C**), we suspected the involvement OmpT, an aspartate outer membrane protease specific for paired basic residues.[157] To test this hypothesis, we introduced the plasmid encoding GFPmut2-Car9 into KS272 and SF100, two isogenic strains containing intact and null *ompT* alleles, respectively. As expected, the extracts of *ompT*$^{+}$ cells contained the expected degradation products after 1h incubation on ice (**Figure 3.5B**, black arrows). Furthermore, conversion of the high molecular mass degradation product into the smaller species was accelerated when extracts were held at 25^{o}C. By contrast, there was no detectable proteolysis of GFPmut2-Car9 when extracts of Δ*ompT* (SF100) cells were incubated at the same temperature, firmly establishing OmpT as the protease responsible for the cleavage of the Car9 extension. Furthermore, GFPmut2-Car9 extracts from SK272 and SF100 were allowed to sit on ice for 24 hours and then added to silica gel to monitor absorption of the proteins. The GFPmut2-Car9 extract from SF100 cells bound to the silica gel as expected, while the GFPmut2-Car9 extract from KS272 cells did not adhere to the silica gel based on fluorescence (**Figure 7.4**).

1.16.5 Removing the Affinity Tag with Whole Cells that Overexpress OmpT

The removal of affinity tags might be desirable if they interfere with biological function or contribute to immunogenicity. This is generally accomplished by engineering the recognition sequence of an endoprotease between affinity tag and fusion partner and making use of the corresponding immobilized or affinity-tagged protease to cleave off the extension.[158] While proteases such as thrombin, tobacco etch virus (TEV) protease and enteropeptidase produce nearly native products when their recognition sequence is specified between a N-terminal affinity tag and the N-terminus of a target protein, they are not as effective at precise excision of C-

terminal affinity tags owing to the fact that the protease specificity determinants are located on the N-terminal side of the cleavage site.[158]

The involvement of OmpT in the processing of the linker-Car9 extension suggested that this protease might be useful within the context of intact cells to inexpensively remove the affinity tag and yield a protein with a native C-terminus (**Figure 3.5C**). To test this idea, SF100 cells transformed or not with pML19 (a pUC derivative that encodes OmpT;[159, 160] were incubated at room temperature with purified GFPmut2-Car9 as described in Materials and Methods. The cells were sedimented by low speed centrifugation and aliquots of the supernatants were subjected to electrophoresis. **Figure 3.6** shows that while the fusion protein remained intact when placed in contact with Δ*ompT* cells (gray arrows), it was converted into its expected degradation products after 30 min of incubation with OmpT-overproducing cells. In addition, tag-free GFPmut2 was the dominant product after 15 additional minutes of incubation (bottom arrow). The samples also contained a small amount of high molecular weight contaminants that were not seen when incubation was conducted with Δ*ompT* cells. These bands likely correspond to host proteins released from SF100 cells that are fragilized or lysed due to OmpT overproduction. The problem should be easy to address by using a different strain and/or adjusting incubation time and temperature.

Overall, our results indicate that the C-terminal linker-Car9 extension is accessible to OmpT and that cells expressing this protease on their surface can be used as an inexpensive reagent to cleave linker and affinity tag in order to produce a properly terminated GFPmut2.

1.16.6 Rapid Purification of Car9-Tagged Proteins

Silica matrices tolerate high pressure drops and have been used for ultrafast (*a.k.a.* Flash) purification of organic species using a scheme in which the mobile phase is driven at high flow rate through the column by applied air pressure.[161] To determine if a similar approach could be used for the rapid purification of Car9-tagged proteins using a disposable setup, we connected two plastic syringes to a control valve and placed washed silica gel above glass wool in the top barrel (**Figure 3.7A**). We next added clarified extract from GFPmut-Car9 producing cells, aspired it through the bed by pulling the piston of the bottom syringe and washed the gel with buffer. Finally, we eluted bound protein by vacuum aspiration of buffer supplemented with L-lysine. This procedure yielded 85% pure GFPmut-Car9 (**Figure 3.7B**). Remarkably, by performing all fluid handling steps at a flow rate of ≈30 mL/min, it was possible to go from clarified extract to pure protein (≈ 0.5 mg/mL) in less than 15 minutes.

1.17 Conclusion

From DNA miniprep kits to next-generation sequencing, rapid and inexpensive methods that simplify formerly complex tasks have revolutionized the practice of life sciences. Protein purification is only halfway there: although affinity tags[135, 136] have transformed what used to be a time-consuming series of chromatography steps into a single-stage process (albeit with some loss of purity), affinity purification remains expensive. Here, we described and validated a new affinity tag and elution conditions for protein purification on unmodified silica. We also demonstrated a disposable companion system that allows for the purification of Car9-tagged proteins from crude cell extracts in a matter of minutes. Finally, we showed that the susceptibility of the linker-Car9 region to proteolysis by outer membrane protease OmpT can be

exploited to remove the C-terminal extension and produce GFPmut2 with a native C-terminus due to the terminal lysine residue and the subsequent lysine residue in the Car9 linker.

In addition to enabling rapid protein purification at the lab scale and inexpensive protein production at the large scale, we anticipate that the strategy described herein will also prove useful for multiplex protein purification using vacuum manifolds. The use of OmpT overproducing cells to remove Car9 extensions should also be applicable to other targets. This will yield proteins that are terminated with a lysine or arginine, but also free of the longer extensions generated by other endoproteases when digesting C-terminal affinity tags. Clearly, the success of the approach will also depend on the absence of other accessible OmpT sites on the target protein.

Even though we have yet to optimize the system, we estimate that the Car9-tag/silica/lysine approach is at least 10-times cheaper than the use of His-tag/Ni-NTA/imidazole. The availability of such a low-cost purification technique should be instrumental in ushering a new era of green manufacturing where functional hybrid materials and systems are fabricated with proteins.[162]

1.18 Figures

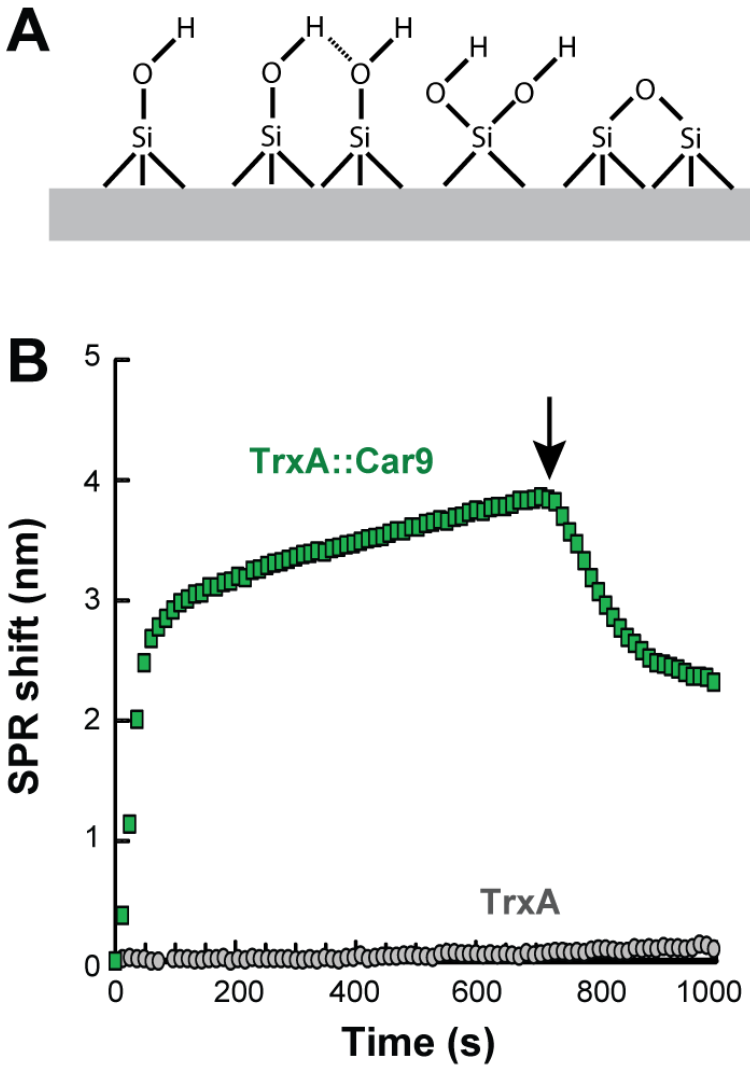

Figure 0.1 Disuflide-constrained Car9 tag binds to silica. (**A**) Surface chemistry of silica. From left to right: free silanol, hydrogen-bonded silanol, germinal silanol, and siloxane (**B**) Surface plasmon resonance (SPR) sensogram of the adsorption of wild type TrxA and TrxA::Car9 on silica chips at 1 μM concentration. The arrow indicates the start of the wash step.

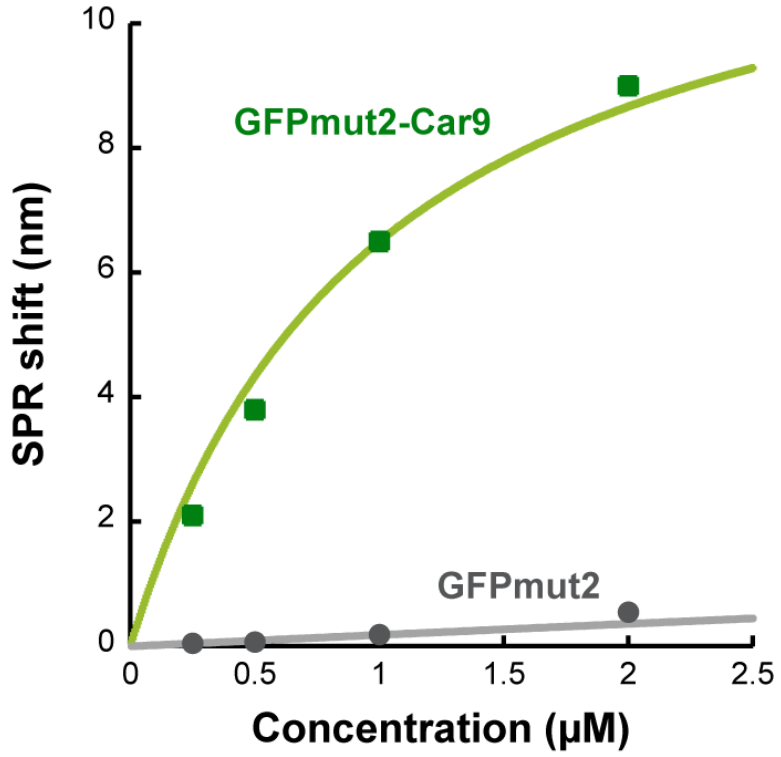

Figure 0.2 Langmuir adsorption isotherms of purified GFPmut2-Car9 and GFPmut2 on silica as determined by SPR experiments conducted at the indicated protein concentrations.

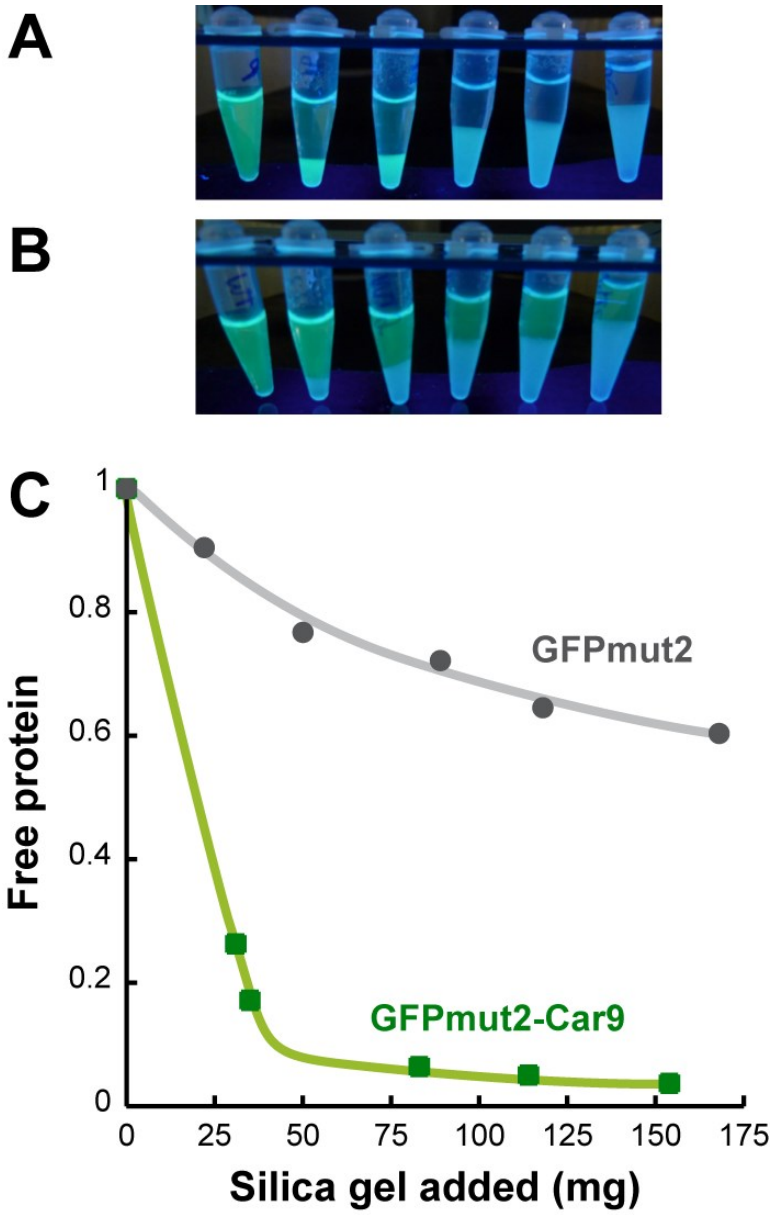

Figure 0.3 Adsorption of GFPmut2 and GFPmut2-Car9 to silica gel. (**A**) GFPmut2-Car9 (2.5 μM) was incubated with increasing amounts of silica and tubes were photographed under UV light. (**B**) As in panel A using 2.5 μM GFPmut2. (**C**) The binding of GFPmut2 and GFPmut2-Car9 to silica gel was quantified by measuring the fluorescence remaining in the supernatant. Fluorescence is normalized to an arbitrary value of 1 in the absence of silica.

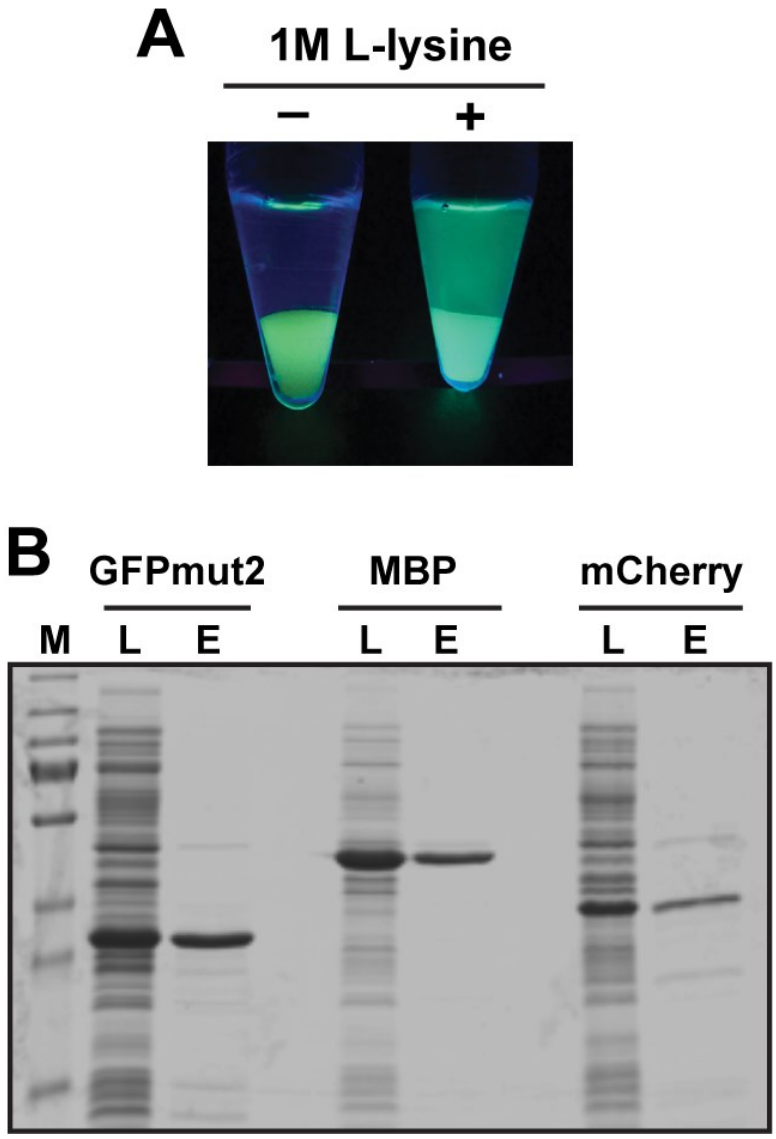

Figure 0.4 Eluting Car9-tagged proteins with L-lysine. **(A)** Release of GFPmut2-Car9 from silica gel upon incubation with 1M L-lysine. **(B)** SDS-PAGE analysis of clarified lysates (L) and lysine-eluted (E) fractions from cells producing GFPmut2-Car9, MBP-Car9 and mCherry-Car9

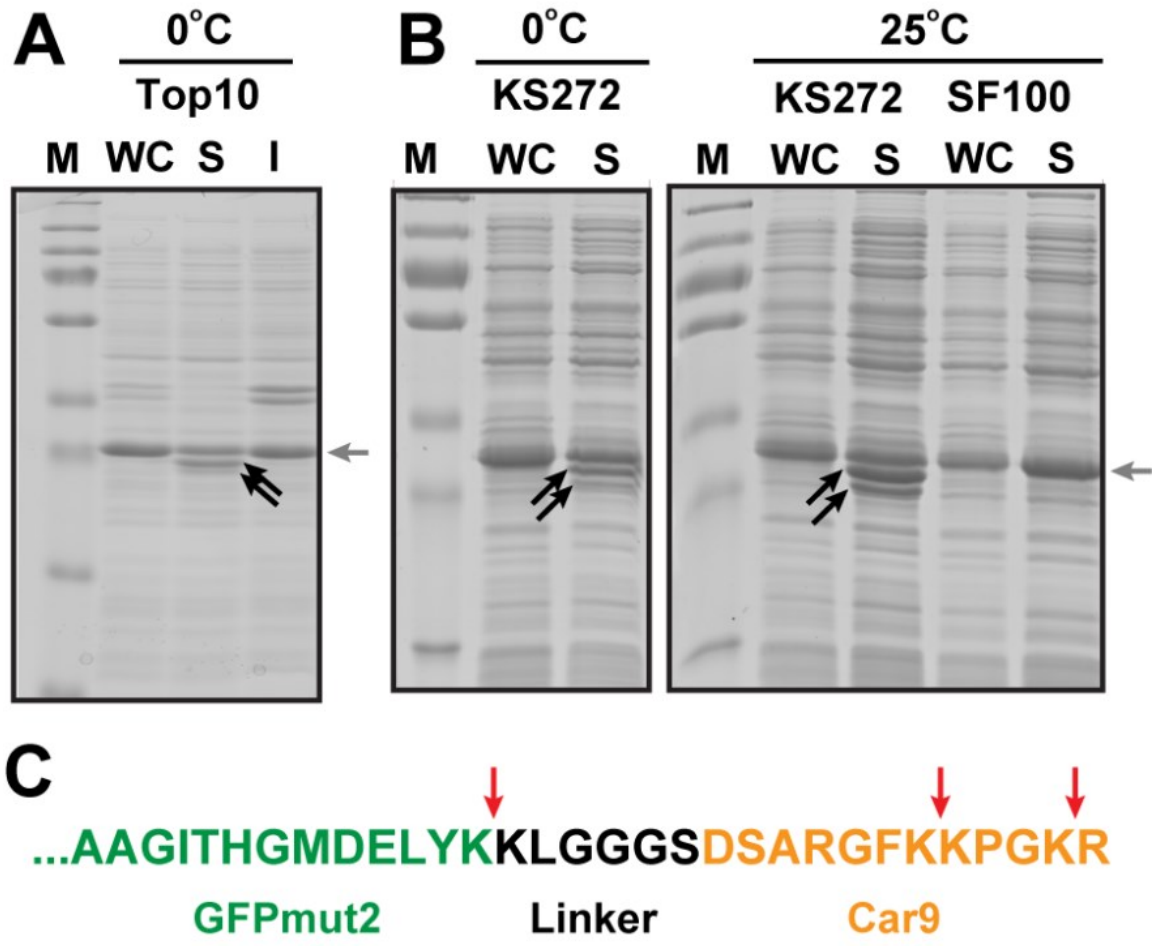

Figure 0.5 The linker-Car9 extension is susceptible to cleavage by OmpT. (A) Top10 (ompT+) cells expressing GFPmut2-Car9 were left unbroken (WC) or disrupted by sonication and centrifuged at 10,000 g to produce soluble (S) and insoluble (I) fractions. Gray arrows show the migration position of intact GFPmut2-Car9, black arrows that of the degradation products. (B) KS272 (ompT+) or SF100 (□ompT) cells expressing GFPmut2-Car9 were left unbroken (WC) or disrupted by sonication and subjected to centrifugation to produce soluble (S) fractions. Proteins were fractionated after 1h incubation at 0°C or 25°C, as indicated. (C) Amino acid sequence at the C-terminal end of GFPmut2-Car9. Regions corresponding to wild type GFPmut2, linker and Car9 sequence are colored and labeled. Arrows show the position of OmpT cleavage sites.

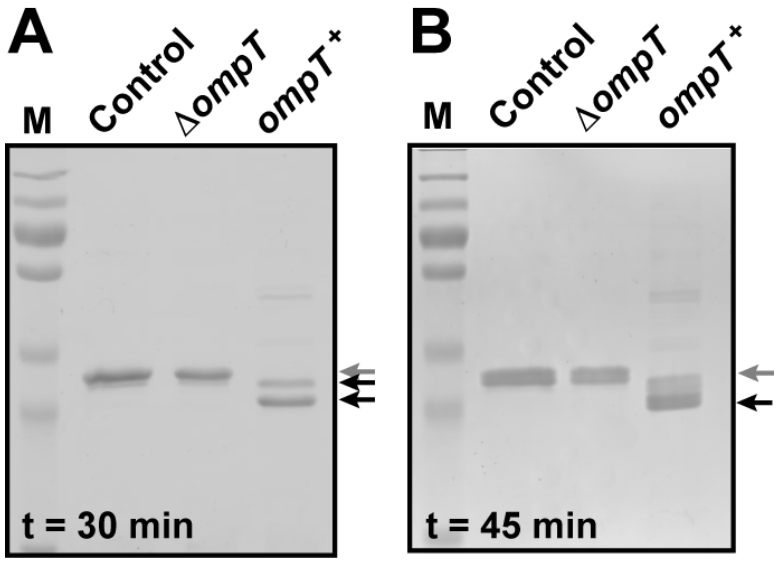

Figure 0.6 Cleaving the linker-Car9 extension of GFPmut2-Car9 with OmpT-producing cells. Purified GFPmut2-Car9 (Control) was incubated with whole cells lacking (Δ*ompT*) or overproducing OmpT (*ompT*$^{+}$). Soluble proteins were fractionated after 30 or 45 min of incubation and removal of the cells.

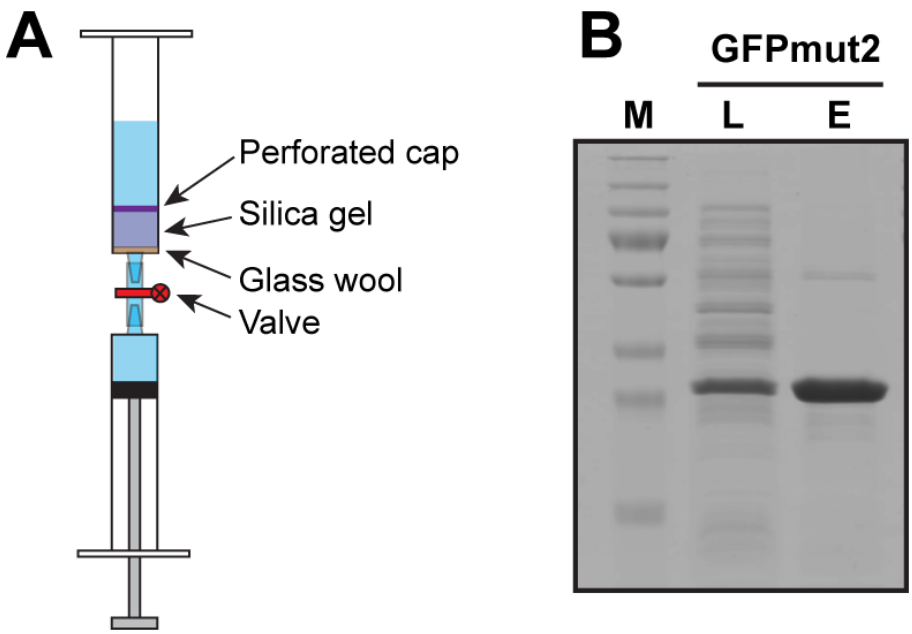

Figure 0.7 Rapid purification of Car9-tagged proteins with a disposable device. (**A**) Schematic representation of the device (**B**) SDS-PAGE analysis of clarified lysate from cells producing GFPmut2-Car9 before loading (L) and after lysine elution (E)

Dual fluorescent, site-specific labeling of carbon nanotubes by protein affinity tags

1.19 Introduction

Carbon nanotubes (CNTs) have been extensively studied due to their extraordinary electronic and thermal properties.[33-37, 50, 163] In biotechnology, these properties can be exploited for the design of new biosensors and drug delivery systems, among other technologies.[163-170] Unfortunately, CNTs are highly hydrophobic and exhibit very poor solubility in water. To overcome this issue, they have been functionalized with biomolecules and various functional groups through chemistries involving both covalent and non-covalent interactions. Conjugating proteins to the CNT surface through covalent interaction requires modification of the sp^2 carbon network to create carboxylic acid groups that can used to create covalent linkages. Creating these carboxylic groups requires treatment with HNO_3/H_2SO_4 or H_2O_2 solutions, but disrupts the integrity of the carbon lattice that is responsible for the electronic and thermal conductance.[58, 59, 73] In addition to the disruption of the carbon lattice, the proteins are often bound in random orientations that can restrict the mobility of the protein or block access to the active site. Both of these issues will reduce protein activity. These issues are similar to those that arise from using silane chemistries as discussed in Chapter 3. Therefore, non-covalent functionalization is rapidly becoming the preferred method for CNT biofunctionalization to retain the underlying integrity of the CNTs.

Non-covalent protein functionalization can also cause a loss in protein activity. Non-covalent interactions can mean proteins that adsorb non-specifically to graphitic nanostructures

[64, 74, 75] or bind only after treatment of the CNTs with polymers, detergents, or esters;[76-78] which allow proteins to adhere as a secondary layer coating graphitic nanostructures. Additionally, often the orientation of the protein is not controlled which can reduce the activity simply by limiting / blocking / reducing access to the active site. While the modifications significantly increase the water solubility without disrupting the CNTs structure, the reduction in protein activity can render them useless for applications such as sensor design that require the activity of the attached protein. For example, Karajanagi *et al* found that α-chymotrypsin lost 99% of its soluble activity when used to coat CNTs that had been sonically separated in dimethylformamide, while soybean peroxidase (SBP) retained 3-28% enzyme activity depending on enzyme loading.[79] Fourier-transform infrared (FTIR) spectroscopy revealed that α-chymotrypsin was unfolded while SBP retained most of its secondary structure, which illustrates that the noncovalent interaction can disrupt protein structure, but even if the secondary structure is maintained, orientation also plays a large role.

In this chapter, we construct and characterize two fluorescent proteins modified with affinity tags that bind to the walls (sp^2-hybridized) or ends (hydroxyl- and ketone-terminated) of CNTs. We demonstrate that these proteins can be used in combination for the dispersion and spatially-controlled labeling of CNTs. From carbon nanostructure manipulation and assembly to the creation of multifunctional CNTs, our results open the door to a broad range of applications that require precision-labeling and solubilization of these promising materials.

1.20 Materials and methods

1.20.1 DNA Manipulations and Protein Purification

Plasmid pBLN200, a pET-24a(+) (Novagen) derivative in which the T7 promoter was replaced by a DNA segment encoding the *araC* gene and the arabinose-inducible P_{BAD} promoter was described elsewhere.[141] Plasmid pBLN200-Car15 was constructed by inserting a *Hin*dIII-*XhoI* cassette encoding a GGGS linker and the linear Car15 dodecamer (RTYLPLPWMAAL) into the same sites of pBLN200. Genes encoding GFPmut2 and sfGFP were PCR-amplified on *Nde*I-*Hin*dIII fragments and inserted into the same sites of pBLN200-Car15. Derivatives of pBLN200 encoding wild type proteins were also built. All DNA constructions and initial expression experiments were conducted in Top10 cells (Top10 (F^- *endA*1 *recA*1 *hsdR*17 (r^-_k,m^+_k) λ^- *supE*44 *thi*1 *gyrA*96 *relA*1 ϕ80Δ*lac*Δ*M15*Δ(*lacZYA-argF*)U169 *deo*R). Plasmids were introduced in *E. coli* KS272 (F' Δ*lacX*74 *galE galK thi rps*L(*strA*) Δ*phoA*) [142] and SF100 (KS272 Δ*ompT,*[143] as indicated. Seed cultures (25 mL) were used to inoculate 500 mL of LB medium supplemented with 50 μg/ml kanamycin and cells were grown to $A_{600} \approx 0.5$ at 37°C. Cultures were transferred to a 25°C water bath for 10 min and protein synthesis was induced by addition of 2% L-Arabinose. After 6h of cultivation at 25°C, cells were harvested by centrifugation at 7,000*g* for 5 min, resuspended in 35 mL of 20 mM Tris-HCl pH 7.5 (Buffer A) supplemented with 2 mM EDTA, and disrupted by 6 rounds of sonication for 3 min at 30% duty cycle using a Branson sonifier. Lysates were clarified by centrifugation at 10,000*g* for 15 min. Clarified lysate of GFPmut2-Car15 was purified to near homogeneity by ion exchange chromatography on a Whatman DE52 column followed by size-exclusion chromatography. The sfGFP-Car15 lysate was immersed in a water bath at 80°C for 15 min and clarified by centrifugation at 14,000 *g* for 15 min. The clarified lysate was purified to near homogeneity by ion exchange chromatography

on a Whatman DE52 column. After dialysis against 50 mM sodium phosphate buffer pH 7.5, proteins were aliquoted at a 10 μM final concentration and stored at -20°C. Purified GFPmut2-Car9 and mCherry-Car9 were obtained as described in Chapter 3.

1.20.2 Characterization of Protein-Carbon Interactions

Glassy carbon (200-400 μm) spherical powder and explosion diamond powder (210-250 μm) were purchased from SPI Supplies. Multi-walled carbon nanotubes (MWNT; 6-9 nm × 5 μm) synthesized by catalytic chemical vapor deposition were purchased from Sigma-Aldrich. For carbon allotrope discrimination experiments, glassy carbon and diamond powders were transferred to a 25 mL glass vial, washed with acetone, methanol and ddH_2O, and subjected to three additional wash cycles in 50 mM sodium phosphate buffer, pH 7.5. Wet powders were transferred to microcentrifuge tubes to reach equivalent surface areas based on mass and average particle size (determined by microscopy analysis). The appropriate proteins (250 μL from a 2.5 μM solution) were added and mixtures were incubated for 1h at room temperature. The supernatant was removed and analyzed in a Hitachi F4500 fluorescent spectrophotometer. With excitation λ = 473 nm and emission measured at λ = 510 nm. Protein concentrations in the supernatant were determined by comparison to standard curves created through purified protein at known concentration.

The glassy carbon and diamond beads were then examined on a laser scanning confocal microscope. After incubation, beads were deposited onto a polyethylene glycol (PEG) coated glass slide. The PEG layer prevents any nonspecific adhesion of the protein to the glass substrate. Single beads were focused in visible mode and fluorescence at the edge of the beads was measured.

To test for activity at sp^2 carbon substrates, purified GFPmut2-Car15 and sfGFP-Car15 were incubated on a freshly cleaved highly ordered pyrolytic graphite (HOPG) surface. 100 μL solution at 1 μM concentration were incubated for 5 min on the HOPG substrate before washing by immersion in large excess of 50 mM phosphate buffer pH 7.5. The HOPG substrate was washed 3 times for 30 seconds each to remove any protein not bound to the HOPG substrate. The sample was then imaged on a Typhoon 9000 gel image scanner with a 475 nm excitation laser and a 510 nm lowpass cutoff filter.

1.20.3 Carbon nanotube resuspension

For multiwalled carbon nanotube (MWNT) resuspension experiments, ≈ 1 mg of material was added to a glass vial containing 2.7 mL of 50 mM phosphate buffer pH 7.5. These solutions were sonicated for 1.5 minutes before adding 300 μL of 10 μM of the designated protein for a final concentration in solution of 1 μM final concentration and sonicated for an additional 1.5 minutes. Mixtures were cooled by immersion in a mixture of EtOH and ice. The sonication was performed using a micro-tipped sonicator at 12W and 100% duty cycle (Branson Sonifier 450). In the cases where mCherry-Car9 was added (0.5 μM), the sonication is repeated for 3 minutes at the same conditions as above. Carbon nanotube suspensions could be centrifuged at 14,000 g for 15 minutes to remove larger aggregates of CNTs or used as sonicated. For samples that were analyzed on the microscope, samples from the supernatant were diluted 4x with 50 mM phosphate buffer pH 7.5. 10 μL of this solution was deposited on a glass microscope slide and examined via fluorescent microscopy at 90x magnification with appropriate excitation for GFPmut2-Car15 (λ = 473 nm) and mCherry-Car9 (λ = 587 nm).

1.21 Results and Discussion

1.21.1 Linearization of the Car9 and Car15 tags does not preclude carbon-binding

The Car9 and Car15 tags used in this study were described in Chapter 2[171] and used within the context of a disulfide-bonded loop inserted within the active site of *E. coli* TrxA.. In Chapter 3, we showed that a linear version of Car 9 fused to the C-terminus of GFPmut2 was capable of binding to silica, providing evidence for tag accessibility and suggesting that linear Car9 should also remain capable of binding to carbon. However, whether linear Car15 retains carbon-binding affinity remains to be determined.

To this end, we fused Car15 to the C-terminus of GFPmut2 via a flexible linker, purified the GFPmut2-Car9 and GFPmut2-Car15 fusion proteins, and evaluated their ability to bind to diamond and glassy carbon substrates, essentially as described in Chapter 3. Briefly, 10 µg of GFPmut2, GFPmut2-Car9, GFPmut2-Car15 was incubated with increasing amounts of glassy carbon or diamond beads for 1h at room temperature. However, rather than measuring how much protein was bound to the beads, we quantified the fluorescence remaining in the supernatant by spectroscopy. Results were similar to those obtained with TrxA::Car15 and TrxA::Car9 (**Figure 2.7**): GFPmut2 had little affinity for either material (**Figure 4.1A**), GFPmut2-Car9 bound equally well to either substrate **(Figure 4.1B**), and GFPmut2-Car15 adhered selectively to glassy carbon beads (**Figure 4.1C**). We conclude that the tags can be ported to different protein frameworks and that the linear versions of Car9 and Car15 retain the carbon binding affinity and allotrope specificity of their disulfide-constrained versions.

1.21.2 Protein stability determines function at carbon interfaces

An important parameter in protein immobilization is retention of biological activity. In the case of transparent silica substrates, visual inspection was sufficient to confirm that GFPmut2-Car9 remained fluorescent, and thus active, upon adsorption to silica gel or surfaces (**Figure 3.2A**). A similar approach is however not possible with opaque carbon substrates. We therefore used confocal microscopy to determine if GFPmut2-Car9 and GFPmut2-Car15 would remain fluorescent upon binding to sp^3-hybridized detonation diamond powder and sp^2-bonded glassy carbon. For these experiments, productive immobilization with retention of activity should be indicated by a decrease in background fluorescence and a sharp signal at the carbon-solvent interface in a confocal slice. Accordingly, wild type GFPmut2, which should only adsorb nonspecifically to either diamond or glassy carbon (**Figure 4.1A**), did not accumulate at interfaces (**Figure 4.2A-B**) or became significantly depleted from solution (compare the background fluorescence of **Figure 4.2A-B** to that of **Figure 4.2C**).

Diamond is fairly hydrophobic and terminated with carboxylate and other CO-containing groups.[172, 173] Because this surface chemistry is comparable to that of silica, we were not surprised to see efficient adsorption of GFPmut2-Car9 to diamond beads and complete disappearance of the background fluorescence (**Figure 4.2A**). On the other hand, while GFPmut2-Car15 was also detected at the solid-liquid interface, the solvent retained some fluorescence. This is fully consistent with the fact that, at a given protein concentration, much less GFPmut2-Car15 than GFPmut2-Car9 binds to diamond (**Figure 4.1B-C**). When the experiment was repeated with glassy carbon beads, we observed a significant amount of solvent fluorescence in the case of GFPmut2 but complete depletion of background fluorescence for either GFPmut2-Car9 or GFPmut2-Car15 (**Figure 4.2**). These results are well explained by the

quantitative adsorption of tagged proteins to glassy carbon beads since both Car9 and Car15 confer GFPmut2 high affinity for sp^2-hybridized surfaces (by contrast, the wild type protein only binds glassy carbon nonspecifically; **Figure 4.1**). The lack of interfacial fluorescence was more surprising and can be attributed to fluorescence quenching (glassy carbon quenches fluorescein emission)[174] or to protein unfolding at the hydrophobic glassy carbon-buffer interface.

To distinguish between these two possibilities, we fused the Car9 and Car15 tags to sfGFP, a variant of GFP containing GFPmut2 mutations (F64L, S65T) and GFP cycle3 mutations (F99S, M153T, V163A) in addition to new mutations (F64L, S65T, S30R, Y39N, N105T, Y145F, I171V, and A206V) that significantly enhance its stability and resistance to chemical denaturation.[175] Indeed, sfGFP derivatives to which Car9 or Car15 tags had been appended remained fluorescent and soluble when crude cell extracts were heated at 80 ^{o}C, allowing for their rapid purification from contaminating proteins. We then examined the fluorescence of GFPmut2-Car15 and sfGFP-Car15 bound to highly-oriented pyrolytic graphite (HOPG), a substrate composed of mostly sp^2 carbon bonds (**Figure 4.3A**). While we did not see a complete loss of fluorescence on HOPG, we believe this is due to the inherently kinetic nature of the fluorescence loss through protein denaturation and believe that with longer incubation times we would see complete loss of fluorescence of the GPFmut2-Car15. These results coincide with previous work on glassy carbon (**Figure 4.2B**). However when examining sfGFP-Car15, we observe a much higher fluorescence at the substrate surface. This can be directly compared to the GFPmut2-Car15 as the 2 proteins share similar emission amplitudes at equal concentration. These results correlate our theory that the loss of fluorescence is manifested through a subtle alteration in the structure of the β-barrel that encases the GFP chromophore since sfGFP-Car15,

which is nearly identical to, but more stable than GFPmut2-Car15, remains fluorescent when bound to carbon surfaces (**Figure 4.3B**)

4.3.4 Implications for the stability of CNT colloidal suspensions

We previously demonstrated that TrxA::Car15, but not TrxA::Car9, was suitable for dispersing CNTs in aqueous solvents (Chapter 2). To determine if proteins modified with linear version of the tag would behave in a similar fashion, we repeated the experiment of **Figure 2.6** with GFPmut2, GFmut2-Car9, GFPmut2-Car15, sfGFP, sfGFP-Car9, and sfGFP-Car15. Results (**Figure 4.3**) confirmed that only GFPmut2-Car15L and sfGFP-Car15 were suitable for CNT solubilization, and Car9 variants were still unable to solubilize CNTs. However, whereas TrxA::Car15-solubilized CNTs precipitated out of solution after about 2 days incubation at room temperature, colloidal suspensions made with GFPmut2-Car15 were stable for over a month. Remarkably, solutions of sfGFP-Car15-dispersed CNTs were stable for more than a year after they had been prepared. Thus, just like fluorescence loss, the colloidal stability of CNTs dispersed using Car15-tagged proteins is determined by the structural stability of these proteins. In view of the fact more than a month is required for GFPmut2-Car15-stabilized CNT to precipitate but that fluorescence is lost quickly upon the adsorption of the same protein to glassy carbon, is likely that progressive accumulation of local unfolding events eventually lead to significant unfolding, and that exposure of the protein's hydrophobic core drives aggregation reactions between nanotubes.

1.21.3 Selective labeling of the side wall and ends of carbon nanotubes

One of the challenges associated with the production of CNT-based devices is the difficulty of accurately controlling their position during part-to-part assembly. Because the side-walls of CNTs consist of sp^2-hybridized carbon while their ends are carboxylated, we reasoned that it might be possible to selectively bind these features using Car15- and Car9-tagged proteins. Indeed, when SWNT were solubilized by sonication in the presence of 1 μM sfGFP-Car15 and further incubated with 0.5 μM mCherry-Car9, the former protein efficiently decorated the sides of the nanotubes (**Figure 4.5A**) while fluorescence corresponding to mCherry emission was only detected in punctuated areas (**Figure 4.5B**) corresponding to the end of nanotubes (**Figure 4.5C**). These preliminary results indicate that selective labeling of CNT geometric features is indeed possible. However, two issues need further attention. First, as previously reported[176, 177] and as can be seen on the images of **Figure 4.5**, sonication fractures and shortens nanotubes. For our experiments, we tested sonication times ranging between 1-5 minutes at a power of 12 W. We found that 3 minutes was the minimum time required for colloidal suspensions sfGFP-Car15-solubilized CNTs to withstand centrifugation at 14,000 *g* without detectable precipitation. However, this treatment also shortens CNTs from the expected 5 μm average length as stated by the manufacturer. A second issue is the incomplete decoration of CNT ends by mCherry-Car9 (**Figure 4.5B**), which is unexpected at the working concentration of 500 nM (10 x K_d) used in the experiment of **Figure 4.5**.

1.22 Conclusion

While CNT-based devices have been used to detect single molecules[178-181] and are very promising in next generation electronics,[182-184] they remain difficult to mass produce and purify in the reliable fashion that will guarantee their commercial success. The highest density of

carbon nanotubes on an electrical device to date is 10^9 per cm^2.[185] To achieve this feat, researchers at IBM coated and solubilized CNTs with sodium dodecyl sulphate (SDS) creating a negatively charged, soluble CNT. These CNTs were then deposited on a positively charged NMPI (4-(*N*-hydroxycarboxamido)-1-methylpyridinium iodide) striped surface by columbic interaction. The wells of NMPI were patterned into SiO_2, which is beneficial as it is negatively charged and would repel the negatively charged, coated CNTs allowing for high density aggregation on the NMPI substrate.[185]

In this chapter, we have shown that Car15 and Car9-tagged proteins have the potential to serve as biological "tacks" to precisely position individual nanotubes or other carbon nanostructures across fabricated circuits. This approach should also prove useful to attach functional proteins to the barrel of the CNT in order to enhance the sensitivity and selectivity of chemical sensing or to monitor enzymatic reaction rates at the single molecule level.

1.23 Figures

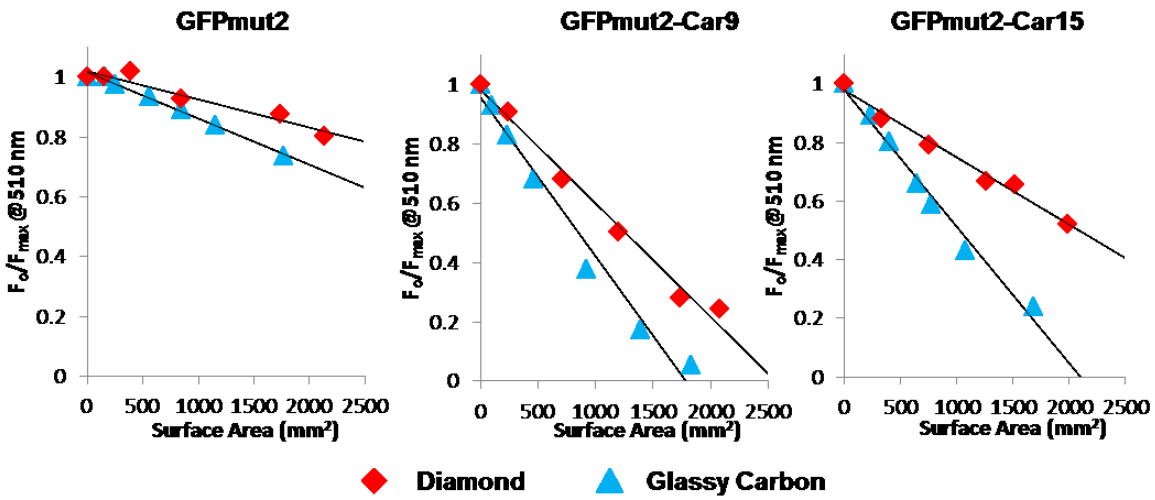

Figure 0.1 Remaining supernatant fluorescence after incubation of GFPmut2, GFPmut2-Car9 and GFPmut2-Car15 to glassy carbon or explosion diamond. Lower values indicate increased adhesion of the target protein.

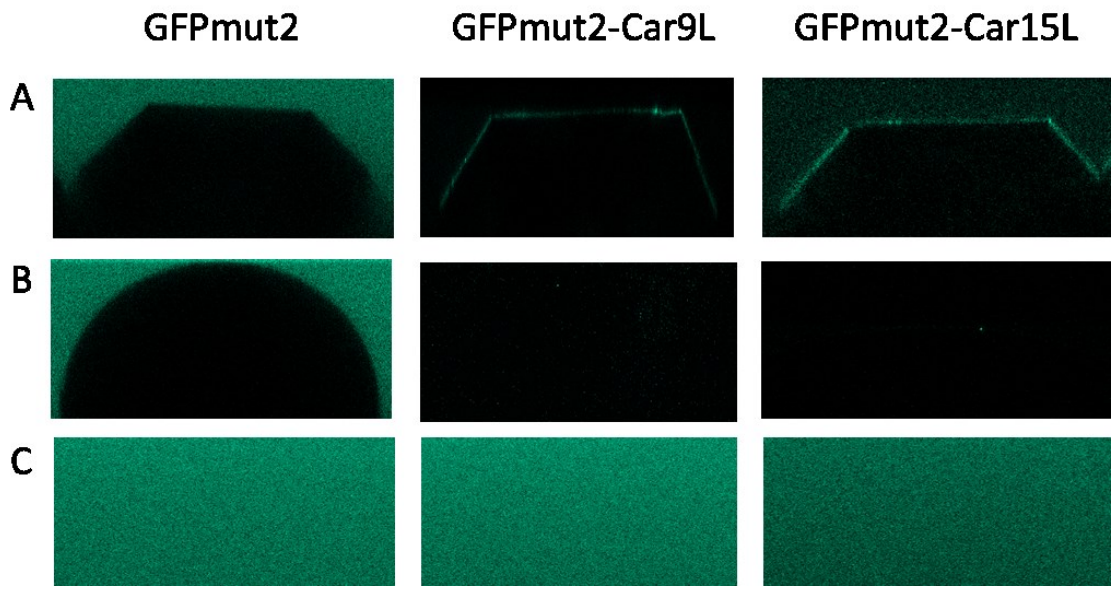

Figure 0.2 Confocal microscopy imaging of GFPmut2, GFPmut2-Car9L, and GFPmut2-Car15L (A) Diamond crystal bead after 1 hr incubation with given protein solution, some fluorescence remains on the surface of the diamond (B) Glassy carbon bead after incubation with protein solution for 1 hr, total loss of fluorescence from solution and on bead. (C) Initial fluorescence of protein solutions before incubation with carbonaceous substrates.

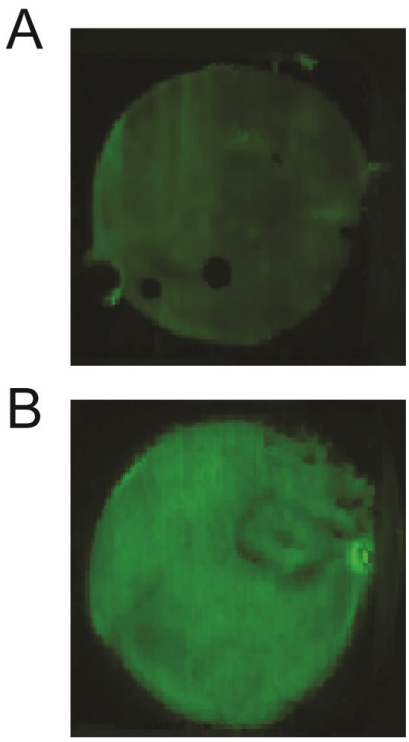

Figure 0.3 Typhoon gel scanner images 1 μM solutions of (A) GFPmut2-Car15 and (B) sfGFP-Car15 after incubation with freshly cleaved HOPG. Images taken after thorough washing of the HOPG substrate with 50 mM phosphate buffer pH 7.5.

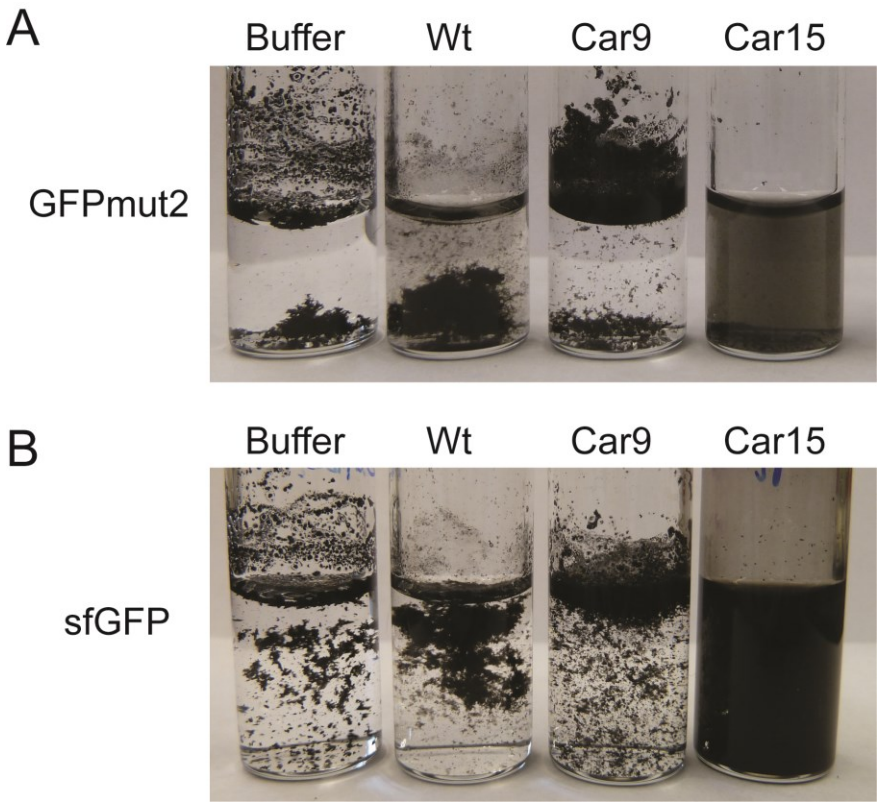

Figure 0.4 Dispersion of multi-walled carbon nanotubes by (A) GFPmut2 (B) sfGFP) derivatives. MWNT (≈ 1mg) were sonicated in the absence of additive or in the presence of 1 μM solutions of indicated protein. Samples were photographed after 24h.

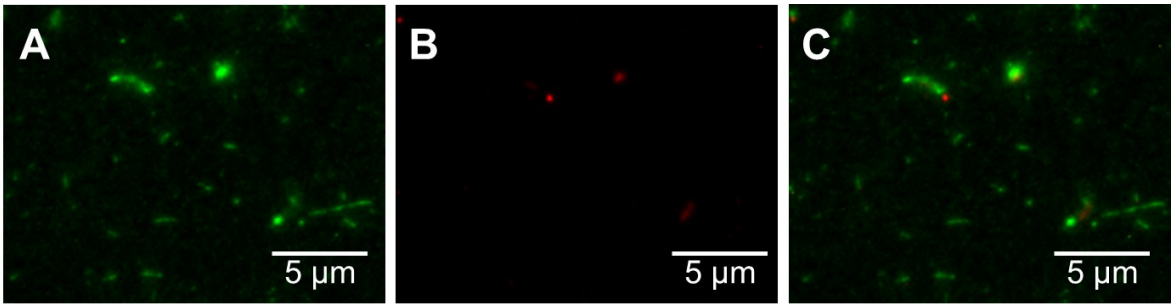

Figure 0.5 Fluorescence microscopy images (90x mag) of SWNT after resuspension with sfGFP-Car15 and subsequent addition of mCherry-Car9 (A) excitation λ = 473 nm (B) excitation λ = 587 nm (C) overlay of (A) and (B)

The Car9 Tag as an Alternative to Silane Chemistry

1.24 Introduction

The micro- and nanoscale organization of proteins on silica substrates is important for a wide array of biotechnologies including controlled cellular growth,[186-189] enzyme immobilization,[190-193] and immunoassays.[194-197] Typically, silane chemistry is used to modify silica substrates with functional carboxylic, amine, or even cyano groups.[198] One of the most common silanes for protein immobilization is APTES (3-Aminopropyl-triethoxysilane), a chemical that terminates a silica substrate with an amine group. This amine can be used for protein conjugation using cross-linkers such as glutaraldehyde (which has the disadvantage of cross-linking proteins to each other)[199, 200] or, more desirably, EDC (*e*thyl-dimethylaminopropy carbodiimide), a compound that reacts with carboxylic acid groups in proteins to form *o*-acylisourea intermediates that react with primary amines. One drawback of EDC chemistry is that it is most efficient under acidic conditions (pH 4.5) where proteins can unfold. To remedy this issue, *N*-Hydroxysuccinimide (NHS; or sulpho-NHS for aqueous conjugation) can be added to create a reactive ester that is stable at physiological pH and results in a similar conjugation of carboxylic acid groups of the protein to the amine-terminated substrate.[201] Although covalent attachment leads to higher protein surface coverage and improved retention compared to simple adsorption, the lack of control over orientation can significantly reduce enzyme activity.[202-204]

An alternative to conjugating proteins to silica relies on the use of aptamers that interact with the surface non-covalently. Previously, Fuchs and Raines used a tag consisting of 9 successive arginines to couple proteins to silica but noticed that the fusion protein was slowly released from

the surface over time.[205] Kuroda and coworkers made use of the *E. coli* ribosomal protein L2 which binds to silica with high affinity but through a poorly understood mechanism that is thought to involve electrostatic interactions and a fairly disordered protein structure.[206] However, L2 is a fairly large (32-kDa) protein[206] and it does not bind well to silica below pH 7.0 or in the presence of high concentrations of salt.[207] These drawbacks deter the use of either of these silica binding tags.

In Chapter 3, we reported that the Car9 dodecamer exhibits high affinity (K_d = 1 μM) for silica and that its binding remained strong under high salt concentrations (5 M $MgCl_2$ or NaCl) and over a broad range of pH (pH 5-10). Here, we show that Car9-tagged proteins can be immobilized onto transparent silica substrates in a single step with retention of activity, control of orientation and chemical addressability. We also demonstrate that GFPmut2-Car9 can be entrapped within silica sol-gels and released from the matrix by arginine addition.

1.25 Materials and Methods

1.25.1 Modification of Silica Surfaces by Protein Immobilization

A glass microscope slide was washed with *dd*H_2O and dried under air. Aliquots (5 μL) of 10 μM solutions of GFPmut2, GFPmut2-Car9L and GFPmut2-Car15L were incubated on the cleaned glass slide for 1 min and imaged with a Typhoon 9000 gel image scanner with a 475 nm excitation laser and a 510 nm lowpass cutoff filter. The slide was also imaged after a 30 sec wash in *dd*H_2O and 30 sec in buffer A supplemented with 1 M L-lysine.

A glass microscope slide was washed with *dd*H_2O and dried under air. Aliquots (5 μL) of 1 μM total concentration mixtures of GFPmut2-Car9 and mCherry-Car9 at ratios of 1:0, 0.75:0.25, 0.5:0.5, 0.25:0.75, 0:1 respectively. The mixtures were incubated on the cleaned glass slide for 1

min and imaged with a Typhoon 9000 gel image scanner with a 475 nm excitation laser and a 510 nm lowpass cutoff filter and then with a 532 nm excitation laser and a 575 nm lowpass cutoff filter The slide was also imaged after a 30 sec wash in 50 mM sodium phosphate buffer pH 7.5

We also tested how multiple proteins with a c-terminal Car9 tag would bind to glass substrates when the proteins were in a solution mixture. In theory, the two proteins should show no segregation at the glass surface if the Car9 tag is equally accessible for each protein. In our study, we mixed different (1:0, 0.75:0.25, 0.5:0.5, 0.25:0.75, 0:1) ratios of GFPmut2-Car9 and mCherry-Car9 incubated them on a glass slide (**Figure 5.2A**). After thorough washing (**Figure 5.2B**) it is apparent that the two proteins showed equal affinity for the silica surface.

1.25.2 Sol-gel Creation and Protein Loading

Silica sol-gels were created using the Stöber method without stirring.[208-210] Briefly, 10 mL of tetramethylorthosilicate (TMOS) was added to 10 mL of methanol and mixed to form solution A. Next, 5 mL of 0.16% w/v ammonium hydroxide was mixed with 10 mL methanol to create the catalyst solution B. Solutions A and B were mixed, poured into petri dishes and allowed to sit for 15 min at room temperature to create silica sol-gels. Sol-gels were covered with methanol and held for 24 hours before the methanol was replaced and aging was allowed to proceed for 72 h changing the methanol every 24 h. The methanol was exchanged for 20 mM Tris buffer pH 7.5 (Buffer A) using the solution replacement as above. Sols were split into pieces approximately 1 x 1 cm and incubated overnight at 4°C with 1 mL of clarified lysate from cells expressing GFPmut2-Car9 (Chapter 3). The sol was removed and immersed in 10 mL of buffer A for 10 min. The process was repeated 5 times and long term storage was in buffer A. Protein-loaded

sols were incubated in 1 mL of buffer A supplemented with 1 M L-lysine and incubated at 4°C for 48 h to release the entrapped protein.

GFPmut2-Car9 was also entrapped in silica sol-gels by directly mixing 100 μL of protein at 2.5 μM concentration with 100 uL of pure TMOS in a microcentrifuge tube. The microcentrifuge tubes were examined after resting overnight at room temperature. All the fluorescence from the GFPmut2-Car9 was located in the bottom of the tube that contained the silica sol-gel.

1.25.3 DNA Manipulations and Protein Purification

A pUC57-Kan derivative encoding a variant of sfGFP specifying *Avr*II and *Spe*I restriction sites at codons 172-173 (a known permissive site within sfGFP),[175] and a 3' extension encoding a GGGS linker and the linear Car15 dodecamer (RTYLPLPWMAAL) on a *Hin*dIII-*Xho*I fragment was ordered from GenScript (Piscataway, NJ). This sfGFP-172-Car15 variant was isolated on a *Nde*I-*Xho*I fragment and inserted into the same sites of pBLN200[141] to place the gene under transcriptional control of the arabinose-inducible P_{BAD} promoter.[141] Complementary primers encoding the Car9 sequence flanked by *Avr*II and *Spe*I sites (5'-GTGGAGCCTAGGGACAGTGCTCGCGGGTTTAAAAAGCCTGGGAAGCGGACTAGTGA TGGC–3') were ordered from Invitrogen. Primers were mixed at 10 μM concentration, boiled for 10 min and allowed to slowly cool to room temperature. Annealed primers were digested with *Avr*II and *Spe*I and inserted into the same sites on the sfGFP-Mut-Car15 to yield sfGFP-MutCar9-Car15, which has a C-terminal sequence of KLGGGSRTYLPLPWMAAL.1

Clarified lysate of sfGFP-MutCar9-Car15 was prepared in sf100 cells, as described in 3.2.1, were immersed in a water bath held at 80°C for 15 min and clarified by centrifugation at 14,000

g for 15 min. The clarified lysate was purified to near homogeneity by ion exchange chromatography on a Whatman DE52 column. After dialysis against 50 mM sodium phosphate buffer pH 7.5, proteins were aliquoted at a 10 μM final concentration and stored at -20°C. GFPmut2, GFPmut2-Car9, GFPmut2-Car15, sfGFP, sfGFP-Car9, sfGFP-Car15 were also expressed and purified as described in section 3.2.1.

1.25.4 Carbon Nanotube Resuspension and Silica Binding

For multiwalled carbon nanotube (MWNT) resuspension experiments, ≈ 1 mg of material was added to a glass vial containing 2.7 mL of 50 mM phosphate buffer pH 7.5. These solutions were sonicated for 1.5 minutes before adding 300 μL of 10 μM of the designated protein (final concentration = 1 μM) and sonicated for an additional 1.5 minutes. Mixtures were cooled by immersion in a mixture of EtOH and ice. The sonication was performed using a micro-tipped sonicator at 12W and 100% duty cycle (Branson Sonifier 450).

Silica pull down experiments were conducted with CNT suspensions of sfGFP-Car15 and sfGFP-mutCar9-Car15. 0.25 mL of resuspended carbon nanotubes were added to 100 mg silica gel in a microcentrifuge tube and gently mixed for 15 minutes. These mixtures were then let to rest overnight and imaged.

1.26 Results and Discussion

1.26.1 Car9 Fusions: an Alternative to Silane Coupling Chemistry

Silane coupling chemistries for protein conjugation to silica surfaces is labor intensive and can lead to partial loss of protein activity. To determine if the Car9 tag that would be suitable single-step immobilization of proteins on silica surfaces, aliquots of purified GFPmut2,

GFPmut2-Car9 and GFPmut2-Car15 were spotted at the surface of a clean microscope slide as indicated in **Figure 5.1a** to form the letters GFP. A wash step with *dd*H_2O, removed control GFPmut2 and GFPmut2-Car15 proteins but not GFPmut2-Car9, as would be expected from a strongly adsorbed species (**Figure 5.2b**). An early indication of protein adhesion is the retention of water on the surface of the hydrophobic glass slide at the location of the protein deposition and adhesion. Nominally, buffer beads and rolls off the glass slide, however, after protein incubation water will be retained in the areas that were exposed to protein. We theorized that this effect is due to the protein creating a hydrophilic area on the nominally hydrophobic surface of the glass substrate. Because Car9-tagged proteins can be eluted from silica gel by incubation with lysine (Chapter 3), we tested the effectiveness of this additive at releasing silica-bound GFPmut2-Car9. **Figure 5.2c** showed that 1 M L-lysine lead to complete removal of the protein. In addition to the loss of fluorescence, the areas regained their hydrophobic character. This non-covalent modification is unique because the protein remains on the silica substrate at high salt concentrations (5 M $MgCl_2$ or 5 M NaCl) and over a large pH range (pH 5-10) (Chapter 3). We conclude that the Car9 tag can be used for the rapid, inexpensive and chemically reversible attachment of proteins to silica surfaces.

We also tested how multiple proteins with a c-terminal Car9 tag would bind to glass substrates when the proteins were in a solution mixture. In theory, the two proteins should show no segregation at the glass surface if the Car9 tag is equally accessible for each protein. In our study, we mixed different (1:0, 0.75:0.25, 0.5:0.5, 0.25:0.75, 0:1) ratios of GFPmut2-Car9 and mCherry-Car9 incubated them on a glass slide (**Figure 5.2A**). After thorough washing (**Figure 5.2B**) it is apparent that the two proteins showed equal affinity for the silica surface.

1.26.2 Protein Decoration of Silica Sol-gels

Entrapment of proteins in silica sol-gels has been shown to increase their stability to chemical denaturation.[211] The traditional process for silica sol-gel creation utilizes the acid or base catalyzed hydrolysis of TMOS or TEOS to form silanols. These silanols then condense in a polymerization reaction to form silica sol-gels. Furthermore, a broad range of proteins can be entrapped within the silica sol-gel during this polymerization process as shown in hundreds of publications in the mid 90's.[212-214] This silica-sol entrapment is non-specific to the protein of interest. Here, we explored two separate methods to encapsulate Car9-tagged proteins in silica sol-gels. In the first approach, we created a silica sol-gel using the method of Stöber.[208-210] **Figure 5.3A** shows that GFPmut2-Car9 partitioned in the sol-gel when clarified extracts of cells expressing this protein were mixed with the gel. These protein-loaded sols could be stored in buffer for over 6 months with no detectable release of fluorescence in the supernatant or decrease in the fluorescence of the sol (**Figure 5.3A**). However, incubation of the samples with 1 M L-lysine for 48h at 4 °C led to quantitative release of the GFPmut2-Car9 (**Figure 5.3B**).

Silica-binding peptides (and in particular the R5 repeat unit peptide from the silica-binding sillifan protein from *Cylindrotheca fusiformis*)[215] have previously been used to entrap enzymes.[216] In these experiments, the R5 peptide was mixed with the enzyme of interest and a 100 mM solution of TMOS to produce a network of ≈ 70 nm silica nanoparticles containing the desired enzyme. **Figure 5.4B** shows that because GFPmut2-Car9 specifies its own silica binding domain, it was possible to produce a protein-rich sol gel by the simple expedient of mixing the tagged protein with a solution of TMOS. By contrast, no polymerization was observed when the experiment was repeated with the GFPmut2 control protein (**Figure 5.4A**). These preliminary data suggest that it should be possible to relying entrap virtually any protein in a silica sol gel by

fusing it to the Car9 tag and using the TMOS technology. It will be instructive to determine the mechanisms by which encapsulation proceeds and how the nature and concentration of the eluent influences the release kinetics of entrapped proteins.

1.26.3 Dual-binding Silica Tag for Complex Nanostructure Creation

Precise positioning of carbon nanostructures such as CNTs and graphene nanoribbons on silicon wafers is a difficult task that will be instrumental for the development of next-generation electronics. IBM recently produced the highest density of CNT-based transistors on a silicon wafer (500 CNTs/μm) by using a Langmuir–Schaefer-based method for CNT self-assembly.[217] (500 CNTs / μm compared to previous devices that averaged 6-10 CNTs / μm.[217-221] Similar methods may be applicable to graphene nanoribbons but have not been reported in the literature. Even with these advances, the methods are extremely delicate and hard to implement on a large scale.

Using interacting proteins pairs or bifunctional proteins engineered to bind both carbon and silica might be a useful alternative since the few nanometer thick oxide layer that spontaneously form on silicon wafers is chemically similar to silica. As a first step towards this goal, we designed and built a variant of sfGFP containing a C-terminal Car15 tag for binding and solubilization of sp^2-hybridized carbon nanostructures, as well as a silica-binding Car9 tag located within a geometrically opposite permissive loop of the protein (sfGFP-mutCar9-Car15).[175] The protein was expressed and purified with no noticeable loss in solubility of fluorescence, which shows that the added tag did not disrupt the structure of the sfGFP. While work on this front is still in the preliminary stages, we have investigated the ability of the sfGFP-mutCar9-Car15 to resuspend CNTs through the Car15 tag as in Chapter 4 (**Figure 5.5A**). These

CNTs were also able to withstand centrifugation at 14,000 *g* similar CNTs resuspended by other Car15 tagged proteins. Additionally, the coated CNTs should still be able to bind silica through the outward facing Car9 tag. To test this ability we incubated 0.25 mL of suspended CNTs with 100 mg of silica gel. Within 15 min, the CNTs that were resuspended with sfGFP-mutCar9-Car15 had left the supernatant and bound to the silica gel. This effect remained 24 hours later (**Figure 5.5B**). We believe this ability to locate CNTs will extend to oxidized silicon substrates used for transistor creation.

1.27 Conclusion

The Car9 tag offers a number of advantages over silane chemistry for protein immobilization at silica surfaces. First, it provides for 1-step decoration under aqueous conditions and without the need for surface modification, activation of the protein and attachment of the protein to the surface with the traditional method. Second, it should improve retention of biological activity, since proteins are not immobilized in random orientations on the surface. Third, and very uniquely, bound proteins can be released from the surface by making use of a lysine buffer. This should enable very useful modalities including surface regeneration and chemical actuation of protein-catalyzed reactions. Finally, we developed a dual-binding protein, sfGFP-mutCar9-Car15, that can solubilize CNTs and co-locate them to silica substrates. We believe this could have many future implications for creation of silicon-CNT hybrid devices.

1.28 Figures

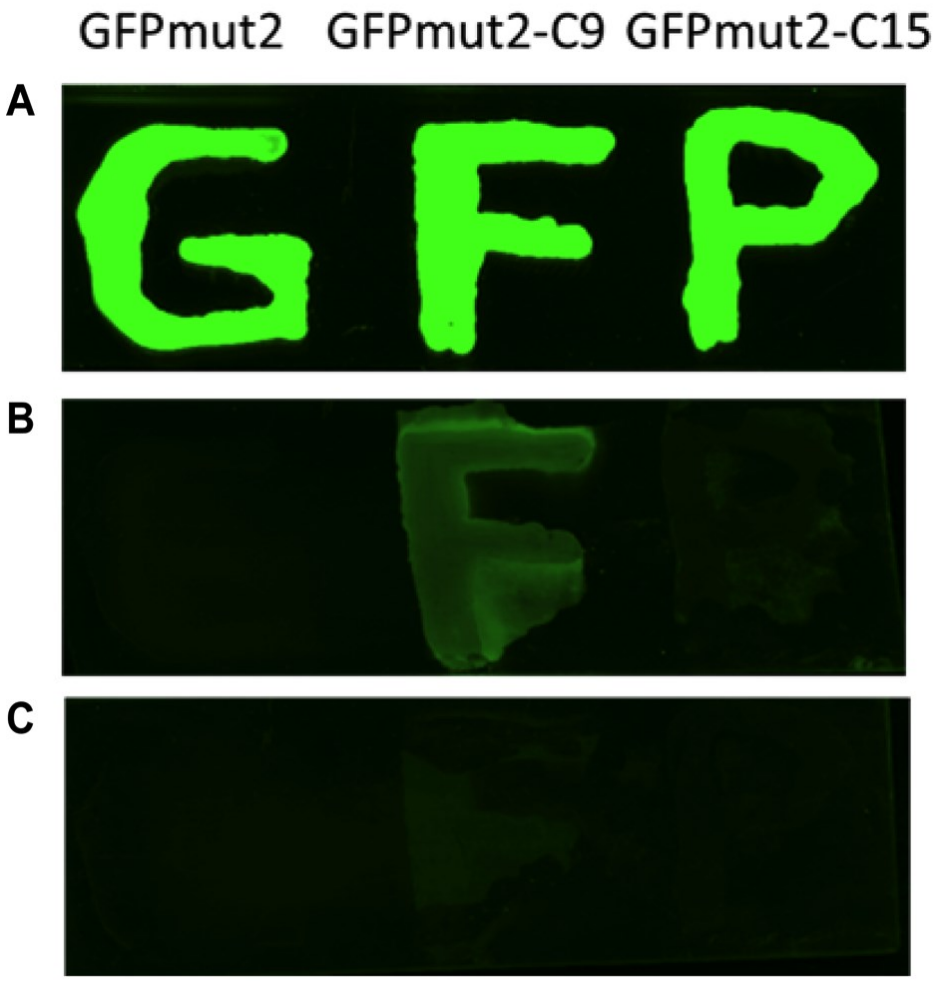

Figure 0.1 Decoration of silica substrates by Car9-tagged proteins (A) 10 μM solutions of GFPmut2, GFPmut2-Car9L and GFPmut2-Car15L incubated on glass slide and imaged by Typhoon 9000 gel analyzer with excitation at 475 nm (B) Glass slide imaged after washing with *dd*H_2O for 30 seconds to remove proteins that did not adhere to the substrate (C) Glass slide imaged after washing with 1 M L-lysine for 5 minutes to specifically remove the Car9-tagged protein.

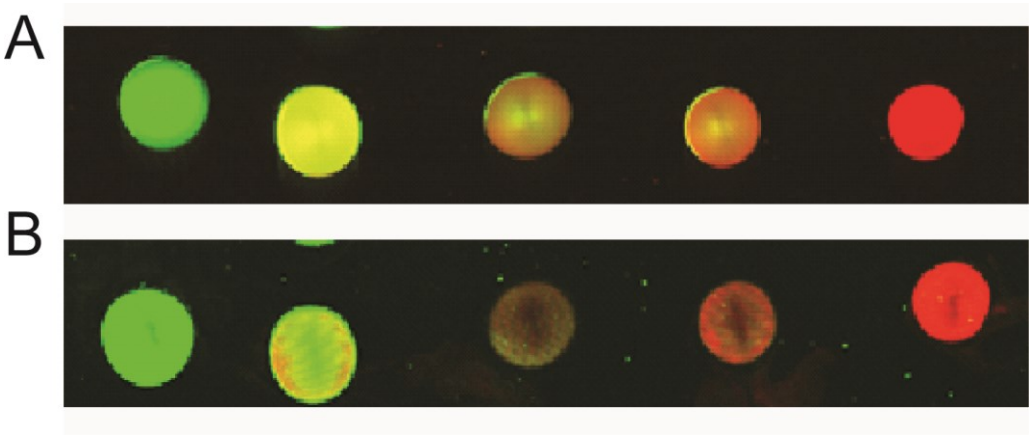

Figure 0.2 Overlaid fluorescent images from Typhoon 9000 gel image scanner (excitation λ = 473 nm and excitation λ = 587 nm) of mixtures of GFPmut2-Car9 and mCherry-Car9 at mixtures of 1:0, 0.75:0.25, 0.5:0.5, 0.25:0.75, 0:1 from left to right. (A) as deposited (B) post-wash with 50 mM sodium phosphate buffer pH 7.5

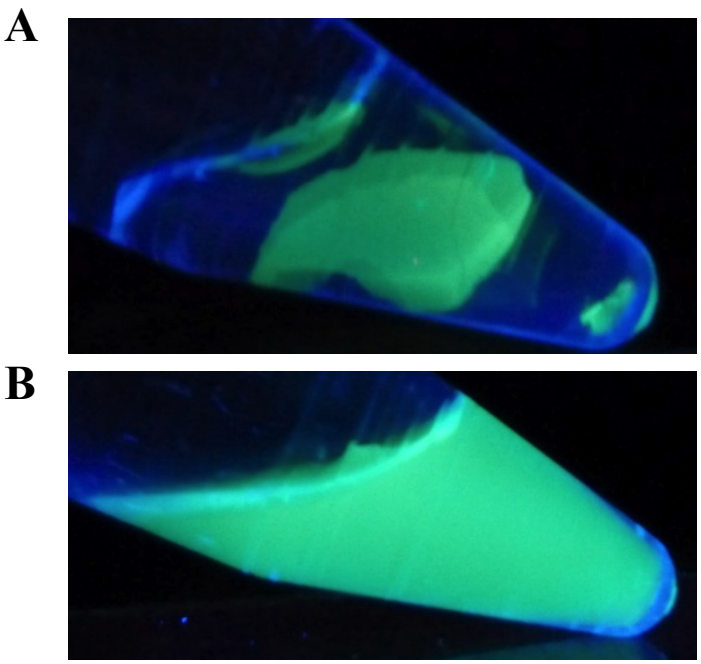

Figure 0.3 GFPmut2-Car9 loaded onto silica sol-gel (A) Silica sol-gel incubated in clarified lysate containing GFPmut2-Car9 and washed with buffer (B) Silica sol-gel after incubation in Buffer A supplemented with 1 M l-lysine

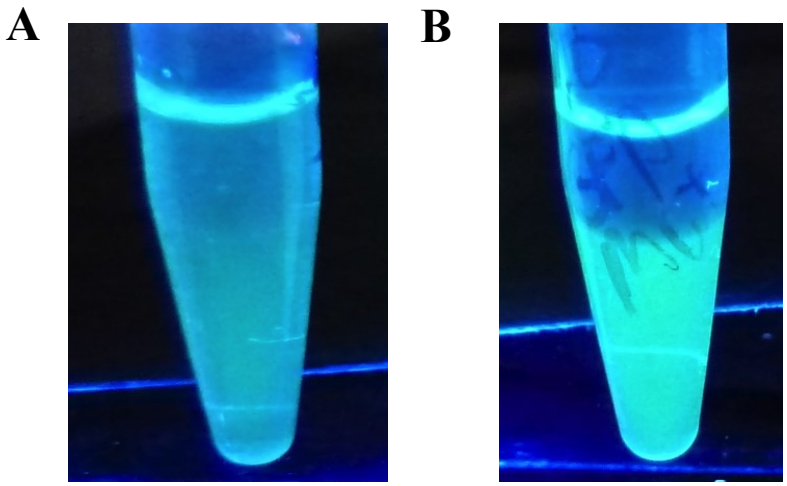

Figure 0.4 Silica sol-gel creation under excitation of UV light (A) GFPmut2 mixed with TMOS solution after overnight incubation remained unpolymerized (B) GFPmut2-Car9 mixed with TMOS solution after overnight incubation with gel formation at bottom of the tube.

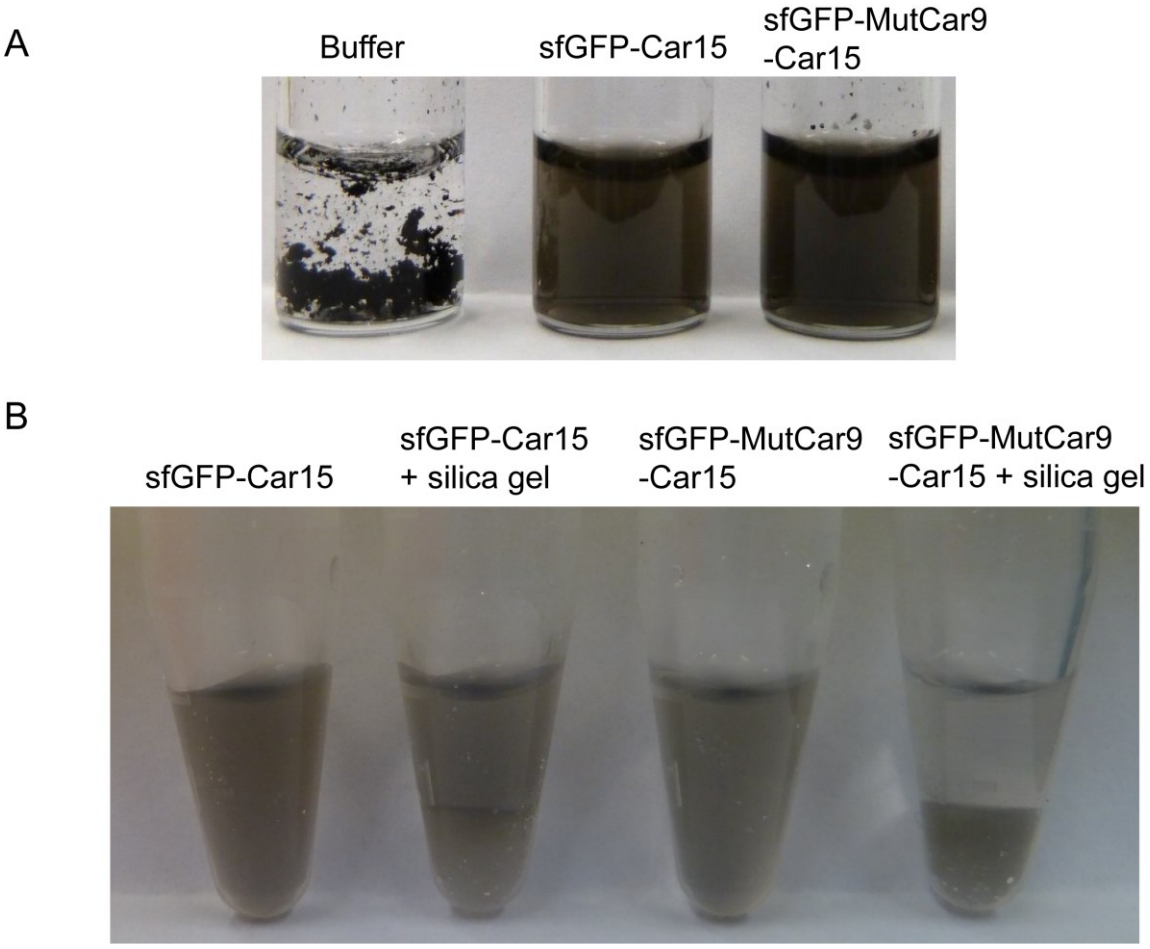

Figure 0.5 Comparison of MWNT suspensions (≈ 1mg MWNT) created by sonication in the presence of (A) 1 μM sfGFP-Car15 or sfGFP-MutCar9-Car15 (B) 0.25 mL of resuspended CNTs incubated with 100 μL silica gel for 24 hours. Samples were photographed after 24h.

Appendix A

1.29 Supplemental information (Chapter 2)

1.29.1 Determination of K_d by Surface Plasmon Resonance (SPR)

Surface Plasmon Resonance measurements were conducted on homemade SPR glass chips coated with a ≈ 2 nm titanium adhesion layer, a ≈ 48 nm evaporated gold film, and a ≈ 4 nm evaporated carbon film. Chips were cleaned with ethanol and UV-ozone as above and mounted on a 4-channel flow cell SPR sensor from the Institute of Photonics and Electronics (Prague, Czech Republic) includes temperature control (25°C) and a peristaltic pump for controlled flow at 50 μL/min. The SPR design is based on an attenuated total reflection and measures wavelength modulation.

Due to the variance between carbon coatings on SPR chips, we relegated the K_d estimation to 4 concentrations due to the restriction of four available flow channels. By assuming a 1st order Langmuir association, K_d can be found by determining rate constant k_{obs} for each concentration. Equation 6.1 was used to fit each SPR curve using a least squares fit method while varying both σ_∞ and k_{obs}. Once the value for k_{obs} has been determine and graphed concentration (Figure 6.1), equation 6.2 can be linearly fit to determine both the k_a and k_d. Finally, the K_d can be determined as shown in equation 6.3 by using the linear fit (**Figure 6.1**).

1.29.2 AFM Analysis of the Adsorption of Authentic TrxA on Highly Oriented Pyrolytic Graphite

AFM was used to analyze samples of HOPG exposed to authentic TrxA (**Figure 6.2**). There was no measureable adhesion of TrxA to HOPG at 1 μM. Additionally, HOPG was examined after exposure to 100 nM TrxA::Car9 (**Figure 6.3 A,B**) and 50 nM TrxA::Car15 (**Figure 6.3 C,D**) TrxA::Car9 appears to bind along the terraces of the HOPG, while TrxA::Car15 shows preferential binding along the planar regions.

1.29.3 Raman Spectroscopy Analysis of Carbon Allotropes

The 5 different carbon substrates used in this study were analyzed by Raman spectroscopy. MWNT, glassy carbon and detonation diamond powders were washed with ddH_2O, deposited on a glass slide and allowed to dry. Spectra were acquired for 10 seconds on a Renishaw inVia Raman microspectrometer through a Leica DM IRBE optical microscope. A 514 nm argon source was used to irradiate samples through a 50x objective lens. Raman-scattered light was captured on a cooled charge-coupled device. Raman-scattered light was captured on a cooled charge-coupled device. The location of the D peaks and G peaks is consistent with literature values (**Figure 6.4**).[222-225]

1.30 Figures

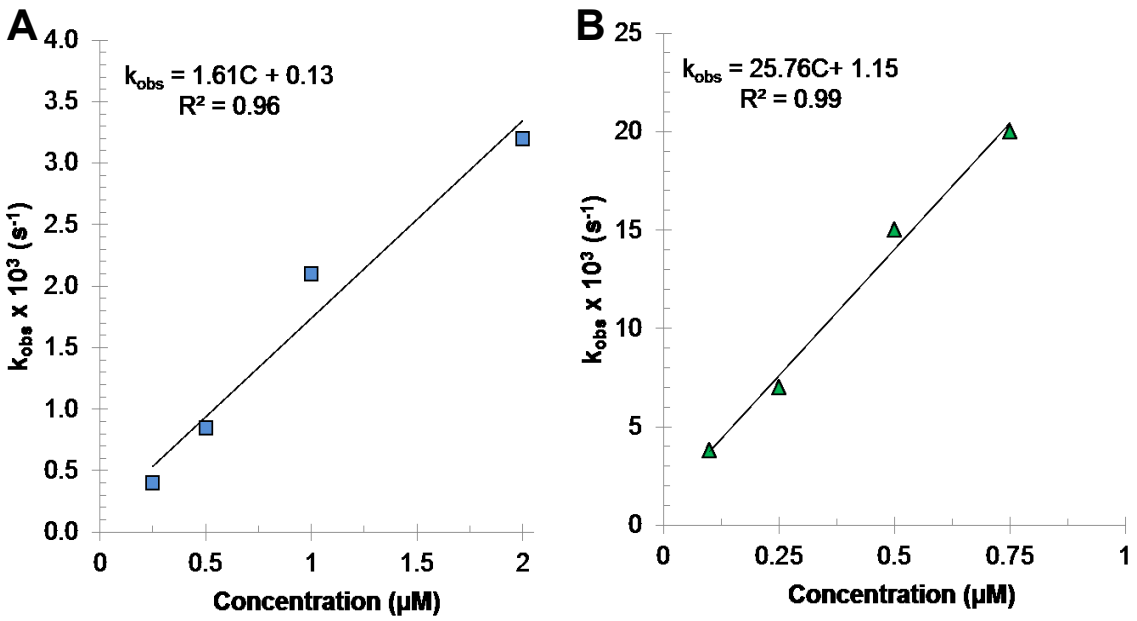

Figure 0.1 Linear fit models to determine K_d of each carbon binding peptide for a carbon surface through SPR. The slow of the linear fit is equal to the k_a for each peptide while the y intercept is the k_d (A) TrxA::Car15 k_{obs} values as determined by SPR at 4 separate concentrations (B) TrxA::Car9 k_{obs} values as determined by SPR at 4 separate concentrations

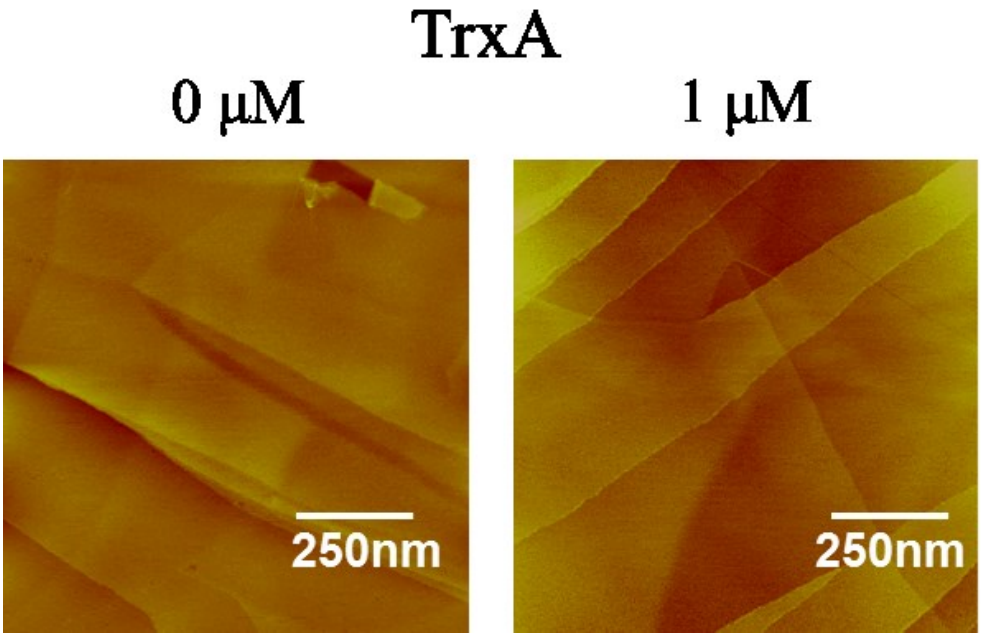

Figure 0.2 Pure 50 mM sodium phosphate buffer pH 7.5 (left) or authentic TrxA at 1 μM concentration were contacted for 10 min with freshly cleaved HOPG. Surfaces were imaged by AFM after washing and drying.

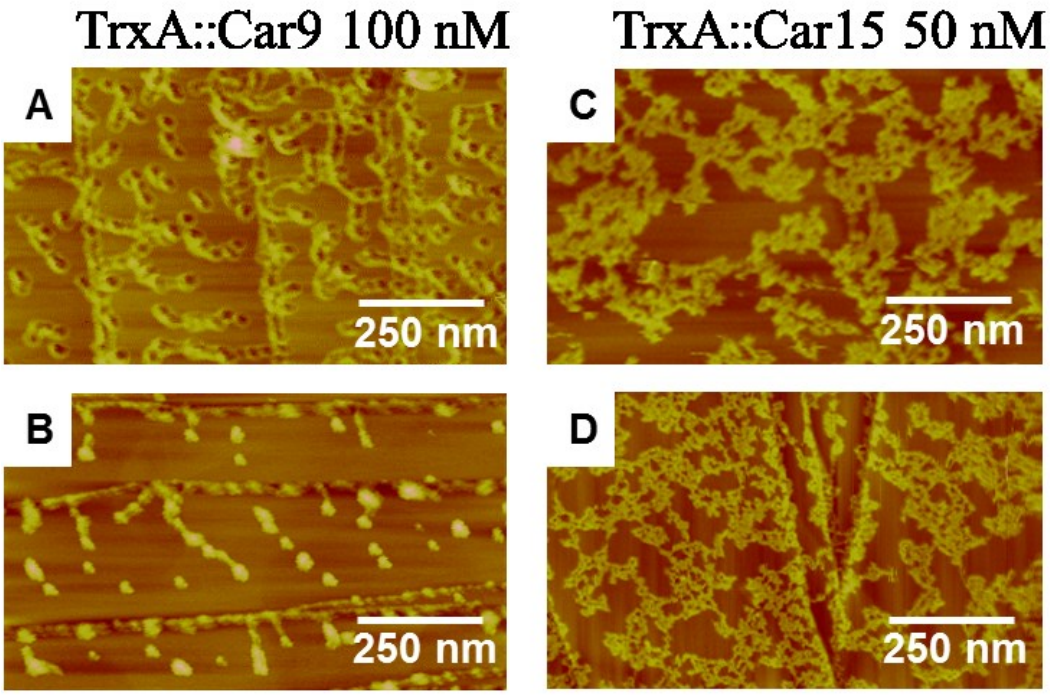

Figure 0.3 AFM images on freshly cleaved HOPG (A) (B) 100 nM TrxA::Car9 (C) (D) 50 nM TrxA::Car15. All solutions were contacted for 10 min with freshly cleaved HOPG. Surfaces were imaged by AFM after washing with ddH_2O and drying.

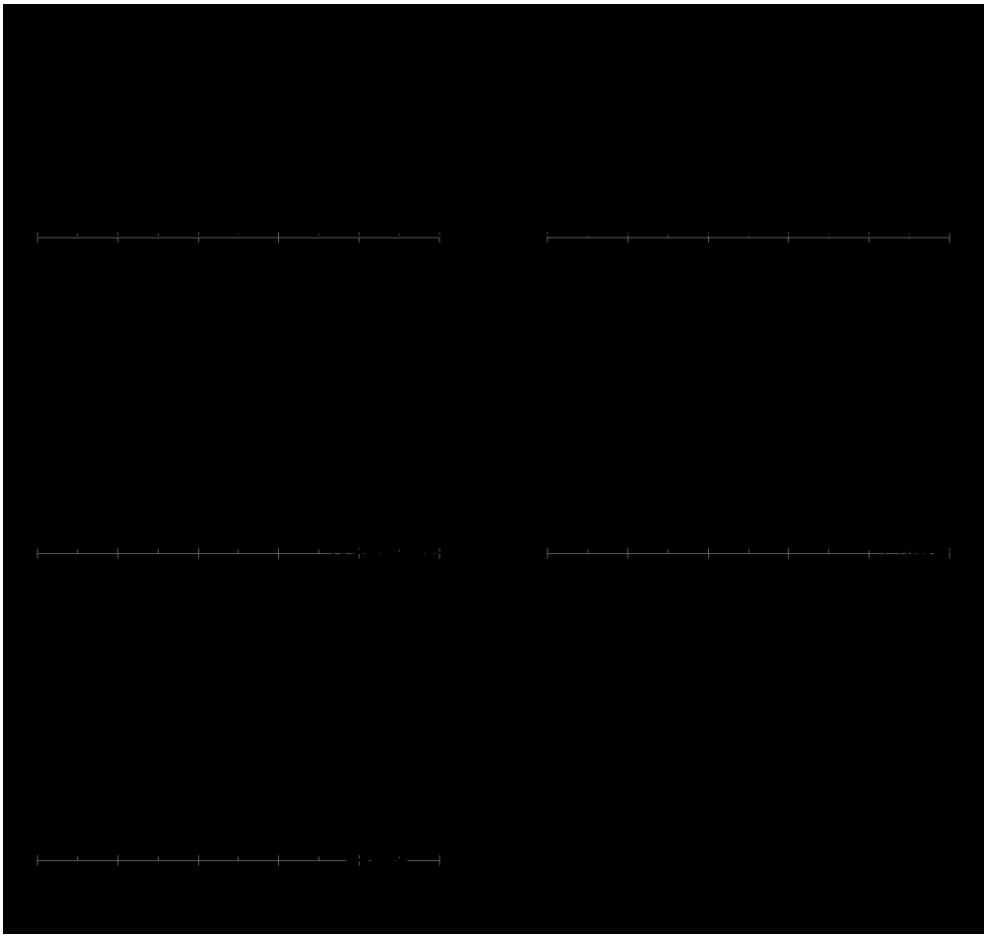

Figure 0.4 Raman spectra of carbon substrates used in this study. (A) HOPG (bar :110 counts/sec); (B) MWNT (bar: 30 counts/sec); (C) evaporated carbon (bar:160 counts/sec); deconvoluted peaks occur at 1364 and 1536 cm^{-1} (D) diamond powder (bar 3000 counts/sec); (E) glassy carbon powder (bar 55 counts/sec).

Appendix B

1.31 Supplemental information (Chapter 3)

1.31.1 Map of plasmid pBLN200-Car9

Diagram of plasmid pBLN200-Car9 (**Figure 7.1**).

1.31.2 The Car9 Tag does not Affect GFPmut2 Function

The fluorescence emission spectra of GFPmut2 and GFPmut2-Car9 (1 μM) were recorded following excitation at 488 nm on a Hitachi F4500 spectrofluorometer (**Figure 7.2**). Measurements of maximum fluorescence intensity at 510 nm were also made on multiple aliquots over a period of 3 months. There was no detectable difference in the optical properties of the two proteins.

1.31.3 GFPmut2 Remains Intact in Extracts of *E. coli* Top10 Cells

Whole cell (WC) and soluble (S) fractions of Top 10 cells expressing GFPmut2 from plasmid pBLN200-GFPmut2 were prepared as described in the Materials and Methods Chapter 3. No degradation products were detected in soluble fractions, indicating that, unlike GFPmut2-Car9, GFPmut2 is resistant to proteolytic degradation by OmpT (**Figure 7.3**).

1.31.4 Truncated GFPmut2-Car9 does not Bind to Silica

To determine if the low molecular mass degradation fragment of GFPmut2-Car9 would retain silica binding activity, soluble extracts from KS272 (*ompT*$^{+}$) or SF100 (Δ*ompT*) cells

expressing GFPmut2-Car9 were prepared as described in the main text and incubated on ice for 24h to ensure quantitative conversion of GFPmut2-Car9 to its low mass fragment in KS272 cells. Aliquots (0.25 mL) were added to 100 mg of silica gel and tubes were photographed under ambient or UV illumination. **Figure 7.4** shows that the truncated product loses silica-binding ability due to proteolytic cleavage of the Car9 tag.

1.31.5 Protein Remaining on Silica Beads Post-Elution

Silica gel, under the buffer conditions used in these experiments, can exhibit negatively charged characteristics through the surface silanol groups and hydrophobic characteristics through the surface siloxane groups. It is reasonable to assume that some proteins from the soluble extract of *E. coli* will non-specifically bind to the silica gel under the loading conditions used. Interestingly with no optimization to buffer conditions, we do not notice a large amount of protein other than the target protein being eluted with 1 M L-lysine. After elution, we examined the protein remaining on the silica beads by immersing 3 g of silica gel in 6 M GndCl. The resulting solution was resuspended in equal amounts of 2x SDS loading buffer and a resulting 90 mg of silica beads were loaded onto the SDS-PAGE gel (**Figure 7.5 beads**). The soluble load is also shown (**Figure 7.5 load**).

1.31.6 Comparing the Economics of His-tagged Protein Purification on a Reusable Ni-NTA Matrix to those of Car9-tagged Protein Purification on Disposable Silica Gel Columns

To compare the cost of purifying a His-tagged protein on a reusable Ni-NTA resin to that of purifying a Car9-tagged protein on a disposable silica gel column, we assumed that: (i) all pre-

chromatography steps (cell growth, induction, harvesting, resuspension, disruption, clarification) were identical; (ii) Ni-NTA and silica gel had comparable protein binding capacity (≈ 5 mg/mL; see main text); and (iii) 3 mL of settled slurry and a 50 mL elution volume was used in both cases. We obtained the cost of chromatography matrices and eluent from Sigma-Aldrich, using products of comparable size and purity (Ni-NTA #p6611 and 100 mL; Silica gel #391484 and 100g; Imidazole #I2399, L-Lysine hydrochloride #L5626 and 500g). **Table 7.1** shows that eluting a His-tagged protein with 100 mM imidazole is 42-times cheaper than eluting a Car9-tagged protein with 1 M L-lysine. However, Ni-NTA is more than 43-times more expensive than silica gel, and the cost of the resin dwarfs that of either eluent. As a result, a Ni-NTA column would have to be reused 15 times for this purification scheme to be more economical than the use of 15 disposable silica gel columns with lysine elution (**Table 7.1**). This is significantly more than the 5 Ni-NTA reuses recommended by the manufacturer, and it does not include the cost of cleaning the resin (which we estimate to be $1.00 per reuse), bulk discounts for lysine, or that a more efficient elution for Car9-tagged proteins may be achieved through optimization.

1.32 Tables

Table 0.1 Comparing the cost of single-use silica purification and reusable Ni-NTA purification.

Purification scheme	Resin cost (3 mL)	Elution cost (50 mL)	One purification	Five purifications	Fifteen purifications
Reusable Ni-NTA	$26.91	$0.03	$26.9	$27.21	$27.36
Disposable silica	$0.62	$1.26	$1.88	$18.8	$28.20

1.33 Figures

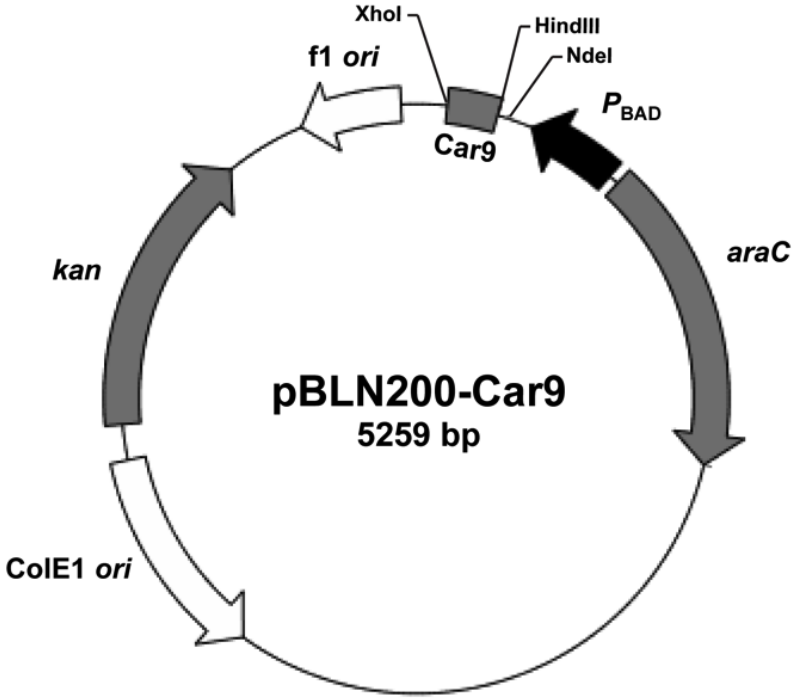

RBS *NdeI*

5′- TCTAGAAATAATTTTGTTTAACTTTAAGAAGGAGATATACATATGGCTAGCATGACTGGT

SalI *HindIII* **Linker**

GGACAGCAATGGGTCGCGGATCCGAATTCGAGCTCCGTCGACAAGCTTGGCGGCGGCTCT

Val Asp Lys Leu Gly Gly Gly Ser

Car9•Tag *XhoI*

GACAGTGCTCGCGGGTTTAAAAAGCCTGGGAAGCGGTAATAACTCGAGCACCACCACCAC -3′

Asp Ser Ala Arg Gly Phe Lys Lys Pro Gly Lys Arg * *

Figure 0.1 Relevant features of plasmid pBLN200-Car9. The plasmid is designed for the construction of C-terminal Car9 fusions by accepting genes on *Nde*I-*Hin*dIII fragments.

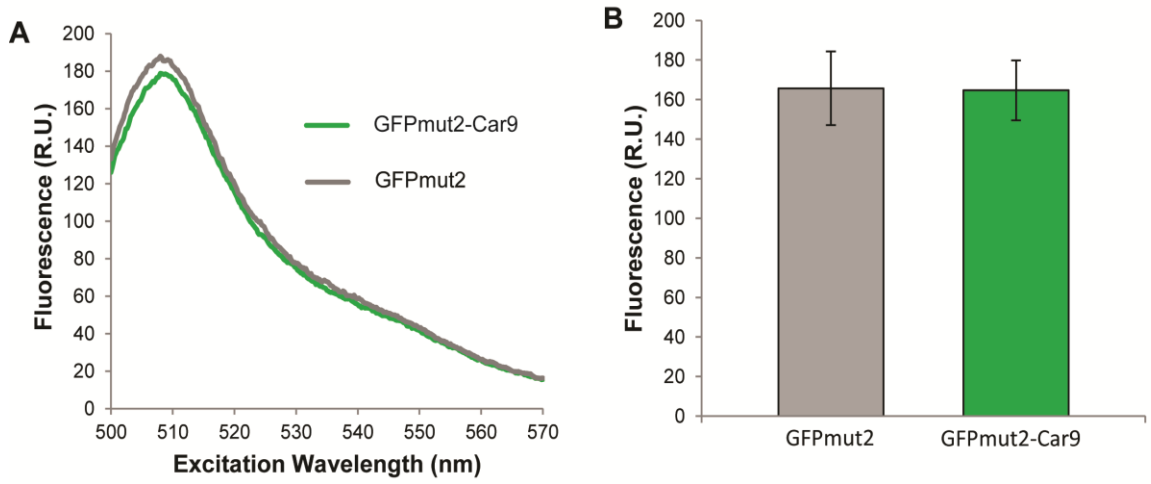

Figure 0.2 Activity comparison between purified GFPmut2 and GFPmut2-Car9 (A) Emission spectra of GFPmut2 and GFPmut2-Car9 (1 µM) following excitation at 488 nm. (B) Maximum emission fluorescence (510 nm) of GFPmut2 and GFPmut2-Car9 aliquots (1 µM) measured over 3 months.

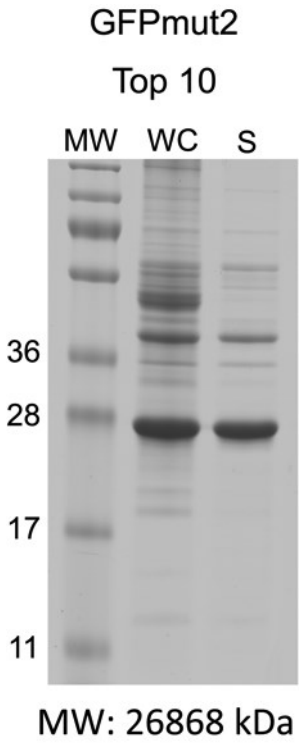

Figure 0.3 SDS-Page gel of the fractionation from GFPmut2 expressed in *E. coli* Top10 cells. Whole (WC) and soluble cell fractions (S) were fractionated by SDS-PAGE.

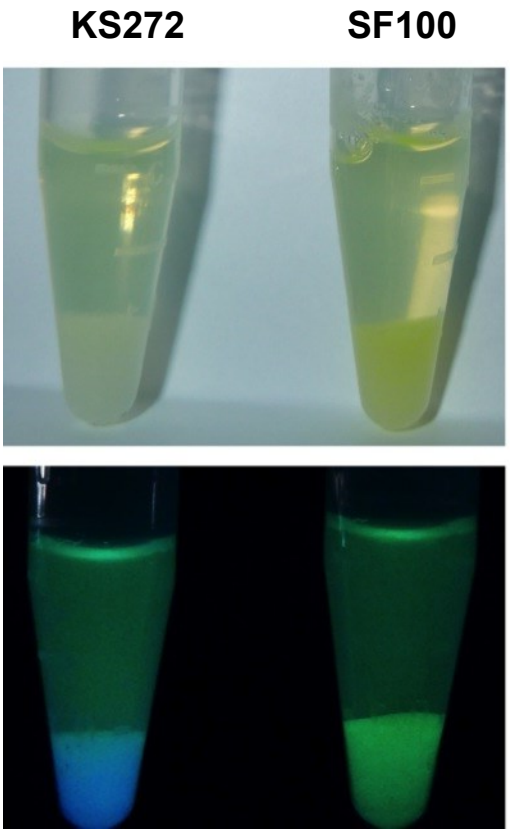

Figure 0.4 Soluble extract from KS272 (*ompT*$^{+}$) or SF100 (Δ*ompT*) cells expressing GFPmut2-Car9 were held on ice overnight and photographed under ambient (top) or UV (bottom) light after 10 minute incubation with silica gel.

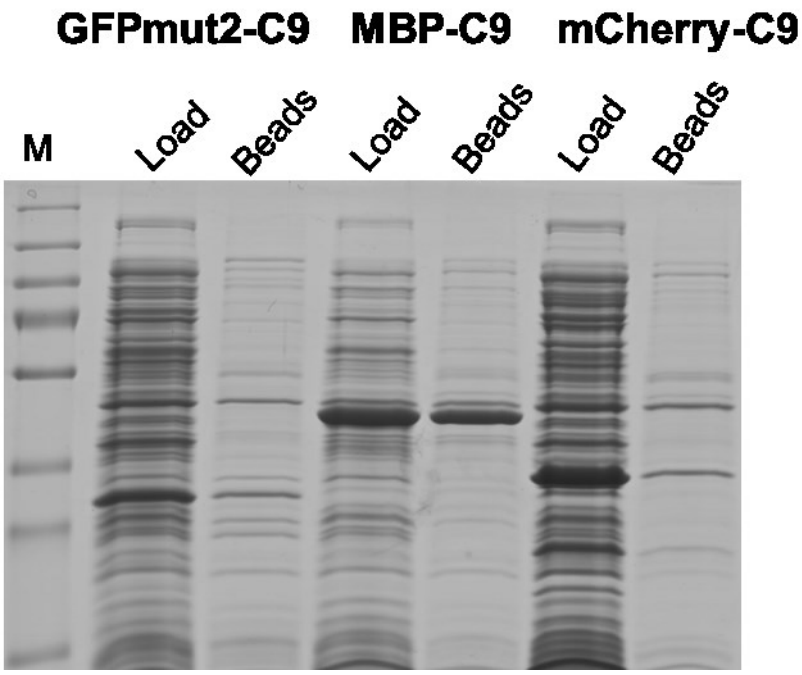

Figure 0.5 SDS-PAGE gel analysis of silica gel beads after purification. Protein is equivalent to 90 mg of silica gel beads post-elution.

References

1. Kyte, J.; Doolittle, R. F., A simple method for displaying the hydropathic character of a protein. *J Mol Biol* **1982,** *157*, 105-132.
2. Ball, P., Life's lessons in design. *Nature* **2001,** *409* (6818), 413-416.
3. Harris, P. J. F., *Carbon nanotubes and related structures: new materials for the twenty-first century*. Cambridge university press: 2001.
4. Mann, S., Molecular tectonics in biomineralization and biomimetic materials chemistry. *Nature* **1993,** *365* (6446), 499-505.
5. Fratzl, P., Biomimetic materials research: what can we really learn from nature's structural materials? *Journal of the Royal Society Interface* **2007,** *4* (15), 637-642.
6. Sarikaya, M.; Tamerler, C.; Jen, A. K. Y.; Schulten, K.; Baneyx, F., Molecular biomimetics: nanotechnology through biology. *Nature Materials* **2003,** *2* (9), 577-585.
7. Currey, J., Mechanical properties of mother of pearl in tension. *Proceedings of the Royal Society of London. Series B. Biological Sciences* **1977,** *196* (1125), 443-463.
8. Sarikaya, M.; Tamerler, C.; Schwartz, D. T.; Baneyx, F., Materials assembly and formation using engineered polypeptides *Annual Review of Materials Research* **2004,** *34* (1), 373-408.
9. Smith, G. P., Filamentous fusion phage: novel expression vectors that display cloned antigens on virion surface. *Science* **1985,** *228* (4705), 3.
10. Parmley, S. F.; Smith, G. P., Antibody-selectable filamentous fd phage vectors: affinity purification of target genes. *Gene* **1988,** *73* (2), 305-318.
11. Endemann, H.; Model, P., Location of filamentous phage minor coat proteins in phage and in infected cells. *Journal of molecular biology* **1995,** *250* (4), 496-506.
12. Kehoe, J. W.; Kay, B. K., Filamentous Phage Display in the New Millennium. *Chem. Rev.* **2005,** *105* (11), 4056-4072.
13. Boder, E. T.; Wittrup, K. D., Yeast surface display for screening combinatorial polypeptide libraries. *Nat Biotech* **1997,** *15* (6), 553-557.
14. Daugherty, P. S., Protein engineering with bacterial display. *Current Opinion in Structural Biology* **2007,** *17* (4), 474-480.
15. Georgiou, G.; Stathopoulos, C.; Daugherty, P. S.; Nayak, A. R.; Iverson, B. L.; Curtiss, R., 3rd, Display of heterologous proteins on the surface of microorganisms: from the screening of combinatorial libraries to live recombinant vaccines. *Nature Biotechnology* **1997,** *15* (1), 29-34.
16. Lu, Z.; Murray, K. S.; Van Cleave, V.; LaVallie, E. R.; Stahl, M. L.; McCoy, J. M., Expression of thioredoxin random peptide libraries on the Escherichia coli cell surface as functional fusions to flagellin: a system designed for exploring protein-protein interactions. *Nature Biotechnology* **1995,** *13* (4), 366-372.
17. Boder, E. T.; Wittrup, K. D., Optimal screening of surface-displayed polypeptide libraries. *Biotechnology Progress* **1998,** *14* (1), 55-62.
18. Gold, L., Oligonucleotides as Research, Diagnostic, and Therapeutic Agents. *Journal of Biological Chemistry* **1995,** *270* (23), 13581-13584.

19. Chiu, D.; Zhou, W.; Kitayaporn, S.; Schwartz, D. T.; Murali-Krishna, K.; Kavanagh, T. J.; Baneyx, F., Biomineralization and Size Control of Stable Calcium Phosphate Core–Protein Shell Nanoparticles: Potential for Vaccine Applications. *Bioconjugate Chem.* **2012**.
20. Thai, C. K.; Dai, H.; Sastry, M.; Sarikaya, M.; Schwartz, D. T.; Baneyx, F., Identification and characterization of Cu2O-and ZnO-binding polypeptides by Escherichia coli cell surface display: toward an understanding of metal oxide binding. *Biotechnology and Bioengineering* **2004,** *87* (2), 129-137.
21. Zhou, W.; Baneyx, F., Aqueous, Protein-Driven Synthesis of Transition Metal-Doped ZnS Immuno-Quantum Dots. *ACS Nano* **2011,** *5* (10), 8013-8018.
22. Zhou, W.; Schwartz, D. T.; Baneyx, F. o., Single-Pot Biofabrication of Zinc Sulfide Immuno-Quantum Dots. *J. Am. Chem. Soc.* **2010,** *132* (13), 4731-4738.
23. Kroto, H. W.; Heath, J. R.; O'Brien, S. C.; Curl, R. F.; Smalley, R. E., C 60: buckminsterfullerene. *Nature* **1985,** *318* (6042), 162-163.
24. Friedman, S. H.; DeCamp, D. L.; Sijbesma, R. P.; Srdanov, G.; Wudl, F.; Kenyon, G. L., Inhibition of the HIV-1 protease by fullerene derivatives: model building studies and experimental verification. *Journal of the American Chemical Society* **1993,** *115* (15), 6506-6509.
25. Gharbi, N.; Pressac, M.; Hadchouel, M.; Szwarc, H.; Wilson, S. R.; Moussa, F., [60]Fullerene is a Powerful Antioxidant in Vivo with No Acute or Subacute Toxicity. *Nano Letters* **2005,** *5* (12), 2578-2585.
26. Käsermann, F.; Kempf, C., Photodynamic inactivation of enveloped viruses by buckminsterfullerene. *Antiviral Research* **1997,** *34* (1), 65-70.
27. Iijima, S., Helical microtubules of graphitic carbon. *Nature* **1991,** *354* (6348), 56-58.
28. Terrones, M., Science and technology of the twenty-first century: synthesis, properties, and applications of carbon nanotubes. *Annual Review of Materials Research* **2003,** *33* (1), 419-501.
29. Dai, H., Carbon nanotubes: synthesis, integration, and properties. *Accounts of Chemical Research* **2002,** *35* (12), 1035-1044.
30. Chaturvedi, P.; Verma, P.; Singh, A.; Chaudhary, P.; Basu, P., Carbon Nanotube-Purification and Sorting Protocols. *Defence Science Journal* **2008,** *58* (5).
31. Arnold, M. S.; Green, A. A.; Hulvat, J. F.; Stupp, S. I.; Hersam, M. C., Sorting carbon nanotubes by electronic structure using density differentiation. *Nature nanotechnology* **2006,** *1* (1), 60-65.
32. Tu, X.; Manohar, S.; Jagota, A.; Zheng, M., DNA sequence motifs for structure-specific recognition and separation of carbon nanotubes. *Nature* **2009,** *460* (7252), 250-253.
33. Dresselhaus, M. S.; Dresselhaus, G.; Eklund, P. C., *Science of fullerenes and carbon nanotubes: their properties and applications*. Academic Press: 1996.
34. Ajayan, P., Nanotubes from carbon. *ChemInform* **1999,** *30* (39), no-no.
35. Pop, E.; Mann, D.; Wang, Q.; Goodson, K.; Dai, H., Thermal conductance of an individual single-wall carbon nanotube above room temperature. *Nano Letters* **2006,** *6* (1), 96-100.
36. Hong, S.; Myung, S., Nanotube Electronics: A flexible approach to mobility. *Nat Nano* **2007,** *2* (4), 207-208.
37. Bellucci, S., Carbon nanotubes: physics and applications. *physica status solidi (c)* **2005,** *2* (1), 34-47.

38. Novoselov, K.; Geim, A.; Morozov, S.; Jiang, D.; Zhang, Y.; Dubonos, S.; Grigorieva, I.; Firsov, A., Electric field effect in atomically thin carbon films. *Science* **2004,** *306* (5696), 666-669.
39. Barth, A.; Marx, W., Graphene-A rising star in view of scientometrics. *arXiv preprint arXiv:0808.3320* **2008**.
40. Lee, C.; Wei, X.; Kysar, J. W.; Hone, J., Measurement of the elastic properties and intrinsic strength of monolayer graphene. *Science* **2008,** *321* (5887), 385-388.
41. Geim, A. K., Graphene: Status and Prospects. *Science* **2009,** *324* (5934), 1530-1534.
42. Geim, A. K.; Novoselov, K. S., The rise of graphene. *Nature Materials* **2007,** *6* (3), 183-191.
43. Castro Neto, A. H.; Guinea, F.; Peres, N. M. R.; Novoselov, K. S.; Geim, A. K., The electronic properties of graphene. *Reviews of Modern Physics* **2009,** *81* (1), 109-162.
44. Wu, J.; Pisula, W.; Mullen, K., Graphenes as potential material for electronics. *Chemical Reviews* **2007,** *107* (3), 718-718.
45. Rao, C. N. R.; Sood, A. K.; Subrahmanyam, K. S.; Govindaraj, A., Graphene: The New Two-Dimensional Nanomaterial. *Angewandte Chemie International Edition* **2009,** *48* (42), 7752-7777.
46. Guo, S.; Dong, S., Graphene nanosheet: synthesis, molecular engineering, thin film, hybrids, and energy and analytical applications. *Chem. Soc. Rev.* **2011,** *40* (5), 2644-2672.
47. Morozov, S. V.; Novoselov, K. S.; Katsnelson, M. I.; Schedin, F.; Elias, D. C.; Jaszczak, J. A.; Geim, A. K., Giant intrinsic carrier mobilities in graphene and its bilayer. *Physical Review Letters* **2008,** *100* (1), 16602-16602.
48. Bolotin, K. I.; Sikes, K. J.; Jiang, Z.; Klima, M.; Fudenberg, G.; Hone, J.; Kim, P.; Stormer, H. L., Ultrahigh electron mobility in suspended graphene. *Solid State Communications* **2008,** *146* (9), 351-355.
49. Zhang, Y.; Tan, Y. W.; Stormer, H. L.; Kim, P., Experimental observation of the quantum Hall effect and Berry's phase in graphene. *Nature* **2005,** *438* (7065), 201-204.
50. Hone, J.; Whitney, M.; Piskoti, C.; Zettl, A., Thermal conductivity of single-walled carbon nanotubes. *Physical Review B* **1999,** *59* (4), R2514-R2516.
51. Tsoukleri, G.; Parthenios, J.; Papagelis, K.; Jalil, R.; Ferrari, A. C.; Geim, A. K.; Novoselov, K. S.; Galiotis, C., Subjecting a graphene monolayer to tension and compression. *Small* **2009,** *5* (21), 2397-2402.
52. Yu, F., Arepalli, Ruoff, Tensile loading of ropes of single wall carbon nanotubes and their mechanical properties. *Physical Review Letters* **2000,** *84* (24), 5552-5555.
53. Dürkop, T.; Getty, S. A.; Cobas, E.; Fuhrer, M. S., Extraordinary Mobility in Semiconducting Carbon Nanotubes. *Nano Letters* **2004,** *4* (1), 35-39.
54. Son, Y. W.; Cohen, M. L.; Louie, S. G., Energy gaps in graphene nanoribbons. *Physical Review Letters* **2006,** *97* (21), 216803.
55. Han, M. Y.; Özyilmaz, B.; Zhang, Y.; Kim, P., Energy band-gap engineering of graphene nanoribbons. *Physical Review Letters* **2007,** *98* (20), 206805.
56. Yang, L.; Park, C. H.; Son, Y. W.; Cohen, M. L.; Louie, S. G., Quasiparticle energies and band gaps in graphene nanoribbons. *Physical Review Letters* **2007,** *99* (18), 186801.
57. Unluer, D.; Tseng, F.; Ghosh, A. W.; Stan, M. R., Monolithically Patterned Wide–Narrow–Wide All-Graphene Devices. *Nanotechnology, IEEE Transactions on* **2011,** *10* (5), 931-939.

58. Dyke, C. A.; James, M., Solvent-free functionalization of carbon nanotubes. *Journal of the American Chemical Society* **2003,** *125* (5), 1156-1157.
59. Hirsch, A., Functionalization of single-walled carbon nanotubes. *Angewandte Chemie International Edition* **2002,** *41* (11), 1853-1859.
60. Moore, V. C.; Strano, M. S.; Haroz, E. H.; Hauge, R. H.; Smalley, R. E.; Schmidt, J.; Talmon, Y., Individually suspended single-walled carbon nanotubes in various surfactants. *Nano Letters* **2003,** *3* (10), 1379-1382.
61. Dieckmann, G. R.; Dalton, A. B.; Johnson, P. A.; Razal, J.; Chen, J.; Giordano, G. M.; Muñoz, E.; Musselman, I. H.; Baughman, R. H.; Draper, R. K., Controlled assembly of carbon nanotubes by designed amphiphilic peptide helices. *Journal of the American Chemical Society* **2003,** *125* (7), 1770-1777.
62. Wang, S.; Humphreys, E. S.; Chung, S. Y.; Delduco, D. F.; Lustig, S. R.; Wang, H.; Parker, K. N.; Rizzo, N. W.; Subramoney, S.; Chiang, Y. M., Peptides with selective affinity for carbon nanotubes. *Nature Materials* **2003,** *2* (3), 196-200.
63. Pender, M. J.; Sowards, L. A.; Hartgerink, J. D.; Stone, M. O.; Naik, R. R., Peptide-mediated formation of single-wall carbon nanotube composites. *Nano Letters* **2006,** *6* (1), 40-44.
64. Karajanagi, S. S.; Yang, H.; Asuri, P.; Sellitto, E.; Dordick, J. S.; Kane, R. S., Protein-assisted solubilization of single-walled carbon nanotubes. *Langmuir* **2006,** *22* (4), 1392-1395.
65. Star, A.; Steuerman, D. W.; Heath, J. R.; Stoddart, J. F., Starched carbon nanotubes. *Angewandte Chemie International Edition* **2002,** *41* (14), 2508-2512.
66. Bandyopadhyaya, R.; Nativ-Roth, E.; Regev, O.; Yerushalmi-Rozen, R., Stabilization of individual carbon nanotubes in aqueous solutions. *Nano Letters* **2002,** *2* (1), 25-28.
67. Zheng, M.; Jagota, A.; Semke, E. D.; Diner, B. A.; McLean, R. S.; Lustig, S. R.; Richardson, R. E.; Tassi, N. G., DNA-assisted dispersion and separation of carbon nanotubes. *Nature Materials* **2003,** *2* (5), 338-342.
68. Patil, A. J.; Vickery, J. L.; Scott, T. B.; Mann, S., Aqueous Stabilization and Self-Assembly of Graphene Sheets into Layered Bio-Nanocomposites using DNA. *Advanced Materials* **2009,** *21* (31), 3159-3164.
69. Tomásio, S. D. M.; Walsh, T., Atomistic modelling of the interaction between peptides and carbon nanotubes. *Molecular Physics* **2007,** *105* (2-3), 221-229.
70. Tomásio, S. M.; Walsh, T. R., Modeling the binding affinity of peptides for graphitic surfaces. Influences of aromatic content and interfacial shape. *The Journal of Physical Chemistry C* **2009,** *113* (20), 8778-8785.
71. Cui, Y.; Kim, S. N.; Jones, S. E.; Wissler, L. L.; Naik, R. R.; McAlpine, M. C., Chemical functionalization of graphene enabled by phage displayed peptides. *Nano Letters* **2010,** *10* (11), 4559-4565.
72. Katoch, J.; Kim, S. N.; Kuang, Z.; Farmer, B. L.; Naik, R. R.; Tatulian, S. A.; Ishigami, M., Structure of a Peptide Adsorbed on Graphene and Graphite. *Nano Letters* **2012,** *12* (5), 2342-2346.
73. Niyogi, S.; Hamon, M.; Hu, H.; Zhao, B.; Bhowmik, P.; Sen, R.; Itkis, M.; Haddon, R., Chemistry of single-walled carbon nanotubes. *Accounts of Chemical Research* **2002,** *35* (12), 1105-1113.
74. Erlanger, B. F.; Chen, B. X.; Zhu, M.; Brus, L., Binding of an anti-fullerene IgG monoclonal antibody to single wall carbon nanotubes. *Nano Letters* **2001,** *1* (9), 465-468.

75. Wang, Y.; Li, Z.; Wang, J.; Li, J.; Lin, Y., Graphene and graphene oxide: biofunctionalization and applications in biotechnology. *Trends in biotechnology* **2011,** *29* (5), 205-212.
76. Carrillo, A.; Swartz, J. A.; Gamba, J. M.; Kane, R. S.; Chakrapani, N.; Wei, B.; Ajayan, P. M., Noncovalent functionalization of graphite and carbon nanotubes with polymer multilayers and gold nanoparticles. *Nano Letters* **2003,** *3* (10), 1437-1440.
77. Lin, Y.; Allard, L. F.; Sun, Y. P., Protein-affinity of single-walled carbon nanotubes in water. *The Journal of Physical Chemistry B* **2004,** *108* (12), 3760-3764.
78. Chen, R. J.; Bangsaruntip, S.; Drouvalakis, K. A.; Wong Shi Kam, N.; Shim, M.; Li, Y.; Kim, W.; Utz, P. J.; Dai, H., Noncovalent functionalization of carbon nanotubes for highly specific electronic biosensors. *Proceedings of the National Academy of Sciences* **2003,** *100* (9), 4984-4989.
79. Karajanagi, S. S.; Vertegel, A. A.; Kane, R. S.; Dordick, J. S., Structure and function of enzymes adsorbed onto single-walled carbon nanotubes. *Langmuir* **2004,** *20* (26), 11594-11599.
80. Brown, S., Protein-mediated particle assembly. *Nano Letters* **2001,** *1* (7), 391-394.
81. Beckett, D.; Kovaleva, E.; Schatz, P. J., A minimal peptide substrate in biotin holoenzyme synthetase-catalyzed biotinylation. *Protein Science* **1999,** *8* (04), 921-929.
82. Ostrov, N.; Gazit, E., Genetic engineering of biomolecular scaffolds for the fabrication of organic and metallic nanowires. *Angewandte Chemie International Edition* **2010,** *49* (17), 3018-3021.
83. Aslan, K.; Lakowicz, J. R.; Geddes, C. D., Rapid deposition of triangular silver nanoplates on planar surfaces: application to metal-enhanced fluorescence. *The Journal of Physical Chemistry B* **2005,** *109* (13), 6247-6251.
84. Haridas, M.; Tripathi, L.; Basu, J., Photoluminescence enhancement and quenching in metal-semiconductor quantum dot hybrid arrays. *Applied Physics Letters* **2011,** *98* (6), 063305-063305-3.
85. Leong, K.; Chen, Y.; Masiello, D. J.; Zin, M. T.; Hnilova, M.; Ma, H.; Tamerler, C.; Sarikaya, M.; Ginger, D. S.; Jen, A. K. Y., Cooperative Near-Field Surface Plasmon Enhanced Quantum Dot Nanoarrays. *Advanced Functional Materials* **2010,** *20* (16), 2675-2682.
86. Coyle, B.; Zhou, W.; Baneyx, F., Protein-aided mineralization of inorganic nanostructures. In *Bionanotechnology: biological self-assembly and its applications*, Rehm, B. H. A., Ed. Caister Academic Press: Norwich, U.K., 2013.
87. Dickerson, M. B.; Sandhage, K. H.; Naik, R. R., Protein- and peptide directed synthesis of inorganic materials. *Chem Rev* **2008,** *108*, 4935-4978.
88. Lee, S.-Y.; Lim, J.-S.; Harris, M. T., Synthesis and application of virus-based hybrid nanomaterials. *Biotechnol Bioeng* **2012,** *109*, 16-30.
89. Seker, U. O. S.; Demir, H. V., Material Binding Peptides for Nanotechnology. *Molecules* **2011,** *16* (2), 1426-1451.
90. Soto, C. M.; Ratna, B. R., Virus hybrids as nanomaterials for biotechnology. *Curr Opin Biotechnol* **2010,** *21*, 426-438.
91. Baneyx, F.; Schwartz, D. T., Selection and analysis of solid-binding peptides. *Curr. Opin. Biotechnol.* **2007,** *18*, 312-317.
92. Sarikaya, M.; Tamerler, C.; Jen, A. K.; Schulten, K.; Baneyx, F., Molecular biomimetics: nanotechnology through biology. *Nat Mater* **2003,** *2*, 577-585.

93. Sarikaya, M.; Tamerler, C.; Schwartz, D. T.; Baneyx, F., Materials assembly and formation using engineered polypeptides. *Annu Rev Mater Res* **2004,** *34*, 373-408.
94. Qureshi, A.; Kang, W. P.; Davidson, J. L.; Gurbuz, Y., Review on carbon-derived, solid-state, micro and nano sensors for electrochemical sensing applications. *Diam Rel Mater* **2009,** *18*, 1401-1420.
95. Liu, Z.; Tabakman, S.; Welsher, K.; Dai, H., Carbon nanotubes in biology and medicine: *in vitro* and *in vivo* detection, imaging and drug delivery. *Nano Res* **2009,** *2*, 85-120.
96. Shen, H.; Zhang, L.; Liu, M.; Zhang, Z., Biomedical applications of graphene. *Theranostics* **2012,** *2*, 283-294.
97. Wang, Y.; Li, Z.; Wang, J.; Li, J.; Lin, Y., Graphene and graphene oxide: biofunctionalization and applictions in biotechnology. *Trends Biotechnol* **2011,** *29*, 205-212.
98. Boul, P.; Liu, J.; Mickelson, E.; Huffman, C.; Ericson, L.; Chiang, I.; Smith, K.; Colbert, D.; Hauge, R.; Margrave, J., Reversible sidewall functionalization of buckytubes. *Chem Phys Lett* **1999,** *310* (3), 367-372.
99. Chan, W. C. W.; Nie, S., Quantum dot bioconjugates for ultrasensitive nonisotopic detection. *Science* **1998,** *281*, 2016-2018.
100. Vigolo, B.; Pénicaud, A.; Coulon, C.; Sauder, C.; Pailler, R.; Journet, C.; Bernier, P.; Poulin, P., Macroscopic fibers and ribbons of oriented carbon nanotubes. *Science* **2000,** *290* (5495), 1331-1334.
101. Dieckmann, G. R.; Dalton, A. B.; Johnson, P. A.; Razal, J.; Chen, J.; Giordano, G. M.; Munoz, E.; Musselman, I. H.; Baughman, R. H.; Draper, R. K., Controlled assembly of carbon nanotubes by designed amphiphilic Peptide helices. *J Am Chem Soc* **2003,** *125* (7), 1770-7.
102. Ortiz-Acevedo, A.; Xie, H.; Zorbas, V.; Sampson, W. M.; Dalton, A. B.; Baughman, R. H.; Draper, R. K.; Musselman, I. H.; Dieckmann, G. R., Diameter-selective solubilization of single-walled carbon nanotubes by reversible cyclic peptides. *J Am Chem Soc* **2005,** *127* (26), 9512-7.
103. Cui, Y.; Kim, S. N.; Jones, S. E.; Wissler, L. L.; Naik, R. R.; McAlpine, M. C., Chemical functionalization of graphene enabled by phage displayed peptides. *Nano Lett* **2010,** *10* (11), 4559-65.
104. Oh, D.; Dang, X.; Yi, H.; Allen, M. A.; Xu, K.; Lee, Y. J.; Belcher, A. M., Graphene sheets stabilized on genetically engineered M13 viral templates as conducting frameworks for hybrid energy-storage materials. *Small* **2012,** *8*, 1006-1011.
105. So, C. R.; Hayamizu, Y.; Yazici, H.; Gresswell, C.; Khatayevich, D.; Tamerler, C.; Sarikaya, M., Controlling self-assembly of engineered peptides on graphite by rational mutation. *ACS Nano* **2012,** *6* (2), 1648-56.
106. Wang, S.; Humphreys, E. S.; Chung, S.-Y.; Delduco, D. F.; Lustig, S. R.; Wang, H.; Parker, K. N.; Rizzo, N. W.; Subramoney, S.; Chiang, Y.-M.; Jagota, A., Peptides with selective affinity for carbon nanotubes. *Nat Mater* **2003,** *2*, 196-200.
107. Yu, T.; Gong, Y.; Lu, T.; Wei, L.; Li, Y.; Mu, Y.; Chen, Y.; Liao, K., Recognition of carbon nanotube chirality by phage display. *RSC Adv* **2012,** *2*, 1466-1476.
108. Thai, C. K.; Dai, H.; Sastry, M. S.; Sarikaya, M.; Schwartz, D. T.; Baneyx, F., Identification and characterization of Cu_2O- and ZnO-binding polypeptides by *Escherichia coli* cell surface display: toward an understanding of metal oxide binding. *Biotechnol Bioeng* **2004,** *87*, 129-137.

109. Zhou, W.; Schwartz, D. T.; Baneyx, F., Single pot biofabrication of zinc sulfide immuno-quantum dots. *J. Am. Chem. Soc.* **2010,** *132*, 4731-4738.
110. Nossal, N. G.; Heppel, L. A., The Release of enzymes by osmotic shock from *Escherichia coli* in exponential phase. *J Biol Chem* **1966,** *241* (13), 3055-3062.
111. Lunn, C. A.; Pigiet, V. P., Localization of thioredoxin from *Escherichia coli* in an osmotically sensitive compartment. *J Biol Chem* **1982,** *257* (19), 11424-11430.
112. Homola, J., Surface plasmon resonance sensors for detection of chemical and biological species. *Chem Rev* **2008,** *108* (2), 462-493.
113. Lu, Z.; Murray, K. S.; Van Cleave, V.; LaVallie, E. R.; Stahl, M. L.; McCoy, J. M., Expression of thioredoxin random peptide libraries on the *Escherichia coli* cell surface as functional fusions to flagellin: a system designed for exploring protein-protein interactions. *Biotechnology* **1995,** *13*, 366-372.
114. Robertson, J., Diamond-like amorphous carbon. *Materials Science and Engineering: R: Reports* **2002,** *37* (4–6), 129-281.
115. Kase, D.; Kulp, J. L., 3rd; Yudasaka, M.; Evans, J. S.; Iijima, S.; Shiba, K., Affinity selection of peptide phage libraries against single-wall carbon nanohorns identifies a peptide aptamer with conformational variability. *Langmuir* **2004,** *20*, 8939-8941.
116. Su, Z.; Mui, K.; Daub, E.; Leung, T.; Honek, J., Single-walled carbon nanotube binding peptides: probing tryptophan's importance by unnatural amino acid substitution. *J Phys Chem B* **2007,** *111* (51), 14411-7.
117. Tomásio, S. M.; Walsh, T. R., Modeling the binding affinity of peptides for graphitic surfaces. Influence of aromatic content and interfacial shape. *J Phys Chem C* **2009,** *113*, 8778-8785.
118. Xie, H.; Becraft, E. J.; Baughman, R. H.; Dalton, A. B.; Dieckmann, G. R., Ranking the affinity of aromatic residues for carbon nanotubes by using designed surfactant peptides. *Journal of peptide science : an official publication of the European Peptide Society* **2008,** *14* (2), 139-51.
119. Zorbas, V.; Smith, A. L.; Xie, H.; Ortiz-Acevedo, A.; Dalton, A. B.; Dieckmann, G. R.; Draper, R. K.; Baughman, R. H.; Musselman, I. H., Importance of aromatic content for peptide/single wall carbon nanotube interactions. *J Am Chem Soc* **2005,** *127*, 12323-12328.
120. Katti, S. K.; LeMaster, D. M.; Eklund, H., Crystal structure of thioredoxin from *Escherichia coli a*t 1.68 A resolution. *J Mol Biol* **1990,** *212* (1), 167.
121. Baneyx, F., Recombinant protein expression in *Escherichia coli*. *Curr Opin Biotechnol* **1999,** *10*, 411-421.
122. Ferrari, A. C.; Robertson, J., Raman spectroscopy of amorphous, nanostructured, diamond-like carbon, and nanodiamond. *Philos Transact A* **2004,** *362* (1824), 2477-512.
123. Dai, H.; Choe, W. S.; Thai, C. K.; Sarikaya, M.; Traxler, B. A.; Baneyx, F.; Schwartz, D. T., Nonequilibrium synthesis and assembly of hybrid inorganic-protein nanostructures using an engineered DNA binding protein. *J Am Chem Soc* **2005,** *127*, 15637-15643.
124. Grosh, C.; Schwartz, D. T.; Baneyx, F., Protein-based control of silver growth habit using electrochemical deposition. *Cryst Growth Des* **2009,** *9*, 4401-4406.
125. Kitayaporn, S.; Zhou, W.; Schwartz, D. T.; Baneyx, F., Laying out ground rules for protein-aided nanofabrication: ZnO synthesis at 70ºC as a case study. *Biotechnol Bioeng* **2012,** *109*, 1912-1918.

126. Sedlak, R. H.; Hnilova, M.; Grosh, C.; Fong, H.; Baneyx, F.; Schwartz, D.; Sarikaya, M.; Tamerler, C.; Traxler, B., Engineered *Escherichia coli* silver-binding periplasmic protein that promotes silver tolerance. *Applied and environmental microbiology* **2012,** *78*, 2289-2296.
127. Sengupta, A.; Thai, C. K.; Sastry, M. S. R.; Schwartz, D. T.; Davis, E. J.; Baneyx, F., A genetic approach for controlling the binding and orientation of proteins on nanoparticles. *Langmuir* **2008,** *24*, 2000-2008.
128. Burghardt, T. P.; Axelrod, D., Total internal reflection/fluorescence photobleaching recovery study of serum albumin adsorption dynamics. *Biophysical journal* **1981,** *33* (3), 455-467.
129. Harris, P. J. F., Fullerene-related structure of commercial glassy carbons. *Philos Mag* **2004,** *84*, 3159-3167.
130. Braden, B. C.; Goldbaum, F. A.; Chen, B. X.; Kirschner, A. N.; Wilson, S. R.; Erlanger, B. F., X-ray crystal structure of an anti-Buckminsterfullerene antibody fab fragment: biomolecular recognition of C(60). *Proc Natl Acad Sci U S A* **2000,** *97* (22), 12193-7.
131. Yang, D. Q.; Sacher, E., Interaction of evaporated nickel nanoparticles with highly oriented pyrolytic graphite: back-bonding to surface fefects, as studied by X-ray photoelectron spectroscopy. *J Phys Chem B* **2005,** *109* (41), 19329-19334.
132. Holmgren, A., Thioredoxin. *Ann. Rev. Biochem.* **1985,** *54*, 237-271.
133. LaVallie, E. R.; Lu, Z.; Diblasio, E. A.; Collins-Racie, L. A.; McCoy, J. M., Thioredoxin as a fusion partner for production of soluble recombinant proteins in *Escherichia coli*. *Methods Enzymol* **2000,** *326*, 322-340.
134. Kim, S. N.; Kuang, Z.; Slocik, J. M.; Jones, S. E.; Cui, Y.; Farmer, B. L.; McAlpine, M. C.; Naik, R. R., Preferential binding of peptides to graphene edges and planes. *J Am Chem Soc* **2011,** *133* (37), 14480-3.
135. Arnau, J.; Lauritzen, C.; Petersen, G. E.; Pedersen, J., Current strategies for the use of affinity tags and tag removal for the purification of recombinant proteins. *Protein expression and purification* **2006,** *48*, 1-13.
136. Waugh, D. S., Making the most of affinity tags. *Trends Biotechnol* **2005,** *23*, 316-320.
137. Kuo, W. H.; Chase, H. A., Exploiting the interactions between poly-histidine fusion tags and immobilized metal ions. *Biotechnol Lett* **2011,** *33* (6), 1075-84.
138. Lichty, J. J.; Malecki, J. L.; Michelson-Horowitz, D. J.; Tan, S., Comparison of affinity tags for protein purification. *Protein expression and purification* **2005,** *41*, 98-105.
139. Ghose, S.; McNemey, T. M.; Hubbard, B., Preparative protein purification on underivatized silica. *Biotechnol Bioeng* **2004,** *87*, 413-423.
140. Coyle, B. L.; Rolandi, M.; Baneyx, F., Carbon-binding designer proteins that discriminate between sp2- and sp3-hybridized carbon surfaces. *Langmuir* **2013,** *29*, 4839-4846.
141. Nannenga, B. L.; Baneyx, F., Reprogramming chaperone pathways to improve membrane protein expression in *Escherichia coli*. *Protein Sci* **2011,** *20*, 1411-1420.
142. Strauch, K. M.; Johnson, K.; Beckwith, J., Characterization of *degP*, a gene required for proteolysis in the cell envelope and essential for growth of *Escherichia coli* at high temperature. *J Bacteriol* **1989,** *171*, 2689-2696.
143. Baneyx, F.; Georgiou, G., In vivo degradation of secreted fusion proteins by the *Escherichia coli* outer membrane protein OmpT. *J. Bacteriol.* **1990,** *172*, 494-494.
144. Wessel, D.; Flügge, U. I., A method for the quantitative recovery of protein in dilute solution in the presence of detergents and lipids. *Anal. Biochem.* **1984,** *138*, 141-143.

145. Thomas, J. G.; Baneyx, F., Protein misfolding and inclusion body formation in recombinant *Escherichia coli* cells overproducing heat-shock proteins. *J. Biol. Chem.* **1996,** *271*, 11141-11147.
146. Iler, R. K., *The chemistry of silica: solubility, polymerization, colloid and surface properties and biochemistry*. Wiley: New York, 1979.
147. Chen, H. B.; Su, X. D.; Neoh, K.-G.; Choe, W. S., Context-dependent adsorption behavior of cyclic and linear peptides on metal oxide. *Langmuir* **2009,** *25*, 1588-1593.
148. Chiu, D.; Zhou, W.; Kitayaporn, S.; Schwartz, D. T.; Murali-Krishna, K.; Kavanagh, T. J.; Baneyx, F., Biomineralization and size control of calcium phosphate core-protein shell nanoparticles: potential for vaccine applications. *Bioconjug. Chem.* **2012,** *23*, 610-617.
149. Choe, W. S.; Sastry, M. S. R.; Thai, C. K.; Dai, H.; Schwartz, D. T.; Baneyx, F., Conformational control of inorganic adhesion in a designer protein engineered for cuprous oxide binding. *Langmuir* **2007,** *23*, 11347-11350.
150. Hnilova, M.; Oren, E. E.; Seker, U. O. S.; Wilson, B. R.; Collino, S.; Evans, J. S.; Tamerler, C.; Sarikaya, M., Effect of molecular conformations on the adsorption behavior of gold-binding peptides. *Langmuir* **2008,** *24*, 12440-12445.
151. Seker, U. O. S.; Wilson, B.; Dincer, S.; Kim, I. W.; Oren, E. E.; Evans, J. S.; Tamerler, C.; Sarikaya, M., Adsorption behavior of linear and cyclic genetically engineered platinum binding peptides. *Langmuir* **2007,** *23*, 7895-7900.
152. Cormack, B. P.; Valdivia, R. H.; Falkow, S., FACS-optimized mutants of the green fluorescent protein (GFP). *Gene* **1996,** *173*, 33-38.
153. Nieba, L.; Nieba-Axmann, E.; Persson, A.; Hämäläinen, M.; Edebratt, F.; Hansson, A.; Lidholm, J.; Magnusson, K.; Karlsson, A. F.; Plückthun, A., BIACORE analysis of histidine-tagged proteins using a chelating NTA sensor chip. *Anal Biochem* **1997,** *252*, 217-228.
154. Patwardhan, S. V.; Emami, F. S.; Berry, R. J.; Jones, S. E.; Naik, R. R.; Deschaume, O.; Heinz, H.; Perry, C. C., Chemistry of aqueous silica nanoparticle surfaces and the mechanism of selective peptide adsorption. *J Am Chem Soc* **2012,** *134*, 6244-6256.
155. Stutz, H., Protein attachment on silica surfaces--a survey of molecular fundamentals, resulting effects and novel preventive strategies in CE. *Electrophoresis* **2009,** *30*, 2032-2061.
156. Shaner, N. C.; Campbell, R. E.; Steinbach, P. A.; Giepmans, B. N. G.; Palmer, A. E.; Tsien, R. Y., Improved monomeric red, orange and yellow fluorescent proteins derived from *Discosoma* sp. red fluorescent protein. *Nat Biotechnol* **2004,** *22*, 1567-1572.
157. Sugimura, K.; Nishihara, T., Purification, characterization, and primary structure of *Escherichia coli* protease VII with specificity for paired basic residues: identity of protease VII and OmpT. *J Bacteriol* **1988,** *170*, 5625-5632.
158. Waugh, D. S., An overview of enzymatic reagents for the removal of affinity tags. *Protein expression and purification* **2011,** *80*, 283-293.
159. Grodberg, J.; Dunn, J. J., ompT encodes the Escherichia coli outer membrane protease that cleaves T7 RNA polymerase during purification. *Journal of bacteriology* **1988,** *170* (3), 1245-1253.
160. Gayda, R. C.; Markovitz, A., Cloned DNA fragment specifying major outer membrane protein a in Escherichia coli K-12. *Journal of bacteriology* **1978,** *136* (1), 369-380.
161. Still, W. C.; Kahn, M.; Mitra, A., Rapid chromatography technique for preparative separations with moderate resolution. *J Org Chem* **1978,** *43*, 2923-2925.

162. Coyle, B. L.; Zhou, W.; Baneyx, F., Protein-aided mineralization of inorganic nanostructures. In *Bionanotechnology: biological self-assembly and its applications*, Rehm, B. H. A., Ed. Caister Academic Press: Norwich, U.K., 2013.
163. Bianco, A.; Kostarelos, K.; Prato, M., Applications of carbon nanotubes in drug delivery. *Current Opinion in Chemical Biology* **2005,** *9* (6), 674-679.
164. Liu, Z.; Tabakman, S.; Welsher, K.; Dai, H., Carbon nanotubes in biology and medicine: in vitro and in vivo detection, imaging and drug delivery. *Nano Research* **2009,** *2* (2), 85-120.
165. Bhirde, A. A.; Patel, V.; Gavard, J.; Zhang, G.; Sousa, A. A.; Masedunskas, A.; Leapman, R. D.; Weigert, R.; Gutkind, J. S.; Rusling, J. F., Targeted killing of cancer cells in vivo and in vitro with EGF-directed carbon nanotube-based drug delivery. *ACS Nano* **2009,** *3* (2), 307-316.
166. Chen, J.; Chen, S.; Zhao, X.; Kuznetsova, L. V.; Wong, S. S.; Ojima, I., Functionalized single-walled carbon nanotubes as rationally designed vehicles for tumor-targeted drug delivery. *Journal of the American Chemical Society* **2008,** *130* (49), 16778-16785.
167. Balasubramanian, K.; Burghard, M., Biosensors based on carbon nanotubes. *Analytical and Bioanalytical Chemistry* **2006,** *385* (3), 452-468.
168. Minot, E. D.; Janssens, A. M.; Heller, I.; Heering, H. A.; Dekker, C.; Lemay, S. G., Carbon nanotube biosensors: the critical role of the reference electrode. *Applied Physics Letters* **2007,** *91* (9), 093507.
169. Lin, Y.; Lu, F.; Tu, Y.; Ren, Z., Glucose biosensors based on carbon nanotube nanoelectrode ensembles. *Nano Letters* **2004,** *4* (2), 191-195.
170. Wang, J., Carbon-nanotube based electrochemical biosensors: A review. *Electroanalysis* **2005,** *17* (1), 7-14.
171. Coyle, B. L.; Rolandi, M.; Baneyx, F. o., Carbon-Binding Designer Proteins that Discriminate between sp2-and sp3-Hybridized Carbon Surfaces. *Langmuir* **2013,** *29* (15), 4839-4846.
172. John, P.; Polwart, N.; Troupe, C. E.; Wilson, J. I. B., The Oxidation of Diamond: The Geometry and Stretching Frequency of Carbonyl on the (100) Surface. *Journal of the American Chemical Society* **2003,** *125* (22), 6600-6601.
173. Huang, L. C. L.; Chang, H.-C., Adsorption and Immobilization of Cytochrome c on Nanodiamonds. *Langmuir* **2004,** *20* (14), 5879-5884.
174. Ray III, K. G.; McCreery, R. L., Characterization of the surface carbonyl and hydroxyl coverage on glassy carbon electrodes using Raman spectroscopy. *Journal of Electroanalytical Chemistry* **1999,** *469* (2), 150-158.
175. Pédelacq, J. D.; Cabantous, S.; Tran, T.; Terwilliger, T. C.; Waldo, G. S., Engineering and characterization of a superfolder green fluorescent protein. *Nature Biotechnology* **2005,** *24* (1), 79-88.
176. Inam, F.; Reece, M. J.; Peijs, T., Shortened carbon nanotubes and their influence on the electrical properties of polymer nanocomposites. *Journal of Composite Materials* **2011**.
177. Lu, K.; Lago, R.; Chen, Y.; Green, M.; Harris, P.; Tsang, S., Mechanical damage of carbon nanotubes by ultrasound. *Carbon* **1996,** *34* (6), 814-816.
178. Sorgenfrei, S.; Chiu, C.-y.; Gonzalez Jr, R. L.; Yu, Y.-J.; Kim, P.; Nuckolls, C.; Shepard, K. L., Label-free single-molecule detection of DNA-hybridization kinetics with a carbon nanotube field-effect transistor. *Nature nanotechnology* **2011,** *6* (2), 126-132.

179. Besteman, K.; Lee, J.-O.; Wiertz, F. G.; Heering, H. A.; Dekker, C., Enzyme-coated carbon nanotubes as single-molecule biosensors. *Nano Letters* **2003,** *3* (6), 727-730.
180. So, H.-M.; Won, K.; Kim, Y. H.; Kim, B.-K.; Ryu, B. H.; Na, P. S.; Kim, H.; Lee, J.-O., Single-walled carbon nanotube biosensors using aptamers as molecular recognition elements. *Journal of the American Chemical Society* **2005,** *127* (34), 11906-11907.
181. Star, A.; Tu, E.; Niemann, J.; Gabriel, J.-C. P.; Joiner, C. S.; Valcke, C., Label-free detection of DNA hybridization using carbon nanotube network field-effect transistors. *Proceedings of the National Academy of Sciences of the United States of America* **2006,** *103* (4), 921-926.
182. Avouris, P., Molecular electronics with carbon nanotubes. *Accounts of Chemical Research* **2002,** *35* (12), 1026-1034.
183. Chau, R.; Doyle, B.; Datta, S.; Kavalieros, J.; Zhang, K., Integrated nanoelectronics for the future. *Nature Materials* **2007,** *6* (11), 810-812.
184. Banerjee, K.; Srivastava, N. In *Are carbon nanotubes the future of VLSI interconnections?*, Proceedings of the 43rd annual Design Automation Conference, ACM: 2006; pp 809-814.
185. Park, H.; Afzali, A.; Han, S.-J.; Tulevski, G. S.; Franklin, A. D.; Tersoff, J.; Hannon, J. B.; Haensch, W., High-density integration of carbon nanotubes via chemical self-assembly. *Nature nanotechnology* **2012,** *7* (12), 787-791.
186. Kleinfeld, D.; Kahler, K.; Hockberger, P., Controlled outgrowth of dissociated neurons on patterned substrates. *J. Neurosci* **1988,** *8* (11), 4098-4120.
187. Britland, S.; Clark, P.; Connolly, P.; Moores, G., Micropatterned substratum adhesiveness: a model for morphogenetic cues controlling cell behavior. *Experimental cell research* **1992,** *198* (1), 124-129.
188. Lom, B.; Healy, K. E.; Hockberger, P. E., A versatile technique for patterning biomolecules onto glass coverslips. *Journal of Neuroscience Methods* **1993,** *50* (3), 385-397.
189. Wilson, K.; Stancescu, M.; Das, M.; Rumsey, J.; Hickman, J., Direct patterning of coplanar polyethylene glycol alkylsilane monolayers by deep-ultraviolet photolithography as a general method for high fidelity, long-term cell patterning and culture. *Journal of Vacuum Science & Technology B* **2011,** *29* (2), 021020.
190. Zhang, F.-F.; Wan, Q.; Li, C.-X.; Wang, X.-L.; Zhu, Z.-Q.; Xian, Y.-Z.; Jin, L.-T.; Yamamoto, K., Simultaneous assay of glucose, lactate, L-glutamate and hypoxanthine levels in a rat striatum using enzyme electrodes based on neutral red-doped silica nanoparticles. *Analytical and Bioanalytical Chemistry* **2004,** *380* (4), 637-642.
191. Yu, A.; Wang, Y.; Barlow, E.; Caruso, F., Mesoporous Silica Particles as Templates for Preparing Enzyme-Loaded Biocompatible Microcapsules. *Advanced Materials* **2005,** *17* (14), 1737-1741.
192. Petri, A.; Gambicorti, T.; Salvadori, P., Covalent immobilization of chloroperoxidase on silica gel and properties of the immobilized biocatalyst. *Journal of Molecular Catalysis B: Enzymatic* **2004,** *27* (2), 103-106.
193. Blanco, R. M.; Terreros, P.; Fernández-Pérez, M.; Otero, C.; Díaz-González, G., Functionalization of mesoporous silica for lipase immobilization: Characterization of the support and the catalysts. *Journal of Molecular Catalysis B: Enzymatic* **2004,** *30* (2), 83-93.

194. Lin, S.; Tseng, F.; Huang, H.; Huang, C.; Chieng, C., Microsized 2D protein arrays immobilized by micro-stamps and micro-wells for disease diagnosis and drug screening. *Fresenius J Anal Chem* **2001,** *371* (2), 202-208.
195. Blawas, A. S.; Huang, C.-Y.; Pirrung, M. C.; Reichert, W. M. In *Patterning antibodies for a multiple analyte sensor via photodeprotection chemistry*, Photonics West'96, International Society for Optics and Photonics: 1996; pp 68-77.
196. Piervincenzi, R. T.; Reichert, W. M.; Hellinga, H. W., Genetic engineering of a single-chain antibody fragment for surface immobilization in an optical biosensor. *Biosensors and Bioelectronics* **1998,** *13* (3), 305-312.
197. Wang, J.; Liu, G.; Engelhard, M. H.; Lin, Y., Sensitive immunoassay of a biomarker tumor necrosis factor-α based on poly (guanine)-functionalized silica nanoparticle label. *Analytical chemistry* **2006,** *78* (19), 6974-6979.
198. Witucki, G. L., A silane primer: chemistry and applications of alkoxy silanes. *Journal of coatings technology* **1993,** *65*, 57-57.
199. Halliwell, C. M.; Cass, A. E., A factorial analysis of silanization conditions for the immobilization of oligonucleotides on glass surfaces. *Analytical chemistry* **2001,** *73* (11), 2476-2483.
200. Yuan, H.; Mullett, W. M.; Pawliszyn, J., Biological sample analysis with immunoaffinity solid-phase microextraction. *Analyst* **2001,** *126* (8), 1456-1461.
201. Tengvall, P.; Jansson, E.; Askendal, A.; Thomsen, P.; Gretzer, C., Preparation of multilayer plasma protein films on silicon by EDC/NHS coupling chemistry. *Colloids and Surfaces B: Biointerfaces* **2003,** *28* (4), 261-272.
202. Uchida, K.; Stadtman, E., Covalent attachment of 4-hydroxynonenal to glyceraldehyde-3-phosphate dehydrogenase. A possible involvement of intra-and intermolecular cross-linking reaction. *Journal of Biological Chemistry* **1993,** *268* (9), 6388-6393.
203. Rao, S. V.; Anderson, K. W.; Bachas, L. G., Oriented immobilization of proteins. *Mikrochim Acta* **1998,** *128* (3-4), 127-143.
204. Leckband, D.; Langer, R., An approach for the stable immobilization of proteins. *Biotechnology and Bioengineering* **1991,** *37* (3), 227-237.
205. Fuchs, S. M.; Raines, R. T., Polyarginine as a multifunctional fusion tag. *Protein Science* **2005,** *14* (6), 1538-1544.
206. Taniguchi, K.; Nomura, K.; Hata, Y.; Nishimura, T.; Asami, Y.; Kuroda, A., The Si-tag for immobilizing proteins on a silica surface. *Biotechnology and Bioengineering* **2007,** *96* (6), 1023-1029.
207. Ikeda, T.; Ninomiya, K.-i.; Hirota, R.; Kuroda, A., Single-step affinity purification of recombinant proteins using the silica-binding Si-tag as a fusion partner. *Protein expression and purification* **2010,** *71* (1), 91-95.
208. Künzelmann, U.; Böttcher, H., Biosensor properties of glucose oxidase immobilized within SiO2 gels. *Sensors and Actuators B: Chemical* **1997,** *39* (1–3), 222-228.
209. Buckley, A. M.; Greenblatt, M., The Sol-Gel Preparation of Silica Gels. *Journal of Chemical Education* **1994,** *71* (7), 599.
210. Stöber, W.; Fink, A.; Bohn, E., Controlled growth of monodisperse silica spheres in the micron size range. *Journal of Colloid and Interface Science* **1968,** *26* (1), 62-69.
211. Ellerby, L. M.; Nishida, C. R.; et al., Encapsulation of Proteins in Transparent Porous Silicate Glasses Prepared by the Sol-Gel Method. *Science* **1992,** *255* (5048), 1113.

212. Avnir, D.; Braun, S.; Lev, O.; Ottolenghi, M., Enzymes and other proteins entrapped in sol-gel materials. *Chemistry of Materials* **1994,** *6* (10), 1605-1614.
213. Dave, B. C.; Dunn, B.; Valentine, J. S.; Zink, J. I., Sol-gel encapsulation methods for biosensors. *Analytical chemistry* **1994,** *66* (22), 1120A-1127A.
214. Livage, J.; Coradin, T.; Roux, C., Encapsulation of biomolecules in silica gels. *Journal of Physics: Condensed Matter* **2001,** *13* (33), R673.
215. Kröger, N.; Deutzmann, R.; Sumper, M., Polycationic peptides from diatom biosilica that direct silica nanosphere formation. *Science* **1999,** *286* (5442), 1129-1132.
216. Naik, R. R.; Tomczak, M. M.; Luckarift, H. R.; Spain, J. C.; Stone, M. O., Entrapment of enzymes and nanoparticles using biomimetically synthesized silica. *Chemical Communications* **2004,** (15), 1684-1685.
217. Cao, Q.; Han, S.-j.; Tulevski, G. S.; Zhu, Y.; Lu, D. D.; Haensch, W., Arrays of single-walled carbon nanotubes with full surface coverage for high-performance electronics. *Nat Nano* **2013,** *8* (3), 180-186.
218. Sangwan, V. K.; Ortiz, R. P.; Alaboson, J. M.; Emery, J. D.; Bedzyk, M. J.; Lauhon, L. J.; Marks, T. J.; Hersam, M. C., Fundamental performance limits of carbon nanotube thin-film transistors achieved using hybrid molecular dielectrics. *ACS Nano* **2012,** *6* (8), 7480-7488.
219. Miyata, Y.; Shiozawa, K.; Asada, Y.; Ohno, Y.; Kitaura, R.; Mizutani, T.; Shinohara, H., Length-sorted semiconducting carbon nanotubes for high-mobility thin film transistors. *Nano Research* **2011,** *4* (10), 963-970.
220. Wang, C.; Chien, J.-C.; Takei, K.; Takahashi, T.; Nah, J.; Niknejad, A. M.; Javey, A., Extremely bendable, high-performance integrated circuits using semiconducting carbon nanotube networks for digital, analog, and radio-frequency applications. *Nano Letters* **2012,** *12* (3), 1527-1533.
221. Sun, D.-m.; Timmermans, M. Y.; Tian, Y.; Nasibulin, A. G.; Kauppinen, E. I.; Kishimoto, S.; Mizutani, T.; Ohno, Y., Flexible high-performance carbon nanotube integrated circuits. *Nature nanotechnology* **2011,** *6* (3), 156-161.
222. Ruel-Gariépy, E.; Leroux, J.-C., In situ-forming hydrogels—review of temperature-sensitive systems. *European Journal of Pharmaceutics and Biopharmaceutics* **2004,** *58* (2), 409-426.
223. Bhattarai, N.; Gunn, J.; Zhang, M., Chitosan-based hydrogels for controlled, localized drug delivery. *Advanced drug delivery reviews* **2010,** *62* (1), 83-99.
224. Peng, C.-C.; Ben-Shlomo, A.; Mackay, E. O.; Plummer, C. E.; Chauhan, A., Drug Delivery by Contact Lens in Spontaneously Glaucomatous Dogs. *Current eye research* **2012,** *37* (3), 204-211.
225. Ali, M.; Horikawa, S.; Venkatesh, S.; Saha, J.; Hong, J. W.; Byrne, M. E., Zero-order therapeutic release from imprinted hydrogel contact lenses within in vitro physiological ocular tear flow. *Journal of Controlled Release* **2007,** *124* (3), 154-162.